

SMALL FUNCTIONAL GROUPS PRESENTED ON PEPTIDE NANOFIBERS  
FOR DETERMINING FATE OF RAT MESENCHYMAL STEM CELLS

A THESIS

SUBMITTED TO THE MATERIALS SCIENCE AND NANOTECHNOLOGY  
PROGRAM OF THE GRADUATE SCHOOL OF ENGINEERING AND SCIENCE

OF BILKENT UNIVERSITY

IN PARTIAL FULFILLMENT OF THE REQUIREMENTS

FOR THE DEGREE OF

MASTER OF SCIENCE

By

Öncay Yaşa

December, 2014

SMALL FUNCTIONAL GROUPS PRESENTED ON PEPTIDE NANOFIBERS  
FOR DETERMINING FATE OF RAT MESENCHYMAL STEM CELLS

By Öncay Yaşa

December, 2014

I certify that I have read this thesis and that in my opinion it is fully adequate, in scope and in quality, as a thesis of the degree of Master of Science.

.....

Assist. Prof. Dr. Ayşe Begüm Tekinay (Advisor)

I certify that I have read this thesis and that in my opinion it is fully adequate, in scope and in quality, as a thesis of the degree of Master of Science.

.....

Assoc. Prof. Dr. Mustafa Özgür Güler

I certify that I have read this thesis and that in my opinion it is fully adequate, in scope and in quality, as a thesis of the degree of Master of Science.

.....

Assoc. Prof. Dr. Çağdaş Devrim Son

Approved for the Graduate School of Engineering and Science:

.....

Prof. Dr. Levent Onural

Director of the Graduate School of Engineering and Science

## **ABSTRACT**

### **SMALL FUNCTIONAL GROUPS PRESENTED ON PEPTIDE NANOFIBERS FOR DETERMINING FATE OF RAT MESENCHYMAL STEM CELLS**

Öncay Yaşa

M.S. in Materials Science and Nanotechnology

Supervisor: Assist. Prof. Dr. Ayşe Begüm Tekinay

December, 2014

Glycosaminoglycans (GAGs) are negatively-charged, unbranched polysaccharides that play important roles in various biological processes and are vital for the regeneration of damaged tissues. Like other natural extracellular matrix components, glycosaminoglycans and proteoglycans show considerable variation in local concentration and chemical composition depending on tissue type. They are found in various connective tissues, including bone, cartilage and fat, and display strong water-binding capacity due to their negative charges. Mechanical characters of GAGs are heavily influenced by the degree and pattern of sulfation, which may greatly alter their viscoelasticity and physiological functions. Variations in GAG sulfation patterns are created principally through extracellular matrix modeling. Due to their extracellular matrix-organizing abilities, glycosaminoglycans are promising biomacromolecules for the design of new bioactive materials for tissue engineering and tissue reconstruction applications. In this study, we functionalized peptide amphiphile molecules with carboxylate and sulfonate groups to develop nanofibrous

networks displaying a range of chemical patterns, and evaluated the effect of the chemical groups over the differentiation fate of rat mesenchymal stem cells. We demonstrate that higher sulfonate-to-glucose ratios are associated with adipogenesis, while higher carboxylate-to-glucose ratios resulted in chondrogenic and osteogenic differentiation of the rat mesenchymal stem cells.

*Keywords:* Peptide nanofibers, extracellular matrix, glycosaminoglycans, biomimetic, mesenchymal stem cells.

# ÖZET

## PEPTİT NANOFİBERLER ÜZERİNDE SUNULAN KÜÇÜK FONKSİYONEL GRUPLARIN RAT MEZENKİMAL KÖK HÜCRELERİ KADERİNİN BELİRLENMESİ İÇİN KULLANILMASI

Öncay Yaşa

Malzeme Bilimi ve Nanoteknoloji Programı, Yüksek Lisans

Tez Yöneticisi: Yrd. Doç. Dr. Ayşe Begüm Tekinay

Aralık, 2014

Glikozaminoglikanlar çeşitli biyolojik olaylarda ve zarar görmüş dokuların yenilenmesinde önemli roller oynayan negatif yüklü, dallanmamış polisakkaritlerdir. Diğer doğal hücre dışı matris elemanları gibi, glikozaminoglikanlar ve proteoglikanlar da dokunun tipine göre yerel konsantrasyon ve kimyasal kompozisyon olarak dikkate değer değişiklikler göstermektedirler. Kemik, kırık ve yağ olmak üzere çeşitli bağ dokularında yer alırlar ve negatif yüklerinden dolayı güçlü su tutma özellikleri vardır. Sülfatlanma dereceleri ve motifleri glikozaminoglikanların mekanik özelliklerini etkileyip, viskoelastik ve fizyolojik fonksiyonlarını önemli derecede değiştirmektedir. Glikozaminoglikanların sülfatlanma motiflerindeki farklılıklar birincil olarak hücre dışı matris modelleme yöntemlerinden kaynaklanmaktadır. Hücre dışı matrisi organize edebilme özelliklerinden dolayı, glikozaminoglikanlar doku mühendisliği ve doku yenilenmesi uygulamalarında kullanılacak yeni biyoaktif malzemelerin geliştirilmesinde umut

vaat eden biyomakromoleküllerdir. Bu çalışmada, nanoipliksi yapıda ve farklı derecelerde kimyasal gruplar içeren ağlar geliştirebilmek adına peptit amfifil molekülleri karboksilat ve sülfonat gruplarıyla fonksiyonlandırılmış, ve elde edilen farklı derecelerde kimyasal gruplar içeren nanoipliksi iskelelerin rat mezenkimal kök hücrelerinde hücre farklılaşmasına olan etkileri araştırılmıştır. Yüksek sülfonat/glikoz oranının yağ doku farklılaşmasıyla, yüksek karboksilat/glikoz oranının ise kıkırdak doku farklılaşmasıyla bağlantılı olduğu rat mezenşim kök hücrelerinde gösterilmiştir.

*Anahtar Kelimeler:* Peptit nanofiberler, hücrelerarası iskele, glikozaminoglikanlar, biyomimetik, mezenkimal kök hücreler

## ACKNOWLEDGEMENTS

I would like to express the deepest appreciation to my advisor Prof. Ayşe Begüm Tekinay for her guidance and support. She always supported my scientific career and pushed me to perform at my best throughout my two years as a Master's student. She also contributed to my personal development and gave me a different perspective about social issues. I also would like to thank Prof. Mustafa Özgür Güler for his guidance and support to my research, without which this work could not have been completed.

I would like to indicate my greatest thanks and most sincere gratitude to my family. In my whole life, I have always felt the love and endless support of my family with me. They always show respect to my decisions and never turn their backs. I am proud of them and I feel very lucky to have such a family.

I would like to express my special thanks to İmmihan Ceren Garip. She was always with me either in good times or bad, and her supports has been invaluable. I can say that the times I spent with her until now were the greatest times of my life.

I would like to express my most sincere thanks to Yasin Tümtaş for his collaboration and friendship in different projects, which would not have been possible without his sincere efforts.

I learned many techniques from my colleagues. I am grateful for their kindness, as well as their contributions to my technical skills and view of science. All NBT and BML laboratory members were there for me when I needed help. It was great to meet, know and work with them. I would like to thank Elif Arslan, Nuray Gündüz, Didem Mumcuoğlu, Berna Şentürk, Melis Göktaş, Seher Yaylacı, Gülistan

Tansık, Gzde Uzunallı, Melike Sever, Glcihan Glseren, Mevhibe Geer, Elif Ergl, Bra Mammadov, Ahmet Emin Tolap, Alper Devrim zkan, mer Faruk Sarıođlu, Nalan Oya San, Giray Bulut, Emre Evin, Duygu Akgn, Melis Őardan and Ashif Shaikh for their support and friendship. I also would like to express my special thanks to Melis Őardan for her contribution to my work. I was lucky to be in such a warm working environment, and to work with such a wonderful friends.

Finally, I would like to thank the National Nanotechnology Research Center (UNAM) and Bilkent University for providing pleasant facilities and latest equipments for my research.

## TABLE OF CONTENTS

CHAPTER 1 .....	1
INTRODUCTION .....	1
1.1 AN OVERVIEW OF REGENERATIVE MEDICINE .....	2
1.1.1 PROGENITOR CELL OR STEM CELL TRANSPLANTATION.....	3
1.1.2 ARTIFICIAL TISSUE IMPLANTATION.....	4
1.1.3 INDUCTION OF REGENERATION BY INTRODUCING CHEMICALS INTO THE SITE OF INJURY.....	4
1.2 MESENCHYMAL STEM CELLS IN REGENERATIVE MEDICINE.....	7
1.2.1 THE DISCOVERY OF MESENCHYMAL STEM CELLS .....	7
1.2.2 ISOLATION OF MESENCHYMAL STEM CELLS .....	9
1.2.3 DIFFERENTIATION OF MESENCHYMAL STEM CELLS .....	9
1.3 EXTRACELLULAR MATRIX AND ITS COMPONENTS .....	10
1.4 NATURAL GLYCOSAMINOGLYCANS AND THEIR ROLES IN TISSUE REGENERATION .....	11
1.5 PEPTIDE AMPHIPHILE MOLECULES AND THEIR USE IN REGENERATIVE MEDICINE.....	16
1.6 MOTIVATION AND GOALS .....	19
CHAPTER 2 .....	20
EXPERIMENTAL .....	20
2.1 CHEMICALS AND SOLUTIONS.....	21
2.2 SYNTHESIS OF PEPTIDE AMPHIPHILE MOLECULES.....	22

2.3 CHARACTERIZATION OF THE SELF-ASSEMBLED PEPTIDE NANOSTRUCTURES.....	23
2.3.1 LIQUID CHROMATOGRAPHY-MASS SPECTROSCOPY.....	24
2.3.2 CIRCULAR DICHROISM .....	25
2.3.3 SCANNING ELECTRON MICROSCOPY .....	25
2.3.4 TRANSMISSION ELECTRON MICROSCOPY .....	26
2.4 PEPTIDE AMPHIPHILE NANOFIBER FORMATION .....	27
2.5 CELL CULTURE .....	27
2.5.1 CELL VIABILITY AND PROLIFERATION.....	28
2.5.2 ALIZARIN RED-S STAINING .....	29
2.5.3 SAFRANIN-O STAINING.....	30
2.5.4 OIL RED-O STAINING .....	31
2.5.5 PROTEIN AND ALKALINE PHOSPHATASE ACTIVITY ASSAYS .	32
2.5.6 QUANTITATIVE REAL-TIME GENE EXPRESSION ANALYSES....	33
2.6 STATISTICAL ANALYSIS.....	34
CHAPTER 3 .....	36
RESULTS AND DISCUSSIONS .....	36
3.1 SYNTHESIS AND CHARACTERIZATION OF PEPTIDE AMPHIPHILE MOLECULES.....	37
3.1.1 PURIFICATION OF THE PEPTIDE AMPHIPHILES WITH HIGH PRESSURE LIQUID CHROMATOGRAPHY .....	41
3.1.2 ANALYSES OF PURITY AND SIZE OF PEPTIDE AMPHIPHILES...	41
3.1.3 SECONDARY STRUCTURE DETERMINATION .....	42

3.1.4 MORPHOLOGICAL ANALYSIS OF PEPTIDE AMPHIPHILES.....	45
3.2 EFFECTS OF PEPTIDE NANOFIBER NETWORKS ON RAT MESENCHYMAL STEM CELLS .....	48
3.2.1 THE DESIGN OF 2D CELL CULTURE EXPERIMENTS .....	48
3.2.2 BIOCOMPATIBILITY OF PEPTIDE NANOFIBER NETWORKS.....	49
3.2.3 PROLIFERATION ANALYSIS OF RAT MESENCHYMAL STEM CELLS ON PEPTIDE NANOFIBER NETWORKS.....	50
3.3 INVESTIGATION OF THE DIFFERENTIATION OF RAT MESENCHYMAL STEM CELLS .....	54
3.3.1 ANALYSIS OF CALCIUM DEPOSITION AND MINERALIZATION	54
3.3.2 ALKALINE PHOSPHATASE ACTIVITY .....	64
3.3.3 EXPRESSION LEVELS OF OSTEOGENIC DIFFERENTIATION MARKERS .....	69
3.3.4 NEUTRAL TRIGLYCERIDE AND LIPID PRODUCTION ANALYSES .....	72
3.3.5 EXPRESSION LEVELS OF ADIPOGENIC DIFFERENTIATION MARKERS .....	73
3.3.6 SULFATED GLYCOSAMINOGLYCAN PRODUCTION ANALYSES .....	78
3.3.7 EXPRESSION LEVELS OF CHONDROGENIC DIFFERENTIATION MARKERS .....	83
CHAPTER 4 .....	85
CONCLUSION AND FUTURE PERSPECTIVES .....	85

BIBLIOGRAPHY ..... 88

## LIST OF FIGURES

- Figure 1.1** Chemical strategies for inducing differentiation. Differentiation *in vitro* is typically carried out in a stepwise manner that recapitulates normal embryonic development. Several strategies have been developed to increase the efficiency of differentiation towards a specific lineage: **(a)** inhibiting stem cell self-renewal by small molecules to accelerate or enhance the differentiation process; **(b)** directing cells into specific cell types by a combination of small molecules that induce desired lineage-specific mechanisms and inhibit the activity of pathways and genes that lead to the induction of undesired cell types; **(c)** promoting progenitor cell expansion by small molecules to generate a large population of intermediate cells for various applications; and **(d)** maturing terminally differentiated cells by small molecules to generate desired functional cells. ESC, embryonic stem cell; iPSC, induced pluripotent stem cell <sup>12</sup>. ..... 6
- Figure 1.2** Mesenchymal stem cells can give rise to osteocytes, hypertrophic chondrocytes and adipocytes, or self-renew to produce identical cells that may later differentiate toward lineages that form the skeleton and bone marrow stroma. Trans-differentiation of MSCs into other non-mesodermal cell types has been also reported *in vitro* but remains controversial *in vivo* <sup>25</sup>. ..... 8
- Figure 1.3** Chemical representations of the disaccharide units of glycosaminoglycans. **(A)** Chondroitin 4-sulfate, **(B)** Chondroitin 6-sulfate, **(C)** Dermatan sulfate, **(D)** Keratan sulfate, **(E)** Heparin, and **(F)** Hyaluronan. .... 12

<b>Figure 3.1</b> Chemical representations of peptide amphiphile molecules. (A) Glc-PA [Lauryl-VVAGKS(Glc)-Am], (B) SO <sub>3</sub> -PA [Lauryl-VVAGEK( <i>p</i> -sulfo benzoate)-Am], (C) E-PA [Lauryl-VVAGE], and (D) K-PA [Lauryl-VVAGK-Am]. .....	39
<b>Figure 3.2</b> Self-assembled nanofiber network systems used in this study. The peptide nanofiber networks self-assemble when mixed with oppositely charged peptide amphiphiles and were modified to incorporate chemical groups found in natural glycosaminoglycans. ....	40
<b>Figure 3.3</b> HPLC chromatogram of purified: (A) Glc-PA, (B) SO <sub>3</sub> -PA, (C) E-PA, and (D) K-PA K molecule at 220 nm.....	43
<b>Figure 3.4</b> Electrospray ionization mass spectra of: (A) Glc-PA, (B) SO <sub>3</sub> -PA, (C) E-PA, and (D) K-PA.....	44
<b>Figure 3.5</b> Circular dichroism (CD) spectra of peptide nanofibers used for the characterization of the secondary structures. CD results indicate that peptide amphiphile nanofibers show a characteristic β-sheet structure at physiological pH. ....	45
<b>Figure 3.6</b> Characterization of the peptide amphiphile nanofiber networks by using scanning electron microscopy. (A) Glc-PA/E-PA, (B) Glc-PA/SO <sub>3</sub> -PA, (C) Glc-PA/SO <sub>3</sub> -PA/E-PA and (D) K-PA/E-PA.....	46
<b>Figure 3.7</b> Characterization of the peptide amphiphile nanofiber networks by using transmission electron microscopy. (A) Glc-PA/E-PA, (B) Glc-PA/SO <sub>3</sub> -PA, (C) Glc-PA/SO <sub>3</sub> -PA/E-PA and (D) K-PA/E-PA.....	47
<b>Figure 3.8</b> Viability analyses of rat mesenchymal stem cells on different peptide nanofiber networks and uncoated tissue culture plate. AlamarBlue® was used to quantitatively determine the viability of rat mesenchymal stem cells at 24 h. One-way ANOVA with Tukey post test (95% confidence interval) was applied for	

analyzing the results, and no significant difference was found between each groups.  
..... 52

**Figure 3.9** Proliferation analyses of rat mesenchymal stem cells cultured with BrdU on different peptide nanofiber networks and uncoated tissue culture plate at day 3. One-way ANOVA with Tukey post test (95% confidence interval) was applied for analyzing the results and significant differences were expressed as (\*  $p < 0.05$ , \*\*  $p < 0.01$ , \*\*\*  $p < 0.001$ ). ..... 53

**Figure 3.10** Alizarin Red-S calcium staining of cells cultured with growth medium at day 7. (A) Glc-PA/E-PA, (B) Glc-PA/SO<sub>3</sub>-PA, (C) Glc-PA/SO<sub>3</sub>-PA/E-PA, (D) K-PA/E-PA, (E) TCP and (F) Quantitative analyses of Alizarin Red-S. One-way ANOVA with Tukey post test was applied to analyze the results and significant differences were expressed as (\*\*  $p < 0.01$  and \*\*\*  $p < 0.001$ ). (Scale bars = 200  $\mu\text{m}$ ) ..... 56

**Figure 3.11** Alizarin Red-S calcium staining of cells cultured with osteogenic medium at day 7. (A) Glc-PA/E-PA, (B) Glc-PA/SO<sub>3</sub>-PA, (C) Glc-PA/SO<sub>3</sub>-PA/E-PA, (D) K-PA/E-PA, (E) TCP and (F) Quantitative analyses of Alizarin Red-S. One-way ANOVA with Tukey post test was applied to analyze the results and significant differences were expressed as (\*  $p < 0.05$ , \*\*  $p < 0.01$  and \*\*\*  $p < 0.001$ ). (Scale bars = 200  $\mu\text{m}$ ) ..... 57

**Figure 3.12** Alizarin Red-S calcium staining of cells cultured with growth medium at day 14. (A) Glc-PA/E-PA, (B) Glc-PA/SO<sub>3</sub>-PA, (C) Glc-PA/SO<sub>3</sub>-PA/E-PA, (D) K-PA/E-PA, (E) TCP and (F) Quantitative analyses of Alizarin Red-S. One-way ANOVA with Tukey post test was applied to analyze the results and significant differences (\*\*) were expressed at  $p < 0.01$ . (Scale bars = 200  $\mu\text{m}$ ) ..... 58

**Figure 3.13** Alizarin Red-S calcium staining of cells cultured with osteogenic medium at day 14. (A) Glc-PA/E-PA, (B) Glc-PA/SO<sub>3</sub>-PA, (C) Glc-PA/SO<sub>3</sub>-PA/E-PA, (D) K-PA/E-PA, (E) TCP and (F) Quantitative analyses of Alizarin Red-S. One-way ANOVA with Tukey post test was applied to analyze the results and significant differences were expressed as (\* p<0.05 and \*\* p<0.01). (Scale bars = 200 μm)..... 59

**Figure 3.14** Alizarin Red-S calcium staining of growth medium without cells at day 7, conducted as a control for non-specific calcium deposition. (A) Glc-PA/E-PA, (B) Glc-PA/SO<sub>3</sub>-PA, (C) Glc-PA/SO<sub>3</sub>-PA/E-PA, (D) K-PA/E-PA and (E) TCP. (Scale bars = 200 μm) ..... 60

**Figure 3.15** Alizarin Red-S calcium staining of osteogenic differentiation medium without cells at day 7, conducted as a control for non-specific calcium deposition. (A) Glc-PA/E-PA, (B) Glc-PA/SO<sub>3</sub>-PA, (C) Glc-PA/SO<sub>3</sub>-PA/E-PA, (D) K-PA/E-PA and (E) TCP. (Scale bars = 200 μm)..... 61

**Figure 3.16** Alizarin Red-S calcium staining of growth medium without cells at day 14, conducted as a control for non-specific calcium deposition. (A) Glc-PA/E-PA, (B) Glc-PA/SO<sub>3</sub>-PA, (C) Glc-PA/SO<sub>3</sub>-PA/E-PA, (D) K-PA/E-PA and (E) TCP. (Scale bars = 200 μm) ..... 62

**Figure 3.17** Alizarin Red-S calcium staining of osteogenic differentiation medium without cells at day 14, conducted as a control for non-specific calcium deposition. (A) Glc-PA/E-PA, (B) Glc-PA/SO<sub>3</sub>-PA, (C) Glc-PA/SO<sub>3</sub>-PA/E-PA, (D) K-PA/E-PA and (E) TCP. (Scale bars = 200 μm)..... 63

**Figure 3.18** *p*-nitrophenol standard curve obtained by using known *p*-nitrophenol standards. The standard curve was used to analyze the ALP activities of the rMSCs. The slope of the best line was 0.0723. .... 66

**Figure 3.19** Alkaline phosphatase activity of rat mesenchymal stem cells at day 3. Different nanofiber networks were used to investigate the changes in ALP activity according to the bio-functionality of the microenvironment. ALP activity of the rMSCs roughly correspond to the lipid accumulation characteristics of these cells. One-way ANOVA with Tukey post test was applied to analyze the results and significant differences were expressed as (\*  $p < 0.05$ , \*\*  $p < 0.01$  and \*\*\*  $p < 0.001$ ).67

**Figure 3.20** Alkaline phosphatase activity of rat mesenchymal stem cells at day 7. Different nanofiber networks were used to investigate the changes in ALP activity according to the bio-functionality of the microenvironment. ALP activity of the rMSCs roughly correspond to the lipid accumulation characteristics of these cells. One-way ANOVA with Tukey post test was applied to analyze the results and significant differences were expressed as (\*  $p < 0.05$ , \*\*  $p < 0.01$  and \*\*\*  $p < 0.001$ ).68

**Figure 3.21** Gene expression analyses of rat mesenchymal stem cells cultured on various nanofiber networks and tissue culture plate with growth medium at day 7. (A) RUNX2 and (B) COL1. The expression level of each gene was normalized against TCP and GAPDH, the latter of which was used as internal control. .... 70

**Figure 3.22** Gene expression analyses of rat mesenchymal stem cells cultured on various nanofiber networks and tissue culture plate with growth medium at day 14. (A) RUNX2 and (B) COL1. The expression level of each gene was normalized against TCP and GAPDH, the latter of which was used as internal control. .... 70

**Figure 3.23** Gene expression analyses of rat mesenchymal stem cells cultured on various nanofiber networks and tissue culture plate with osteogenic differentiation medium at day 7. (A) RUNX2 and (B) COL1. The expression level of each gene was normalized against TCP and GAPDH, the latter of which was used as internal

control. One-way ANOVA with Tukey post test was applied to analyze the results and significant differences were expressed as (\*\* p<0.01 and \*\*\* p<0.001). ..... 71

**Figure 3.24** Gene expression analyses of rat mesenchymal stem cells cultured on various nanofiber networks and tissue culture plate with osteogenic differentiation medium at day 14. (A) RUNX2 and (B) COL1. The expression level of each gene was normalized against TCP and GAPDH, the latter of which was used as internal control. One-way ANOVA with Tukey post test was applied to analyze the results and significant differences were expressed as (\* p<0.05 and \*\* p<0.01). ..... 71

**Figure 3.25** Oil Red-O staining of cells in growth medium at day 7, showing the extent of lipid deposition. (A) Glc-PA/E-PA, (B) Glc-PA/SO<sub>3</sub>-PA, (C) Glc-PA/SO<sub>3</sub>-PA/E-PA, (D) K-PA/E-PA, (E) TCP and (F) Quantification of Oil Red O. One-way ANOVA with Tukey post test was applied to analyze the results and significant differences were expressed as (\* p<0.05 and \*\* p<0.01). (Scale bars = 200 μm)..... 75

**Figure 3.26** Oil Red-O staining of cells in growth medium at day 14, showing the extent of lipid deposition. (A) Glc-PA/E-PA, (B) Glc-PA/SO<sub>3</sub>-PA, (C) Glc-PA/SO<sub>3</sub>-PA/E-PA, (D) K-PA/E-PA, (E) TCP and (F) Quantification of Oil Red O. One-way ANOVA with Tukey post test was applied to analyze the results and significant differences were expressed as (\*\* p<0.01 and \*\*\* p<0.001). (Scale bars = 200 μm) ..... 76

**Figure 3.27** Gene expression analyses of rat mesenchymal stem cells cultured on various nanofiber networks and tissue culture plate with growth medium at day 7. (A) FABP4 and (B) ADIPOQ. The expression level of each gene was normalized against TCP and GAPDH, the latter of which was used as internal control. One-way

ANOVA with Tukey post test was applied to analyze the results and significant differences were expressed as (\*  $p < 0.05$  and \*\*  $p < 0.01$ ). ..... 77

**Figure 3.28** Gene expression analyses of rat mesenchymal stem cells cultured on various nanofiber networks and tissue culture plate with growth medium at day 14. (A) FABP4 and (B) ADIPOQ. The expression level of each gene was normalized against TCP and GAPDH, the latter of which was used as internal control. .... 77

**Figure 3.29** Safranin-O staining at day 7 for the analysis of sulfated glycosaminoglycan incorporation. Cells were cultured with growth medium. (A) Glc-PA/E-PA, (B) Glc-PA/SO<sub>3</sub>-PA, (C) Glc-PA/SO<sub>3</sub>-PA/E-PA, (D) K-PA/E-PA and (E) TCP. (Scale bars = 200  $\mu$ m) ..... 81

**Figure 3.30** Safranin-O staining at of cells in growth medium at day 7, showing the extent of sulfated glycosaminoglycan incorporation. (A) Glc-PA/E-PA, (B) Glc-PA/SO<sub>3</sub>-PA, (C) Glc-PA/SO<sub>3</sub>-PA/E-PA, (D) K-PA/E-PA and (E) TCP. (Scale bars = 200  $\mu$ m) ..... 82

**Figure 3.31** Gene expression analyses of rat mesenchymal stem cells cultured on various nanofiber networks and tissue culture plate with growth medium at day 7. (A) SOX9 and (B) COL2. The expression level of each gene was normalized against TCP and GAPDH, the latter of which was used as internal control. .... 84

**Figure 3.32** Gene expression analyses of rat mesenchymal stem cells cultured on various nanofiber networks and tissue culture plate with growth medium at day 14. (A) SOX9 and (B) COL2. The expression level of each gene was normalized against TCP and GAPDH, the latter of which was used as internal control. One-way ANOVA with Tukey post test was applied to analyze the results and significant differences were expressed as (\*  $p < 0.05$  and \*\*  $p < 0.01$ ). ..... 84

## LIST OF TABLES

<b>Table 1.1</b> The localization and primary functions of the natural glycosaminoglycans in the body.....	15
<b>Table 2.1</b> Sequences, molecular weights, and charges of the synthesized peptide amphiphile molecules.....	23
<b>Table 2.2</b> Primer sequences and annealing temperatures of runt-related transcription factor 2, collagen 1, transcription factor SOX-9, collagen 2, adiponectin and fatty acid binding protein 4 for rat mesenchymal stem cells.....	35

## LIST OF ABBREVIATIONS

<b>ECM</b>	:	Extracellular Matrix
<b>PA</b>	:	Peptide Amphiphile
<b>GAG</b>	:	Glycosaminoglycan
<b>DIEA</b>	:	<i>N,N</i> -diisopropylethylamine
<b>TFA</b>	:	Trifluoroacetic Acid
<b>TIS</b>	:	Triisopropylsilane
<b>DMF</b>	:	Dimethylformamide
<b>DCM</b>	:	Dichloromethane
<b>LC-MS</b>	:	Liquid Chromatography Mass Spectroscopy
<b>HPLC</b>	:	High Pressure Liquid Chromatography
<b>CD</b>	:	Circular Dichroism
<b>SEM</b>	:	Scanning Electron Microscopy
<b>TEM</b>	:	Transmission Electron Microscopy
<b>FBS</b>	:	Fetal Bovine Serum
<b>DMEM</b>	:	Dulbecco's Modified Eagle Medium
<b>PS</b>	:	Penicillin/Streptomycin
<b>BrdU</b>	:	Bromodeoxyuridine
<b>ALP</b>	:	Alkaline phosphatase
<b>ORO</b>	:	Oil Red O
<b>TCP</b>	:	Tissue Culture Plate
<b>rMSC</b>	:	Rat Mesenchymal Stem Cell

<b>GAPDH</b>	:	Glyceraldehyde 3-phosphate dehydrogenase
<b>COL1</b>	:	Collagen 1
<b>COL2</b>	:	Collagen 2
<b>RUNX2</b>	:	Runt-related Transcription Factor 2
<b>SOX9</b>	:	Transcription Factor SOX-9
<b>ADIPOQ</b>	:	Adiponectin
<b>FABP4</b>	:	Fatty Acid Binding Protein 4
<b>qRT-PCR</b>	:	Quantitative Real-Time Polymerase Chain Reaction
<b>GE</b>	:	Glc-PA/E-PA
<b>GS</b>	:	Glc-PA/SO <sub>3</sub> -PA
<b>GES</b>	:	Glc-PA/SO <sub>3</sub> -PA/E-PA
<b>KE</b>	:	K-PA/E-PA

## **CHAPTER 1**

### **INTRODUCTION**

## 1.1 AN OVERVIEW OF REGENERATIVE MEDICINE

Regenerative medicine researches aim to assist the natural tissue regeneration process, and employ a variety of approaches to repair, renew or replace tissues or organs that have lost their functionality due to traumatic injury, disease, age or hereditary defects <sup>1</sup>. The human body is a complex system, and its maintenance mechanisms include natural repair processes that operate at molecular, cellular and systemic levels to continuously regenerate lost tissue in healthy individuals. However, the body's natural capacity for regeneration may not be enough in cases of severe injury or chronic disease, necessitating external assistance to fully restore the functions of the damaged tissue. Regenerative medicine studies deal with the organizational complexity and functional diversity of the cells and their surroundings to recover and regenerate tissues following traumatic injury. Its success, therefore, depends on our ability to understand the cellular and molecular mechanisms of regeneration, and to transfer this information to facilitate the functional regeneration of damaged tissues with limited capacity for renewal. Three main approaches are used in regenerative medicine studies in order to regenerate damaged tissues or organs. These approaches are: **(1)** differentiated cell (progenitor cell) or stem cell transplantation either alone or as part of a biomaterial <sup>2-3</sup>, **(2)** artificial tissue implantation <sup>4</sup> and **(3)** induction of the regeneration by using chemicals at the sites of injuries <sup>5</sup>. These methods can be employed alone or in combination to overcome the engineering limitations of the bionic devices and the donor shortage inherent to organ transplants <sup>6</sup>.

The effectiveness of regenerative medicine hinges on its ability to mimic the microenvironment normally experienced by cells in their native tissues. This microenvironment typically contains at least one of these features:

1. The presence of the requisite bio-signals for cell attachment and migration;
2. The retention and presentation of biochemical factors;
3. A porous environment for the adequate diffusion of nutrients, and waste; and
4. Mechanical characteristics, such as rigidity or elasticity, that are naturally experienced by each cell type <sup>7</sup>.

#### **1.1.1 PROGENITOR CELL OR STEM CELL TRANSPLANTATION**

Cell transplantation is an attractive alternative to whole organ transplantation because (1) it allows early intervention in diseases, (2) it reduces the immunogenicity of transplantation and the risk of organ rejection, and (3) it eliminates the risk of proper donor finding. Cells used in transplantation studies should be easy to access and propagate, be pluripotent and not subject to immunorejection. Progenitor cells and stem cells show these properties, and therefore can be used in cell transplantation studies either alone or part of a biomaterial. There are two main types of stem cells, embryonic stem cells and adult stem cells. Embryonic stem cells are totipotent cells, *i.e.* they can differentiate into all three embryonic germ layers. Adult stem cells are multipotent cells, and have more limited differentiation potentials compared to embryonic stem cells. They can differentiate into mesodermal and non-mesodermal cell types <sup>8</sup>.

### **1.1.2 ARTIFICIAL TISSUE IMPLANTATION**

Artificial tissue implantation involves the development of biomimetic devices or functionalized platforms that can be used to replace areas of damaged tissue and provide a suitable environment for the survival and regeneration of the remaining cells. Various artificial tissue transplants have been developed for the replacement of several tissue types, using methods such as hydrogels or 3D bio-printing. For example, it was shown that a mixture of human liver precursor cells and two other cell types can form 3D structures called “liver buds”, which were able to form functional connections with natural blood vessels and perform liver-specific functions *in vivo* <sup>9</sup>. In another study, a complex 3D architecture with designed patterns was created by using pressure activated micro-syringe equipped with a fine-bore exit needle and used to constitute implantable bioartificial organs. It was demonstrated that cells remain viable and continue their biological functions in this platform because the microchannels present in the system provide an easy access to nutrients and facilitate the removal of waste materials <sup>10</sup>.

### **1.1.3 INDUCTION OF REGENERATION BY INTRODUCING CHEMICALS INTO THE SITE OF INJURY**

Small molecules can be used to induce regeneration directly at the site of injury. This method has several advantages compared to artificial tissue implantation and cell transplantation. First, these chemicals have physicochemically well-defined structures and can be synthesized in large quantities with little batch-to-batch

variation. In addition, most of these chemicals have the ability to penetrate the cells and modulate intracellular processes. Finally, being small molecules, they are relatively non-immunogenic compared to other regeneration strategies <sup>11</sup>.

It is well-demonstrated that small chemicals with the ability to target specific signaling pathways and/or proteins can be used for the manipulation of cell fate, state and function <sup>12</sup>. There are various strategies for efficient directed differentiation of the cells as shown in Figure 1.1. To illustrate; Noggin is a BMP4 inhibitor and SB431542 is a TGF $\beta$  receptor inhibitor, and the inhibition of BMP pathway and TGF $\beta$  pathway at the same time by using these molecules increased the efficiency of neural differentiation of a monolayer culture of human embryonic stem cells <sup>13</sup>. Pumorphamine which is an adenine derivative is another example for the small molecules used in regenerative medicine applications. It is used as an inducer of osteoblast formation from multipotent mesenchymal progenitor cells and lineage-committed preosteoblasts <sup>14</sup>.

The *in vivo* potential of small chemicals is also well-established. For instance, the 1,2-isoxazoles were shown to repair damaged heart tissue after infarction, activating a cardiac program in the Notch-activated epicardium-derived progenitor cells <sup>15</sup>. Finally, in another *in vivo* study, a compound named as P7C3 was shown to improve the survival of newly formed neurons from apoptotic cell death and promote neurogenesis in the subgranular zone of the hippocampal dentate gyrus, but did not affect neural stem cell differentiation <sup>16</sup>.

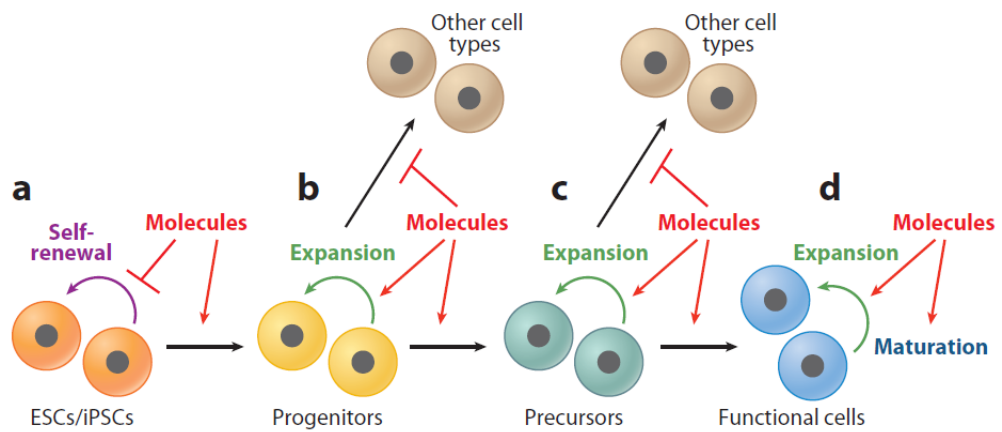


**Figure 1.1** Chemical strategies for inducing differentiation. Differentiation *in vitro* is typically carried out in a stepwise manner that recapitulates normal embryonic development. Several strategies have been developed to increase the efficiency of differentiation towards a specific lineage: **(a)** inhibiting stem cell self-renewal by small molecules to accelerate or enhance the differentiation process; **(b)** directing cells into specific cell types by a combination of small molecules that induce desired lineage-specific mechanisms and inhibit the activity of pathways and genes that lead to the induction of undesired cell types; **(c)** promoting progenitor cell expansion by small molecules to generate a large population of intermediate cells for various applications; and **(d)** maturing terminally differentiated cells by small molecules to generate desired functional cells. ESC, embryonic stem cell; iPSC, induced pluripotent stem cell <sup>12</sup>.

## 1.2 MESENCHYMAL STEM CELLS IN REGENERATIVE MEDICINE

Mesenchymal stem cells (MSCs), also known as multipotent marrow stromal cells or mesenchymal stromal cells, are stromal cells that have the ability to self-renew and/or differentiate into mesodermal (bone, adipose and cartilage) and non-mesodermal lineages (**Figure 2.1**)<sup>17-20</sup>. MSCs can be distinguished from other cell types due to their four intrinsic characteristics. (1) They show plastic adherent properties under standard culture conditions. (2) They express the surface markers CD73, CD90 and CD105. (3) They have a fibroblast-like morphology. (4) They lack the expression of the surface markers CD45, CD34, CD14 or CD11b, CD79a and HLA-DR<sup>21</sup>.

### 1.2.1 THE DISCOVERY OF MESENCHYMAL STEM CELLS

The presence of stem cells for non-hematopoietic cells in bone marrow was first recognized 130 years ago, by the observations of the German pathologist Cohnheim. In his research, Cohnheim suggested the possibility that bone marrow may be the source of fibroblasts, and that these fibroblasts initiate collagen fiber deposition as part of the normal wound repair process<sup>22</sup>.

Starting with the work of Friedenstein and colleagues, it was known that bone marrow contains cells that can differentiate into other mesenchymal cells, as well as developing into fibroblastic colony forming cells<sup>23</sup>. Ever since, these findings were also confirmed by numerous scientists and it was also demonstrated that these cells can also be found in the human bone marrow<sup>24</sup>.

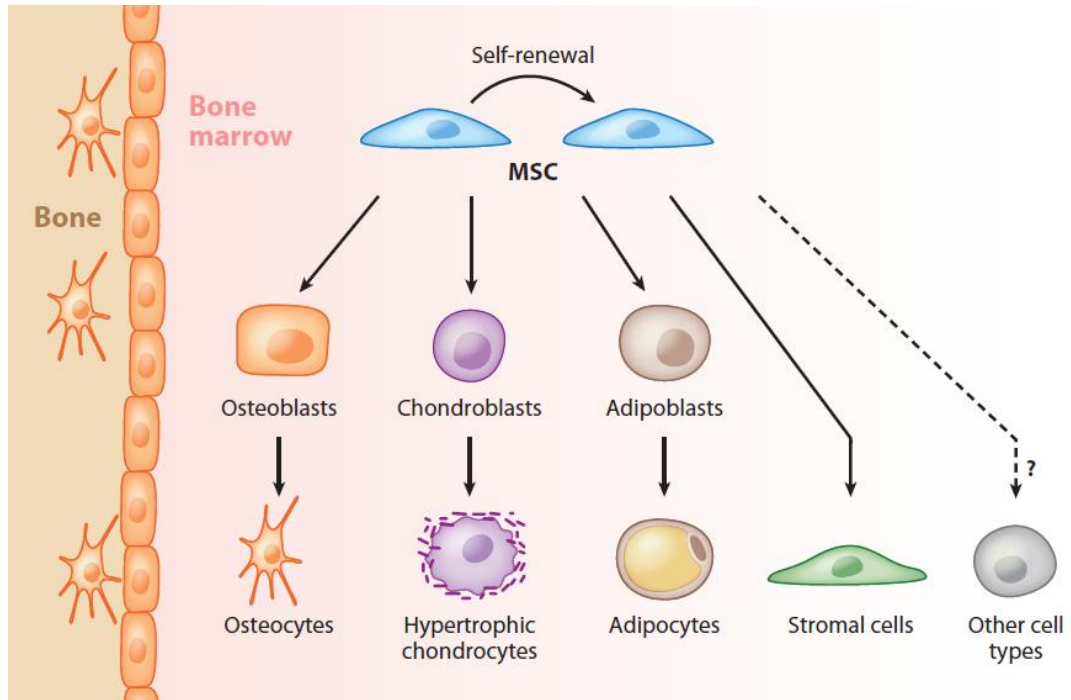


**Figure 1.2** Mesenchymal stem cells can give rise to osteocytes, hypertrophic chondrocytes and adipocytes, or self-renew to produce identical cells that may later differentiate toward lineages that form the skeleton and bone marrow stroma. Trans-differentiation of MSCs into other non-mesodermal cell types has been also reported *in vitro* but remains controversial *in vivo* <sup>25</sup>.

### **1.2.2 ISOLATION OF MESENCHYMAL STEM CELLS**

Mesenchymal stem cells can be isolated from many different sites of the body including the superior iliac crest of the pelvis in humans, the tibial and femoral marrow compartments and the thoracic and lumbar spine<sup>26-29</sup>. MSCs can be isolated and enriched with standard cell culture methods in which samples are fractionated on a density gradient and plating the isolated cells at densities from  $1.0 \times 10^4$  to  $0.4 \times 10^6$  cells/cm<sup>2</sup><sup>30</sup>.

### **1.2.3 DIFFERENTIATION OF MESENCHYMAL STEM CELLS**

It was demonstrated in many studies that MSCs can differentiate into bone, cartilage and fat tissues<sup>31-33</sup>.  $\beta$ -glycerophosphate, ascorbic acid-2-phosphate, dexamethasone and fetal bovine serum are required for the activation of osteogenic differentiation. When cultured with these supplements, mesenchymal stem cells increase their alkaline phosphatase activities and deposit a calcium-rich mineralized extracellular matrix, in addition to showing osteoblastic morphology. Chondrogenic differentiation of mesenchymal stem cells requires a three-dimensional culture configuration, a serum free nutrient medium and a member of the TGF- $\beta$  superfamily. In the presence of these factors, MSCs upregulate the expression of cartilage specific extracellular matrix components and start to lose their fibroblastic morphology. Adipogenic differentiation can be initiated by culturing MSCs in a monolayer culture in the presence of isobutylmethylxanthine, and confirmed visually by the formation of large lipid vacuoles in differentiating cells. Peroxisome

proliferator-activated receptor-gamma and fatty acid synthetase also play important roles in the induction of adipogenic differentiation in MSCs <sup>34</sup>.

### **1.3 EXTRACELLULAR MATRIX AND ITS COMPONENTS**

Extracellular matrix (ECM) is the material that surrounds the cells. It is paramount for cell-to-cell communication and the maintenance of tissue integrity. The ECM is highly complex and consists of a great variety of proteins, primarily in the form of proteoglycans, glycoproteins and long nanofibers. Natural extracellular matrix components provide structural and biochemical support for cells, and direct cellular behaviors such as adhesion, migration, proliferation, and differentiation. The extracellular matrix microenvironment therefore has an indispensable role for the survival and the regeneration of the cells. The composition, topology and physicochemical characteristics of the extracellular matrix show differences according to cell and tissue types, wound- and disease-states, and age. In addition to these, the ECM has a very dynamic structure even within a single type of tissue, as it is constantly being remodeled by enzymatic and non-enzymatic processes <sup>35</sup>. Extracellular matrix receptors, such as integrins and syndecans, take roles in the adhesion of the cells <sup>36-37</sup>. The adhesion of the cells to the ECM triggers cytoskeletal changes and can facilitate the migration of these cells through the ECM <sup>38</sup>. Collagens, elastins, fibronectins and laminins are the main fibrous extracellular matrix proteins <sup>39</sup>. From these fibrous proteins, collagen is the most abundant one found in the extracellular matrix and it gives tensile strength, helps cell adhesion and support migration and chemotaxis <sup>40</sup>. Collagens are defined by the triple helical

organization of component pro- $\alpha$ -chains that is formed as a result of the glycine amino acid being used in every third residue. There are now 28 known collagen types<sup>41</sup>. Fibronectin takes roles in extracellular matrix organization, cell attachment and function<sup>42</sup>. Fibronectin also has important functions in cell migration during embryonic development, tumor metastasis and cardiovascular disease<sup>43</sup>. Mechanical and biochemical changes in the extracellular matrix are perceived and acted upon by the cells through the crosstalk between integrins and the actin cytoskeleton<sup>44</sup>.

#### **1.4 NATURAL GLYCOSAMINOGLYCANS AND THEIR ROLES IN TISSUE REGENERATION**

Glycosaminoglycans (GAGs) are highly polar, negatively charged, unbranched polysaccharides which play important roles in various biological processes, and are vital for the regeneration of damaged tissues. They have extremely heterogeneous and complex structures due to degree of substitution and positioning of sulfate/sulfonate and acetyl groups<sup>45</sup>. GAGs are mainly composed of repeating disaccharide units (**Figure 1**). The repeating disaccharide unit always contains an amino sugar; either *N*-acetylglucosamine or *N*-acetylgalactosamine, along with a uronic acid, usually D-glucuronic or L-iduronic acid<sup>46</sup>. GAGs can be classified into four basic groups according to their repeating disaccharide structures and functions in the body. These four basic groups are: (1) Heparin/Heparan sulfate, (2) Chondroitin sulfate/Dermatan sulfate, (3) Keratan sulfate, and (4) Hyaluronic acid/Hyaluronan<sup>47</sup>. Except for hyaluronan, they contain sulfate/sulfonate groups, form proteoglycans by substituting protein cores, and are synthesized in the

endoplasmic reticulum and Golgi bodies<sup>48</sup>. GAGs have diverse intracellular and extracellular actions, and play crucial roles in different biological processes (**Table 1**) including growth, proliferation and differentiation of the cells, regeneration of nerve, cartilage and bone tissues, angiogenesis, and tumor metastasis through specific interactions with growth factors, growth factor receptors, extracellular matrix proteins, and other chemokines<sup>49-54</sup>.

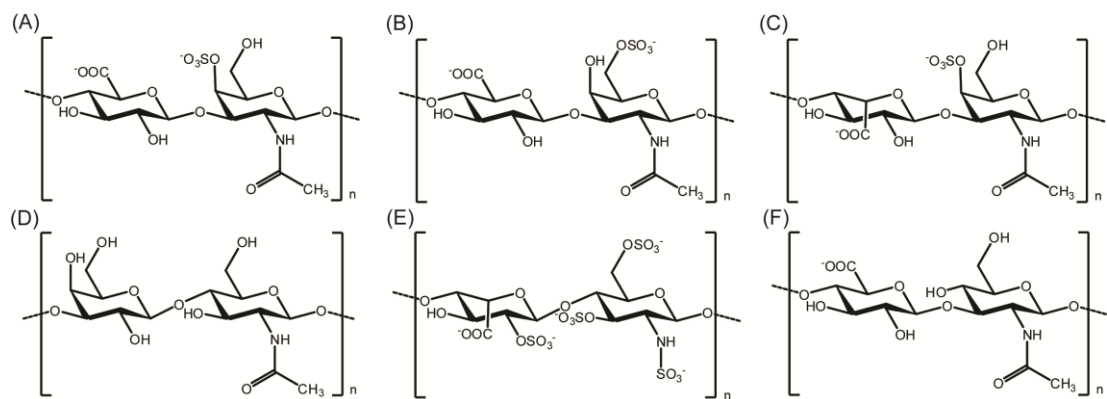


**Figure 1.3** Chemical representations of the disaccharide units of glycosaminoglycans. **(A)** Chondroitin 4-sulfate, **(B)** Chondroitin 6-sulfate, **(C)** Dermatan sulfate, **(D)** Keratan sulfate, **(E)** Heparin, and **(F)** Hyaluronan.

Hyaluronan (HA), which is composed of alternating units of  $\beta$ -1,4-linked D-glucuronic acid- $\beta$ -1,3-N-acetyl-D-glucosamine, is the only non-sulfated glycosaminoglycan<sup>55</sup>. Unlike other glycosaminoglycans, it is synthesized in the plasma membrane and its primary structure does not contain a peptide component<sup>48</sup>. It especially forms the extracellular matrix of soft connective tissues, and interactions between hyaluronan receptor and extracellular polysaccharides have effects on

locomotion and cell migration <sup>56</sup>. HA also has important biological functions in wound healing and remodeling, and serves to initiate inflammatory responses, maintain structural cell integrity and promote recovery from tissue injuries <sup>57</sup>.

Chondroitin sulfate (CS) is composed of  $\beta$ -1,3-linked D-glucuronic acid- $\beta$ -1,4-*N*-acetyl-D-galactosamine. CS is a sulfated glycosaminoglycan commonly found in the cartilage extracellular matrix, where it serves to increase the resistance of this tissue against frictional and compressive stress <sup>58-60</sup>. The CS disaccharides are sulfated on either C-4 or C-6 position of the *N*-acetyl-D-galactosamine residues and classified according to their sulfation patterns <sup>61</sup>. Besides cartilage extracellular matrix, it is also the major element of the brain extracellular matrix and takes roles in plasticity, neural development, and regeneration. In adults, chondroitin sulfate proteoglycans also play roles in learning and memory processes <sup>62</sup>.

Dermatan sulfate (DS) is another natural and sulfated glycosaminoglycan. DS is composed of  $\beta$ -1,3-linked L-iduronic acid- $\beta$ -1,4-*N*-acetyl-D-galactosamine units and is also known as chondroitin sulfate B <sup>63</sup>. In the cornea, it plays a crucial role in optical clarity by regulating fibril spacing <sup>64</sup>. It also has roles in bone metabolism in pathological conditions by regulating osteoclast formation through interaction with receptor activator of NF- $\kappa$ B ligand and inhibition of signal transduction in osteoclast progenitor cells <sup>65</sup>. DS can selectively inhibit thrombin without interfering with platelets. Therefore, it can also be used as anticoagulant for patients with acute renal failure after a major cardiovascular surgery <sup>66</sup>.

Heparan sulfate (HS) is composed of alternating units of  $\alpha$ -D-glucosamine and uronic acid, either  $\beta$ -D-glucuronic acid or  $\alpha$ -L-iduronic acid, and linked by 1,4 glycosidic bond. The  $\alpha$ -D-glucosamine can be either N-sulfated or N-acetylated <sup>67</sup>.

Bearing one of the highest natural complexities among glycosaminoglycans, HS performs a wide range of biological activities including roles in blood coating, angiogenesis, and the protection of proteins from degradation<sup>68</sup>. It also takes role in regulation of bone morphogenetic proteins' activities and induction of morphogenesis. For instance, cell surface heparan sulfate proteoglycans can intercede BMP-2 internalization and it was shown that these heparan sulfate supramolecules lead to transdifferentiation of C2C12 myoblasts into osteoblasts through direct regulation of BMP-2 activities<sup>69</sup>.

Keratan sulfate (KS) is composed of  $\beta$ -1,3-linked D-galactose- $\beta$ -1,4-*N*-acetyl-D-glucosamine units and sulfated on C-6 of either or both hexose moieties<sup>70</sup>. KS is associated with a vast variety of biological functions in different tissue types and developmental stages. It is mainly found in cornea, cartilage, and brain. It is the major GAG in cornea and takes role in corneal hydration and maintenance of ECM structure<sup>71</sup>. Due to its highly hydrated nature, KS suppresses cartilage damage in joints and exogenous KS application can be used for treatment of inflammatory arthritis<sup>72</sup>. KS is also synthesized in central nervous system and takes an important role in modulating axonal growth after spinal cord injury<sup>73</sup>.

In the extracellular matrices of all mammalian tissues, GAGs are found covalently attached to proteins, and classified as proteoglycans except for hyaluronan<sup>74</sup>. Proteoglycans are classified according to their GAG composition, localization and core proteins. Their molecular sizes, abundances, and sulfation and acetylation patterns change based on tissue types and developmental stages. Proteoglycans can be separated into three main families which are small leucine-rich proteoglycans, modular proteoglycans and cell-surface proteoglycans<sup>75</sup>. Small leucine-rich

proteoglycans take roles in various signaling pathways and regulation of inflammatory response reactions. To illustrate, they can bind to and activate epidermal growth factor receptor, insulin-like growth factor 1 receptor, and TGF- $\beta$ <sup>76-77</sup>. Modular proteoglycans take roles in mainly cell adhesion, migration and proliferation. Cell-surface proteoglycans can act as co-receptors facilitating ligand encounters with signaling receptors<sup>35</sup>.

**Table 1.1** The localization and primary functions of the natural glycosaminoglycans in the body.

<b>Glycosaminoglycan</b>	<b>Localization</b>	<b>Functions</b>	<b>References</b>
Heparin/Heparan sulfate	basement membranes, mast cells, lung, liver and skin	takes roles in the allergic and inflammatory reactions driven by mast cells functions as an anticoagulant primarily through activation of AT-mediated inhibition of blood coagulation factors	78-79
Chondroitin sulfate/Dermatan sulfate	cartilage, bone, skin, blood vessels, heart valves, tendons, lung	provides resistance to compression take roles in coagulation, infection, wound repair, and fibrosis	60,63
Keratan sulfate	cornea, bone, cartilage	takes roles in the cellular recognition of protein ligands, axonal guidance, cell motility and in embryo implantation	70
Hyaluronic acid/Hyaluronan	synovial fluid, articular cartilage, skin	have functions in joints lubricate and protect cartilage surfaces prevent capillary growth	80

## 1.5 PEPTIDE AMPHIPHILE MOLECULES AND THEIR USE IN REGENERATIVE MEDICINE

Peptide amphiphiles (PAs) are peptide-based molecules that can self-assemble into high-aspect ratio nanofibers. A typical peptide amphiphile macromolecule consists of four main regions. The hydrophobic domain that consists of a long alkyl tail forms the first region. A short peptide sequence which takes role in the formation of intermolecular hydrogen bonds forms the second region. The third region is formed from charged amino acids to enhance solubility of the macromolecule in water and to design pH and salt-responsive nanostructures and networks. The fourth region contains bioactive signals that is usually designed by mimicking epitopes and used for providing special signals that take roles in nanostructure-cell interactions and differentiation of the cells <sup>81</sup>.

The amphiphilic nature of the peptide amphiphile molecules comes from the incorporation of a hydrophobic alkyl tail after the peptide sequence. This hydrophobic alkyl tail that forms the first region of the macromolecules as previously mentioned allows the presentation of peptide signals specifically on the periphery of self-assembled nanostructures. The hydrophobic tails can also be adjusted by using different alkyl chain lengths or by using different hydrophobic components <sup>82</sup>. The short peptide sequence that forms the second region of the macromolecules usually consists of hydrophobic amino acids. This short peptide sequence allows formation of intermolecular hydrogen bonds generally in the form of  $\beta$ -sheets and leads for the presentation of bioactive signals on the nanofiber surface at a high density. Charged amino acids that form the third region of a peptide amphiphile molecule come after

the short peptide sequences and their number and identity determine the solubility of the peptide amphiphile molecules under physiological conditions. The bioactive peptide sequence formed by mimicking various epitopes constitutes the last and the most important region of the peptide amphiphile molecules if they will be used in a biological study. This region may consist of different biological signals such as one that promotes cell adhesion<sup>83-84</sup> or one that generates a pronounced therapeutic effect<sup>85-86</sup>.

Peptide amphiphile molecules were first presented approximately a decade ago as a regenerative tool for bio-mineralization. In this study, it was shown that peptide nanofibers with phosphoserine residues self-assembled into nanofibers that can nucleate thin hydroxyapatite crystals on their surfaces *in vitro* as observed in bone formation<sup>87</sup>. The importance of phosphoserine residue for nucleation of hydroxyapatite was also proved *in vivo* using an orthotopic rat femoral critical-size defect model. In this study performed by Mata *et al.*, the combined effects of fibronectin epitope RGDS and the phosphoserine residues on bone regeneration were determined by the analysis of hydroxyapatite nucleation, and it was concluded that the presence of phosphoserine residues on the peptide nanofibers enhances formation of biomimetic bone crystals<sup>88</sup>.

Recently, various peptide amphiphile nanofibers that contain bioactive signals have been used to mimic natural sulfated glycosaminoglycans and to constitute a suitable microenvironment for the survival and differentiation of the osteogenic cells. In one study, a heparin-mimetic peptide amphiphile scaffold system was used to analyze osteogenic differentiation of Saos-2 cells. The BMP-2 binding capacity of these heparin-mimetic peptide scaffold was shown by using an ELISA based growth

factor binding assay. The nanofiber scaffold showed osteoinductive properties by stabilizing BMP-2 and providing a convenient microenvironment for bone regeneration with their sulfonate and carboxylate groups. These nanofiber networks also enhance the viability, proliferation and mineralization of the osteogenic cells by binding to BMP-2 <sup>89</sup>.

Ustun *et al.* used heparin mimetic PA macromolecule to analyze differentiation of chondroprogenitor ATDC5 cells. Heparin mimetic peptide scaffold was found to give both structural and functional assistance for the cells, causing rapid aggregation of the cells in insulin-free medium, which culminate in the formation of cartilage-like nodules. The sulfated glycosaminoglycan deposition was shown with Safranin-O staining, and the bioactive role of the nanofiber system was also revealed with qRT-PCR which was used to show expression levels of collagen II and aggrecan genes <sup>90</sup>.

In a different study, the effect of heparin-mimetic PA on neurite outgrowth was analyzed in combination with laminin-derived PA. It was revealed that hydrogels composed of self-assembly of a laminin-derived PA and heparin mimetic PA increase the efficiency of the neurite outgrowth compared to laminin-derived PAs alone. It was also revealed that the inhibitory effect of chondroitin sulfate proteoglycans on the central nervous system can be overcome by using this scaffold <sup>91</sup>.

## 1.6 MOTIVATION AND GOALS

Despite vast advancements in biology and its sub-disciplines, it is still not possible to fully mimic sophisticated biological materials in either form or function. As such, regenerative medicine often aims to partially replicate the effect of biological structures by identifying and utilizing functional regions that contain crucial biological signals. Peptide amphiphile macromolecules allow direct incorporation of these functional regions into their primary sequences. By using peptide amphiphile molecules, nanostructures with high aspect ratios, complex architectures and desired biochemical characteristics can be easily produced under physiological conditions. These peptide nanostructures can then be used in various regenerative medicine applications, where they are expected to enhance the natural regeneration process due to their resemblances to the native microenvironments of their target tissues.

It was previously shown that synthetic matrices containing small-molecule chemical functional groups can be used for controlled induction of differentiation to multiple mesenchymal stem cell lineages<sup>92</sup>. In this study, peptide amphiphile molecules modified with different small functional groups were used to determine the effect of GAG composition on rat mesenchymal stem cell fate. Our hypothesis was that the functions of natural glycosaminoglycans can be mimicked using a combination of various small functional groups; and we tested this hypothesis under *in vitro* conditions by investigating the differentiation tendency of rat mesenchymal stem cells over functionalized bioactive nanofibrous networks towards mesodermal lineages.

## **CHAPTER 2**

## **EXPERIMENTAL**

## 2.1 CHEMICALS AND SOLUTIONS

### *Solid State Peptide Synthesis Reagents:*

9-Fluorenylmethoxycarbonyl (Fmoc) and *tert*-butoxycarbonyl (Boc) protected amino acids except glyco amino acid, [4-[ $\alpha$ -(2',4'-dimethoxyphenyl) Fmoc-aminomethyl]phenoxy] acetamidonorleucyl-MBHA resin (Rink amide MBHA resin), Fmoc-Glu(OtBu)-Wang resin, and 2-(1*H*-Benzotriazol-1-yl)-1,1,3,3-tetramethyluronium hexafluoro-phosphate (HBTU) were purchased from NovaBiochem and ABCR. Fmoc-Ser[ $\beta$ -Glc(OAc)<sub>4</sub>]-OH was purchased from AAPPTec. *N,N*-diisopropylethylamine (DIEA) and lauric acid were purchased from Merck. Piperidine, acetic anhydride, dichloromethane (DCM), dimethylformamide (DMF), trifluoroacetic acid (TFA) and triisopropylsilane (TIS) were purchased from Sigma-Aldrich. The remaining chemicals were purchased from Fisher and/or Alfa Aesar; all chemicals were used as provided. Deionized water with a resistance of 18 M $\Omega$ .cm (Millipore Milli-Q) was used in all experiments.

### *Cell Culture Reagents:*

Dulbecco's Modified Eagle Medium (DMEM), Penicillin/Streptomycin (PS) antibiotic combination and Fetal Bovine Serum (FBS) were purchased from Gibco, Life Technologies. Alamar Blue was purchased from Invitrogen. BrdU (colorimetric) was purchased from Roche. Safranin-O, Oil Red-O and Alizarin Red-S were purchased from Sigma-Aldrich.

## 2.2 SYNTHESIS OF PEPTIDE AMPHIPHILE MOLECULES

Peptide amphiphile molecules were synthesized by using a standard solid phase peptide synthesis method with Rink amide MBHA resin or glutamic acid loaded Wang resin. GLC-PA [Lauryl-VVAGKS(Glc)-NH<sub>2</sub>], SO<sub>3</sub>-PA [Lauryl-VVAGEK(*p*-sulfobenzoate)-NH<sub>2</sub>] and K-PA [Lauryl-VVAGK-NH<sub>2</sub>] were synthesized on Rink amide MBHA resin. E-PA [Lauryl-VVAGE] was synthesized on Fmoc-Glu-Wang resin. Prior to the first coupling reaction, the resins were swelled in DCM for 30 min and the solvent was exchanged to DMF, in which all remaining reactions were carried out. In the synthesis of every peptide amphiphile molecules, the solid state was washed three times with DMF, three times with DCM and finally again three times with DMF respectively between each step to remove unreacted chemicals. Each coupling reaction started with the removal of the Fmoc protecting group by using 20% (v/v) piperidine/dimethylformamide solution for 20 min. Amino acids were then prepared for the coupling reaction by dissolving in DMF and amino acid coupling reactions were performed by using 2 equivalents of amino acid, 1.95 equivalents of HBTU and 3 equivalents of DIEA in 10 mL DMF for 2.5 h. At the end of each coupling step, the completeness of the coupling reaction was determined with Kaiser test. If the reaction was complete, the amino acid chain was exposed to 10% (v/v) acetic anhydride/dimethylformamide solution for 30 min in order to acetylate unreacted amine groups prior to the next coupling cycle. These steps were repeated until the desired amino acid sequences were obtained (Table 2.1). The lauric acid tail was then added in a similar fashion to the amino acid coupling reaction, except that the coupling time was 4 h. After the synthesis procedure, peptide cleavage from the

solid phase was carried out for 2 h at room temperature with 95% cleavage cocktail (95:2.5:2.5 TFA:TIS:ddH<sub>2</sub>O) and excess TFA and DCM were subsequently removed with rotary evaporator. The remaining peptide amphiphile solution was then precipitated using overnight incubation in ice cold diethyl ether at -20 °C. The solution was then centrifuged at 8000 rpm for 15 min to completely precipitate peptide amphiphile molecules; diethyl ether was then decanted and the remainder in the flask was evaporated, and the peptide amphiphile molecules were dissolved with ddH<sub>2</sub>O. Finally, the peptide amphiphile solution was frozen at -80 °C for 4 h, lyophilized for 3 days and stored at -20 °C.

**Table 2.1** Sequences, molecular weights, and charges of the synthesized peptide amphiphile molecules.

Name	Sequence	Molecular Weight	Charge
GLC-PA	Lauryl-VVAGKS(Glc)-Am	903.12	+1
SO <sub>3</sub> -PA	Lauryl-VVAGEK( <i>p</i> -sulfobenzoate)-Am	967.18	-2
K-PA	Lauryl-VVAGK-Am	653.90	+1
E-PA	Lauryl-VVAGE	655.82	-2

### 2.3 CHARACTERIZATION OF THE SELF-ASSEMBLED PEPTIDE NANOSTRUCTURES

High Pressure Liquid Chromatography (HPLC) was used to purify the synthesized peptide amphiphile molecules, while Liquid Chromatography-Mass

Spectroscopy (LC-MS), Circular Dichroism (CD), Scanning Electron Microscopy (SEM) and Transmission Electron Microscopy (TEM) were used to perform chemical and mechanical characterizations of peptide amphiphile molecules.

### **2.3.1 LIQUID CHROMATOGRAPHY-MASS SPECTROSCOPY**

A quadruple time of flight (Q-TOF) mass spectrometer with electrospray ionization (ESI) source equipped with a reverse phase analytical high performance liquid chromatography was used to characterize the synthesized peptide amphiphile molecules. For the characterization of negatively and positively charged PA molecules, Agilent Zorbax Extend-C18 (2.1 x 50 mm) column and Zorbax SB-C8 (4.6 x 100 mm) column were used as stationary phases respectively. A gradient of water (0.1% formic acid or 0.1% NH<sub>4</sub>OH) and acetonitrile (0.1% formic acid or 0.1% NH<sub>4</sub>OH) was used as mobile phase during liquid chromatography.

#### *High Pressure Liquid Chromatography:*

Reverse phase preparative HPLC equipped with either Zorbax Extend-C18 (21.2 x 150 mm) column or Zorbax SB-C8 (21.2 x 150 mm) column as a stationary phase were used to purify negatively and positively charged PA molecules, respectively. A gradient of water (0.1% acetonitrile or 0.1% NH<sub>4</sub>OH) and acetonitrile (0.1% formic acid or 0.1% NH<sub>4</sub>OH) were used as a mobile phase during HPLC purification of the synthesized PA molecules. Furthermore; according to their synthesis purity, positively charged PA molecules were only treated with 0.1 M HCl

solution in dialysis bags, in which the remaining TFA removed through chloride ion exchange.

### **2.3.2 CIRCULAR DICHROISM**

Circular dichroism analyses were performed by using a J-815 Jasco spectrophotometer in the far ultra-violet region. PA molecules were prepared and used at a final concentration of 200  $\mu\text{M}$  during all analysis. Quartz cuvette with 1 mm pathlength was used for all measurements. Measurement parameters were selected as: digital integration time of 1 sec, band width of 1 nm, data pitch of 0.1 nm, and with standard sensitivity. The scanning results were the average of three readings in a spectral range between 190 nm and 300 nm. Following scanning, ellipticity data obtained from the measurements were converted to molar ellipticity (with the unit  $\text{degree}\cdot\text{cm}^2\cdot\text{mole}^{-1}$ ) using the following formula:

$$[\theta] = \frac{100 \times \theta}{(C \times l)}$$

$[\theta]$ : Molar ellipticity,  $\theta$ : Ellipticity, C: Concentration in Molar, l: Length in cm

### **2.3.3 SCANNING ELECTRON MICROSCOPY**

Scanning electron microscopy samples were prepared by mixing 10 mM Glc-PA and 10 mM E-PA at 1:1 ratio, 10 mM Glc-PA and 10 mM  $\text{SO}_3$ -PA at 1:1 ratio, 10 mM Glc-PA, 10 mM  $\text{SO}_3$ -PA and 10 mM E-PA at 2:1:1 ratio, and finally 10 mM

K-PA and 10 mM E-PA at 1:1 ratio to have overall negatively charged hydrogels. Hydrogels were placed onto silicon wafers and incubated for 30 minutes before applying serial ethanol dehydration protocol. Hydrogels were dehydrated sequentially in 20% (v/v), 40% (v/v), 60% (v/v), 80% (v/v) and absolute ethanol, and subsequently dried by using a critical point dryer (Tousimis, Autosamdri-815B, Series C critical point dryer). Finally, samples were coated with 5 nm Au/Pd and analyzed by using a SEM (SEM, FEI Quanta 200 FEG) with an ETD detector at high vacuum mode at 10 keV beam energy.

#### **2.3.4 TRANSMISSION ELECTRON MICROSCOPY**

Lacey mesh ultrathin carbon coated copper grids were used for transmission electron microscopy analysis. TEM samples were prepared by mixing 2 mM Glc-PA and 2 mM E-PA at 1:1 ratio, 2 mM Glc-PA and 2 mM SO<sub>3</sub>-PA at 1:1 ratio, 2 mM Glc-PA, 2 mM SO<sub>3</sub>-PA and 2 mM E-PA at 2:1:1 ratio, and finally 2 mM K-PA and 2 mM E-PA at 1:1 ratio to have overall negatively charged hydrogels. The upper parts of grids were dipped for 1 min into samples that were previously diluted 100 times with distilled water; the grids were then stained with 2 wt% uranyl acetate for 40 seconds and kept in a fume hood until a dried film was obtained. Finally; samples were kept in a fume hood until a dried film was obtained, and analyzed by using a FEI Tecnai G2 F30 transmission electron microscope. STEM images were also obtained with a FEI Tecnai G2 F30 TEM working at HAADF mode. All TEM and STEM images were acquired at 300 kV.

## **2.4 PEPTIDE AMPHIPHILE NANOFIBER FORMATION**

Peptide amphiphile nanofibers were formed by mixing different combinations of positively (Glc-PA and K-PA) and negatively (SO<sub>3</sub>-PA and E-PA) charged PA molecules at neutral pH. In this study, four different PA nanofiber network systems were used and these nanofiber networks were prepared by mixing: **1)** 2 mM Glc-PA and 2 mM E-PA at a 1:1 ratio, **2)** 2 mM Glc-PA and 2 mM SO<sub>3</sub>-PA at a 1:1 ratio, **3)** 2 mM Glc-PA, 2 mM SO<sub>3</sub>-PA and 2 mM E-PA at a 2:1:1 ratio, respectively, and finally **4)** 2 mM K-PA and 2 mM E-PA at a 1:1 ratio. The overall charges of the PA nanofiber networks were negative. All peptide amphiphile solutions were sterilized for 30 min under UV light shortly after they were prepared. Before the formation of nanofiber networks, pH of the peptide amphiphile solutions were checked by using pH-indicator strips and adjusted to neutral pH with NaOH or HCl. Finally, the solutions were sonicated for 30 min and mixed as above mentioned.

## **2.5 CELL CULTURE**

Cell culture experiments were performed by using rat mesenchymal stem cells. Cells were incubated at 37 °C in a humidified atmosphere supplied with 5% CO<sub>2</sub>. Cell maintenance was done in low glucose DMEM (Dulbecco's modified eagle's medium) supplemented with 10% (v/v) Fetal Bovine Serum (FBS) and 1% (v/v) Penicillin/Streptomycin (PS). Cell culture was performed in 75 cm<sup>2</sup> flasks and cells were seeded in these flasks as 3 x 10<sup>3</sup> cells/cm<sup>2</sup>. Cell medium was replenished every 3 days and the cells were used in experiments or subcultured when they

reached ~90% confluency. Osteogenic differentiation medium was used in mineralization experiments including Alizarin Red-S staining and alkaline phosphatase activity assay. The growth medium of cells was changed to osteogenic medium after the cells reached ~90% confluency. Osteogenic medium contains low glucose DMEM, 10% (v/v) FBS and 1% (v/v) Penicillin/Streptomycin supplemented with 10 mM  $\beta$ -glycerophosphate, 50  $\mu$ g/mL ascorbic acid and 10 nM dexamethasone.

In order to perform 2D cell culture experiments, well plates were coated with peptide amphiphile nanofiber networks which were formed as previously mentioned. Then, the well plates were incubated at 37 °C for 30 minutes and dried in a biological safety cabinet. After overnight drying, peptide coated well plates were additionally sterilized with ultraviolet light for 30 minutes and cells were seeded in different amounts according to the experiments.

### **2.5.1 CELL VIABILITY AND PROLIFERATION**

Cell viability and proliferation analyses were performed by seeding rMSCs onto PA-coated and uncoated wells (TCP). 96-well plates were used for all analyses and cells were seeded at a density of  $5 \times 10^3$  cells/well. rMSCs were seeded in low glucose DMEM supplemented with 10% (v/v) FBS and 1% (v/v) Penicillin/Streptomycin under conditions of 5% CO<sub>2</sub> at 37 °C in a humidified chamber.

Biocompatibilities of peptide amphiphile nanofiber networks were evaluated by using Alamar Blue assay (Invitrogen) at 24 h. At the end of 24 h, medium was

discarded and cells were washed with phosphate buffered saline (PBS). Then, cells were incubated with 10% (v/v) Alamar Blue in serum free media for 4 h. Absorbance at 570/600 nm excitation/emission was measured with a microplate reader (Molecular Devices Spectramax M5). Absorbance values that were showing the viability of the cells were normalized to uncoated wells.

The proliferation of the rMSCs on peptide amphiphile nanofiber networks was evaluated by using BrdU (colorimetric) at 72 h. At the end of 70 h, medium was discarded and then cells were incubated with standard cell culture medium supplemented with 100  $\mu$ M BrdU labeling solution for 2 h. At the end of this incubation period, BrdU incorporation assay was performed as follows. First, cells were fixed with FixDenat solution for 30 minutes. Then, anti-BrdU-POD working solution was added to the wells and cells were incubated for 90 minutes. After that, the wells were washed with washing solution and finally substrate solution was added into the wells and proliferation rates of the cells were quantified by measuring absorbance (370 nm with 492 nm reference wavelength) with a microplate reader (Molecular Devices Spectramax M5).

### **2.5.2 ALIZARIN RED-S STAINING**

Alizarin Red-S staining was performed by using 96-well plates that were PA-coated and uncoated. Cells were seeded at a density of  $5 \times 10^3$  cells/well under conditions of 5% CO<sub>2</sub> at 37 °C in a humidified chamber either in low glucose DMEM supplemented with 10% (v/v) FBS and 1% (v/v) Penicillin/Streptomycin or in osteogenic differentiation medium (low glucose DMEM, 10% (v/v) FBS and 1%

(v/v) Penicillin/Streptomycin supplemented with 10 mM  $\beta$ -glycerophosphate, 50  $\mu$ g/mL ascorbic acid and 10 nM dexamethasone). Calcium deposition was assessed by staining the wells and the cells with Alizarin Red-S reagent at the end of day 7 and day 14 as previously described<sup>93</sup>. Briefly, medium was discarded and cells were washed with 1 x PBS. Then, cells were fixed with ice cooled 70% (v/v) ethanol for 1 h at room temperature. After the fixation step, cells were washed with ddH<sub>2</sub>O on a shaker for 15 min and then stained with 40 mM Alizarin Red-S solution (pH 4.2) for 30 min at room temperature on a shaker. Finally, the Alizarin Red-S solution was discarded and the wells were washed with ddH<sub>2</sub>O 5 times to get rid of non-specific binding of the dye. The stained calcium nodules were observed under a light microscope and all images were acquired at a 10x magnification. After image taking, to quantify Alizarin Red-S staining, wells were destained by using 10% (w/v) cetylpyridinium chloride in 10 mM sodium phosphate for 15 min at room temperature and absorbance was read at 562 nm by using a microplate reader.

### **2.5.3 SAFRANIN-O STAINING**

Safranin-O staining was performed by using 96 well plates that were PA-coated and uncoated. Cells were seeded at a density of  $5 \times 10^3$  cells/well in low glucose DMEM supplemented with 10% (v/v) FBS and 1% (v/v) Penicillin/Streptomycin under conditions of 5% CO<sub>2</sub> at 37 °C in a humidified atmosphere. Sulfated glycosaminoglycan depositions were assessed by staining the wells with Safranin-O reagent at the end of day 7 and day 14. Briefly, the culture medium was discarded and cells were washed with 1x PBS. After washing step, cells

were fixed by using 10% (v/v) formalin in PBS for 15 min at room temperature. Then, the cells were again washed with 1x PBS and afterwards blocked with 1% (w/v) BSA/PBS for 30 min at room temperature. After blocking, cells were stained with 0.1% (w/v) Safranin O in 1% (v/v) acetic acid for 5 min at room temperature. Finally, the wells were extensively washed 3 times with 0.1% (v/v) acetic acid in PBS to remove unbound dye and stained glycosaminoglycan depositions were observed under a light microscope. All images were acquired at a 10x magnification.

#### **2.5.4 OIL RED-O STAINING**

Oil Red-O staining was performed by using 96 well plates that were PA-coated and uncoated. Cells were seeded at a density of  $5 \times 10^3$  cells/well in low glucose DMEM supplemented with 10% (v/v) FBS and 1% (v/v) Penicillin/Streptomycin under conditions of 5% CO<sub>2</sub> at 37 °C in a humidified chamber. Lipid vacuoles were assessed by staining the wells with Oil Red-O reagent at the end of day 7 and day 14. Briefly, the culture medium was discarded and cells were washed with 1x PBS and then incubated with 10% (v/v) formalin in PBS for 10 min at room temperature. After that, the cells were fixed by changing formalin with fresh formalin and incubating for additional 1 h at room temperature. Then, the cells were washed with ddH<sub>2</sub>O and incubated with 60% (v/v) isopropanol for 5 min at room temperature. In the next step, isopropanol was removed and wells were completely air dried. After that, the cells were stained with Oil Red-O working solution for 10 min at room temperature and washed 4 times with ddH<sub>2</sub>O. Finally, images were acquired under a light microscope at 10x magnification. For the

quantification of Oil Red-O staining, Oil Red-O dye was eluted by incubating the cells with absolute isopropanol for 10 min at room temperature with gentle shaking. After that, the absorbance was measured at 500 nm by using 100% isopropanol as a blank with a microplate reader (Molecular Devices Spectramax M5).

### **2.5.5 PROTEIN AND ALKALINE PHOSPHATASE ACTIVITY ASSAYS**

Protein and alkaline phosphatase activity assays were performed by using 48-well plates that were PA-coated and uncoated. Cells were seeded at a density of  $20 \times 10^3$  cells/well in low glucose DMEM supplemented with 10% (v/v) FBS and 1% (v/v) Penicilin/Streptomycin under conditions of 5% CO<sub>2</sub> at 37 °C in a humidified chamber. Briefly, cells were washed with 1x PBS prior to protein extraction experiment. Protein extraction experiment was briefly performed first by adding PEK (Protein Extraction Kit)/PIK (Protease Inhibitor Cocktail) at a 95:5 ratio onto the cells and incubating on a shaker for 30 min. Then, the cells were lysed by vortexing and protein containing solutions from each well were transferred into eppendorf tubes by pipetting. After that, protein samples were centrifuged at 14000 g at 4 °C for 10 min and supernatants that contain proteins were taken into new eppendorf tubes. Pierce<sup>®</sup> BCA protein assay (Thermo Scientific) was performed to quantify protein amount obtained from the cells as described in manufacturer's protocol. Absorbance was determined at 562 nm by using a micro plate reader (Molecular Devices Spectramax M5).

For the analyses of alkaline phosphatase (ALP) activities of rMSCs seeded onto different peptide nanofiber networks, 50 µL of protein sample obtained from the

protein assay was incubated with 150  $\mu$ L of *p*-nitrophenol phosphate substrate in a 96-well plate for 30 min on a shaker. Serial dilutions of *p*-nitrophenol in 0.25 M NaOH were used as standards. Finally, optical density was determined at 405 nm wavelength by using a microplate reader. The alkaline phosphatase activity values were normalized to total protein amounts.

### **2.5.6 QUANTITATIVE REAL-TIME GENE EXPRESSION ANALYSES**

Quantitative real-time polymerase chain reaction (qRT-PCR) was used for determining the gene expression profiles of rMSCs. Total RNA was isolated from rat mesenchymal stem cell samples by using TRIzol (Invitrogen) reagent. Nanodrop 2000 (Thermoscientific) was used to assess the yield and purity of the extracted RNA. Primer sequences were designed using Primer 3 software (Table 2.2). The reaction efficiencies of each primer set were evaluated with standard curve by using 2-fold serial dilutions of total RNA. cDNA synthesis from RNA and qRT-PCR were performed by using SuperScript III Platinum SYBR Green One-Step qRT-PCR Kit (Invitrogen). The qRT-PCR reaction conditions were briefly as follows: 55 °C for 5 min, 95 °C for 5 min and 40 cycles of 95 °C for 15 sec, X °C (where X is the annealing temperature of the primers, see below) for 30 sec, and 40 °C for 1 min, followed by a melting curve to confirm product specificity. For analysis of the expression data, primary gene expression data was normalized to the expression level of GAPDH. A comparative Ct method was used to analyze the results. Gene expression was normalized to GAPDH and TCP. The expression levels of six different genes were analyzed and quantified by using qRT-PCR. These genes were

runt-related transcription factor 2, collagen 1, transcription factor SOX-9, collagen 2, adiponectin and fatty acid binding protein 4.

## **2.6 STATISTICAL ANALYSIS**

All quantitative values are represented as means  $\pm$  standard error of the mean (SEM). All experiments were performed with at least three replicates for each group and for at least three independent repeats. One-way analysis of variance (ANOVA) with Tukey post test or two-way analysis of variance (ANOVA) were used for statistical analysis and a P value of less than 0.05 was considered statistically significant.

**Table 2.2** Primer sequences and annealing temperatures of runt-related transcription factor 2, collagen 1, transcription factor SOX-9, collagen 2, adiponectin and fatty acid binding protein 4 for rat mesenchymal stem cells.

<b>Gene</b>	<b>Primer Sequence: Forward/Reverse</b>	<b>Annealing Temperature (°C)</b>
Runt-related Transcription Factor 2 ( <b>RUNX2</b> )	5'-GGACGAGGCAAGAGTTTCACT-3' 5'-CCCTAAATCACTGAGGCGGT-3'	59.5 °C
Collagen 1 ( <b>COL1</b> )	5'-GAATATGTATCACCAGACGCAGA-3' 5'-GGACATCTGGGAAGCAAAGT-3'	59.5 °C
Transcription Factor SOX-9 ( <b>SOX9</b> )	5'-CCACCCCGATTACAAGTACC-3' 5'-CAGCCACCTGGGACTCTAA-3'	61.5 °C
Collagen 2 ( <b>COL2</b> )	5'-CGAGGTGACAAAGGAGAAGC-3' 5'-TCCCGGTCTTCATGGGACTA-3'	55.0 °C
Adiponectin ( <b>ADIPOQ</b> )	5'-AAGGGAGACGCAGGTGTTCTTGG-3' 5'-ATGGGAACATTGGGGACAGTGAC-3'	58.0 °C
Fatty Acid Binding Protein 4 ( <b>FABP4</b> )	5'-CCCAGATGACAGGAAAGTGAAGAGC-3' 5'-CTTTCATGACACATTCCACCACAG-3'	59.0 °C

## **CHAPTER 3**

### **RESULTS AND DISCUSSIONS**

### 3.1 SYNTHESIS AND CHARACTERIZATION OF PEPTIDE AMPHIPHILE MOLECULES

Four different peptide amphiphile molecules were designed and synthesized by using solid phase peptide synthesis protocol. These molecules were used to form nanofiber networks and to mimic natural extracellular matrix microenvironment. Peptide amphiphile molecules were designed as a composition of hydrophobic alkyl group,  $\beta$ -sheet driving group, and charged group. Lauric acid that was added at the end of peptide sequences gives a hydrophobic character to peptide amphiphile molecules and triggers hydrophobic collapse during self-assembly<sup>94</sup>. Before the lauric acid hydrophobic tail, four non-polar amino acids were incorporated into the peptide sequences to constitute the  $\beta$ -sheet forming units of the peptide amphiphile molecules. Sequence of these non-polar amino acids that were used in all peptide amphiphile molecules was Val-Val-Ala-Gly (VVAG). The peptide amphiphile molecules that were used in this study to mimic glycosaminoglycan components of natural extracellular matrix were; Glc-PA [Lauryl-VVAGKS(Glc)-Am], K-PA [Lauryl-VVAGK-Am], E-PA [Lauryl-VVAGE] and SO<sub>3</sub>-PA [Lauryl-VVAGEK(*p*-sulfobenzoate)-Am] (**Figure 3.1**). Glc-PA that contains one lysine and one serine, where a glucose group was attached to side chain of serine residue, after the  $\beta$ -sheet forming unit was designed to mimic the saccharide backbone of glycosaminoglycans. SO<sub>3</sub>-PA that contains one glutamic acid and one lysine, where a sulfonate group was attached to the side chain of lysine residue, after the  $\beta$ -sheet forming unit was designed to mimic sulfated glycosaminoglycans. E-PA which contains only one glutamic acid after VVAG sequence was designed to mimic unsulfated

glycosaminoglycans. K-PA which contains only one lysine after VVAG sequence ( $\beta$ -sheet forming sequence) was designed and used as a counter positively charged peptide amphiphile molecule. Glc-PA and K-PA are positively charged at neutral pH whereas SO<sub>3</sub>-PA and E-PA are negatively charged. Glc-PA was used to form glycosaminoglycan mimetic hydrogels by adding negatively charged SO<sub>3</sub>-PA and/or E-PA molecules. Positively charged K-PA was mixed with negatively charged E-PA at neutral pH to form non-bioactive control group. By using these peptide amphiphile molecules, four different nanofiber network systems were formed and used in the experiments. These nanofiber network systems were Glc-PA/E-PA, Glc-PA/SO<sub>3</sub>-PA, Glc-PA/SO<sub>3</sub>-PA/E-PA and K-PA/E-PA (**Figure 3.2**). Glc-PA/E-PA network was used to mimic natural hyaluronan, which is a non-sulfated glycosaminoglycan and is widely distributed throughout connective and neural tissues. Glc-PA/SO<sub>3</sub>-PA and Glc-PA/SO<sub>3</sub>-PA/E-PA networks were used to mimic sulfated glycosaminoglycans. Glc-PA/SO<sub>3</sub>-PA nanofiber network system generally used to mimic heparan sulfate which contains one sulfate molecule in each saccharide residue. Glc-PA/SO<sub>3</sub>-PA/E-PA nanofiber network system was generally used to mimic chondroitin sulfate and dermatan sulfate which contain one sulfate and one carboxyl molecules in each disaccharide residue. After the synthesis of peptide amphiphile molecules, they were purified according to their charges and molecular complexities by using high pressure liquid chromatography or 0.1 mM HCl (acid) treatment protocols. Then, the purity of synthesized molecules was checked again according to their charges by using liquid chromatography-mass spectroscopy. Finally, secondary structures of the nanofibers were analyzed by using circular dichroism, scanning electron microscopy and transmission electron microscopy.

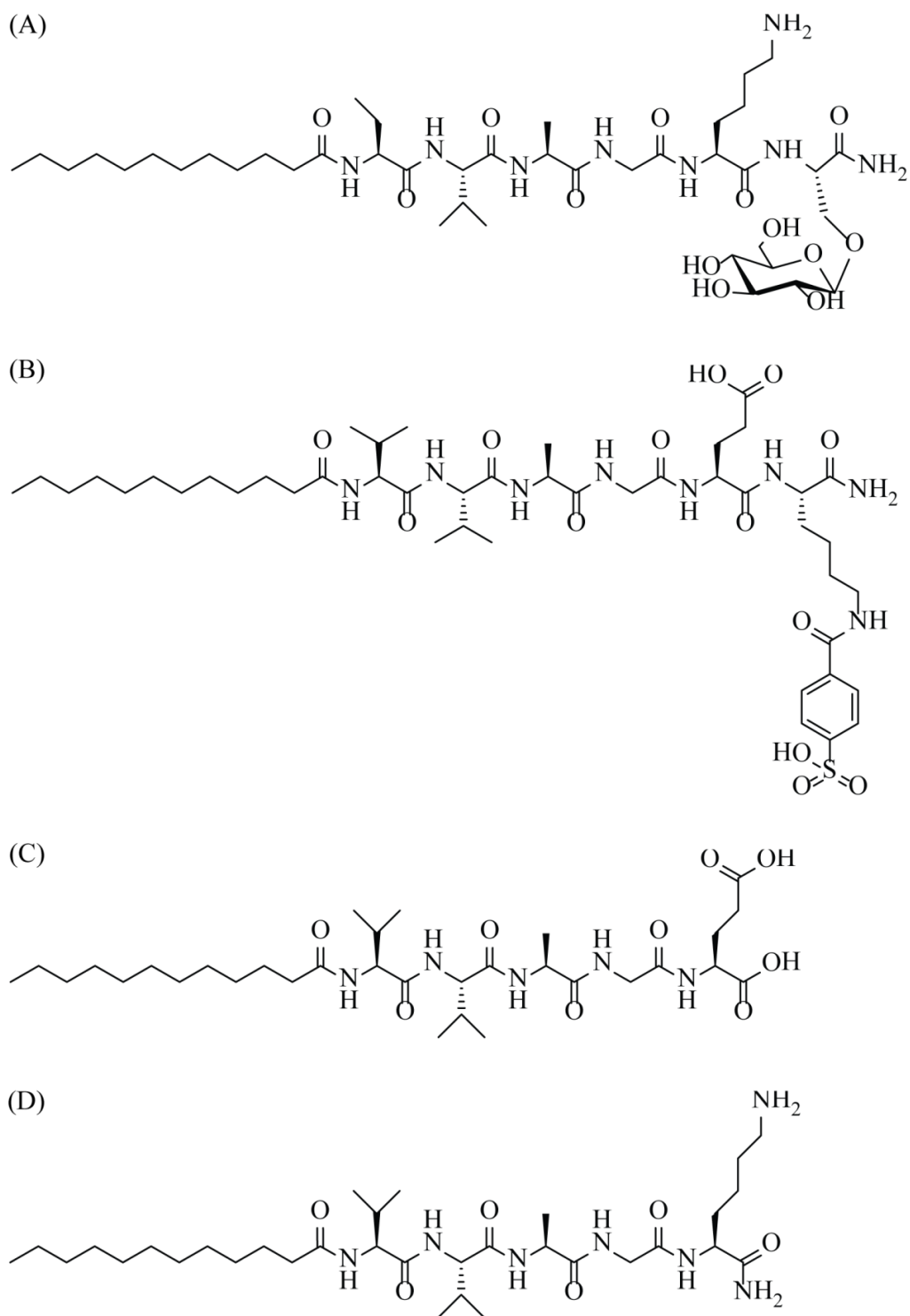


**Figure 3.1** Chemical representations of peptide amphiphile molecules. **(A)** Glc-PA [Lauryl-VVAGKS(Glc)-Am], **(B)** SO<sub>3</sub>-PA [Lauryl-VVAGEK(*p*-sulfo benzoate)-Am], **(C)** E-PA [Lauryl-VVAGE], and **(D)** K-PA [Lauryl-VVAGK-Am].

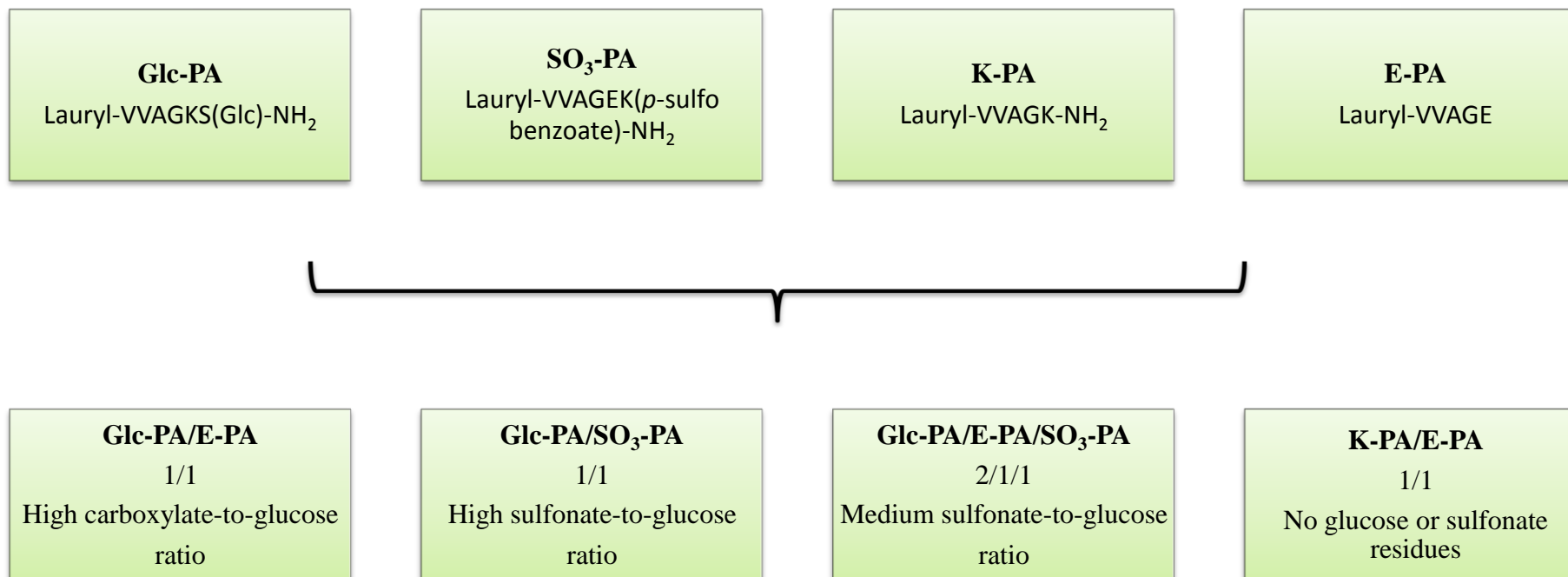


**Figure 3.2** Self-assembled nanofiber network systems used in this study. The peptide nanofiber networks self-assemble when mixed with oppositely charged peptide amphiphiles and were modified to incorporate chemical groups found in natural glycosaminoglycans.

### **3.1.1 PURIFICATION OF THE PEPTIDE AMPHIPHILES WITH HIGH PRESSURE LIQUID CHROMATOGRAPHY**

Reverse phase preparative HPLC equipped with either Zorbax Extend-C18 (21.2 x 150 mm) column or Zorbax SB-C8 (21.2 x 150 mm) column as a stationary phase were used to purify negatively and positively charged peptide amphiphile molecules, respectively. A gradient of water (0.1% acetonitrile or 0.1% NH<sub>4</sub>OH) and acetonitrile (0.1% formic acid or 0.1% NH<sub>4</sub>OH) were used as a mobile phase during HPLC purification of the synthesized peptide amphiphile molecules. Negatively charged PA molecules were always purified with reverse phase HPLC to get rid of the unwanted molecules. However; according to their synthesis purity, positively charged PA molecules were sometimes only treated with 0.1 M HCl (acid) solution in dialysis bags in which the remaining TFA was exchanged with chloride ions and passed to outside through the pores of dialysis bags due to simple diffusion and therefore removed at the end. The purities of the synthesized peptide amphiphile molecules became more than 95% after HPLC and/or acid purifications and then these molecules used in characterization and cell culture experiments.

### **3.1.2 ANALYSES OF PURITY AND SIZE OF PEPTIDE AMPHIPHILES**

Q-TOF LC/MS was used to verify the purity of the synthesized peptide amphiphile molecules. Expected masses for the PA molecules are theoretically 902.57 for Glc-PA, 966.51 for SO<sub>3</sub>-PA, 655.42 for E-PA and 653.48 for K-PA as shown in Table 2.1. Q-TOF LC/MS measurements were first performed subsequent

to synthesis of PA molecules to determine the completion and efficiency of the solid state peptide synthesis procedure and to decide which purification method will be used for further experiments. After performing the reverse phase preparative HPLC purification or acid treatment protocols as a purification method, Q-TOF LC/MS analyses were applied second time to indicate the final purity of the synthesized PA molecules. The elution time graphics which were obtained from Q-TOF LC/MS analyses as shown in Figure 3.3 gave information about the purity of the synthesized PA molecules. From Q-TOF LC/MS analyses, we obtained 903.59 for Glc-PA, 965.47 for SO<sub>3</sub>-PA, 654.42 for E-PA and 654.48 for K-PA as shown in Figure 3.4. These results indicated that the solid phase peptide synthesis protocol was correctly applied for all synthesis reactions and therefore completely synthesized PA molecules were obtained at the end of the reactions.

### 3.1.3 SECONDARY STRUCTURE DETERMINATION

Circular Dichroism (CD) analyses were performed to understand the secondary structure of PA molecules. CD measures the differential absorbance of left-handed and right-handed circularly polarized light which exhibited on optically active chiral molecules. In the case of PA molecules, the absorbance is provided by the amide group forming the peptide backbone and acting as a chromophore in the far UV region. The CD spectra of the PA hydrogels revealed a negative minimum at around 220 nm and a positive maximum at around 200 nm, which indicated the formation of  $\beta$ -sheet structure driven by the self-assembly of PAs in Glc-PA/E-PA, Glc-PA/SO<sub>3</sub>-PA, Glc-PA/SO<sub>3</sub>-PA/E-PA and K-PA/E-PA combinations (**Figure 3.5**).

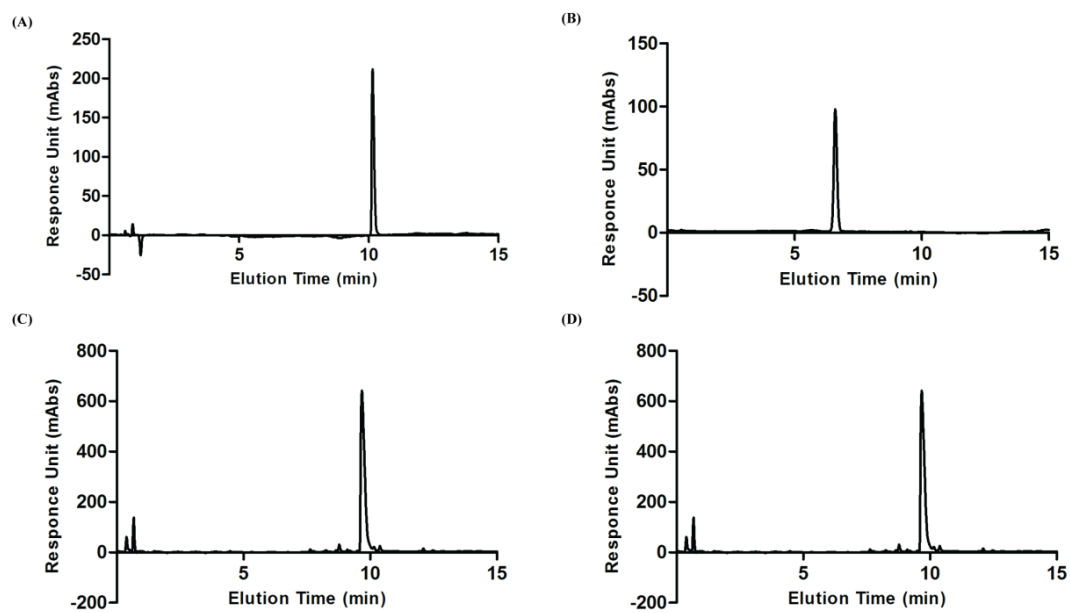


**Figure 3.3** HPLC chromatogram of purified: (A) Glc-PA, (B) SO<sub>3</sub>-PA, (C) E-PA, and (D) K-PA K molecule at 220 nm.

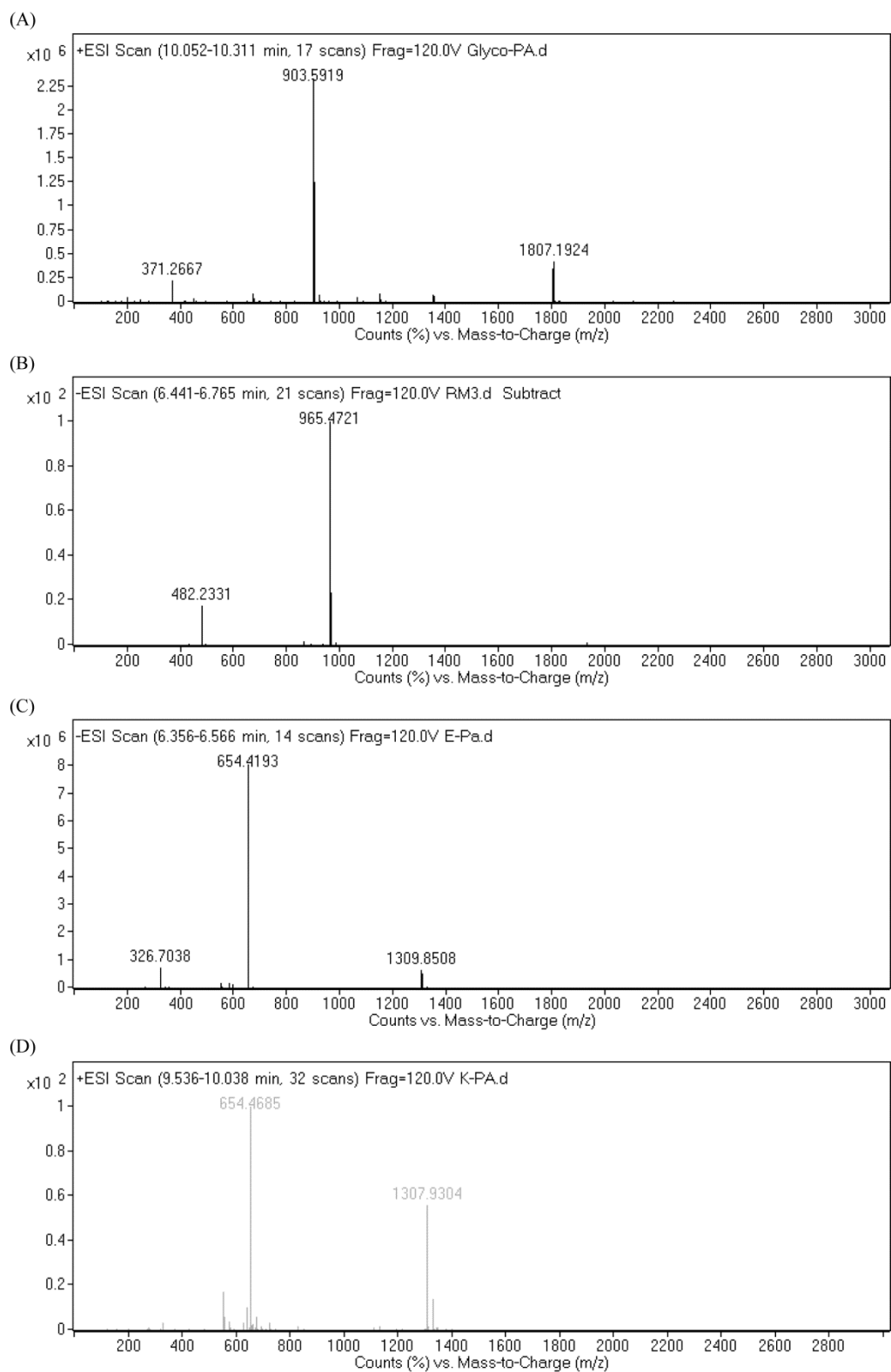


**Figure 3.4** Electrospray ionization mass spectra of: (A) Glc-PA, (B) SO<sub>3</sub>-PA, (C) E-PA, and (D) K-PA.

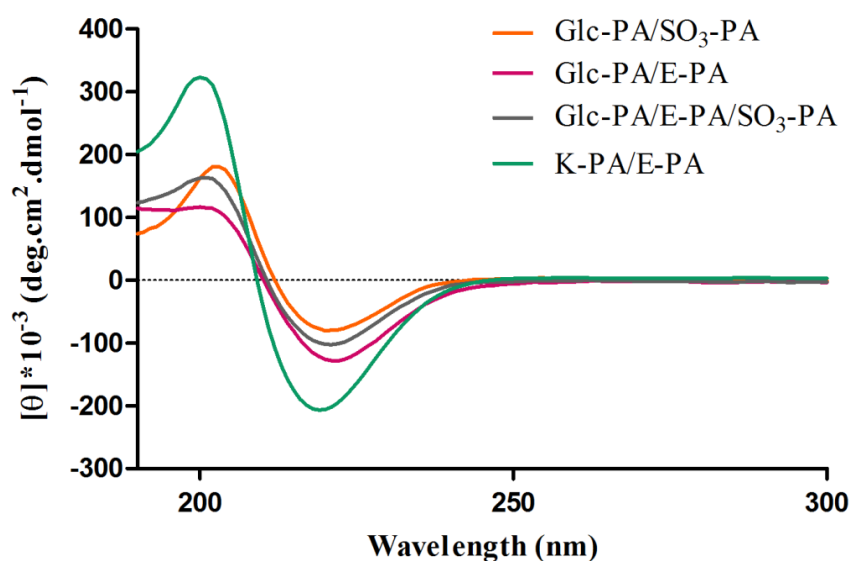


**Figure 3.5** Circular dichroism (CD) spectra of peptide nanofibers used for the characterization of the secondary structures. CD results indicate that peptide amphiphile nanofibers show a characteristic  $\beta$ -sheet structure at physiological pH.

### 3.1.4 MORPHOLOGICAL ANALYSIS OF PEPTIDE AMPHIPHILES

Scanning electron microscopy analyses were performed to characterize the self-assembly of peptide amphiphile molecules, the nanofiber formation and the morphology of the nanofiber networks. SEM analyses showed the formation of nanofibrous networks upon mixing oppositely charged peptide amphiphile molecules as Glc-PA/E-PA, Glc-PA/SO<sub>3</sub>-PA, Glc-PA/SO<sub>3</sub>-PA/E-PA and K-PA/E-PA combinations (**Figure 3.6**). The observed porous and nanofibrous network morphology of the PA hydrogels structurally resemble the native extracellular matrix found around the cells and therefore present a suitable microenvironment for the cells.

Transmission electron microscopy analyses were performed to further verify the nanofiber formation and to analyze the individual nanofibers. TEM analyses revealed the formation of nanofibers upon charge neutralization of oppositely charged peptide amphiphile molecules as Glc-PA/E-PA, Glc-PA/SO<sub>3</sub>-PA, Glc-PA/SO<sub>3</sub>-PA/E-PA and K-PA/E-PA combinations (**Figure 3.7**). Nanofibers were observed with 6 – 10 nm diameters and lengths up to a few microns. Moreover, bundling of the nanofibers was observed for K-PA/E-PA combination. These nanofibers resemble the fibrous macromolecules found in the native extracellular matrix of the cells.

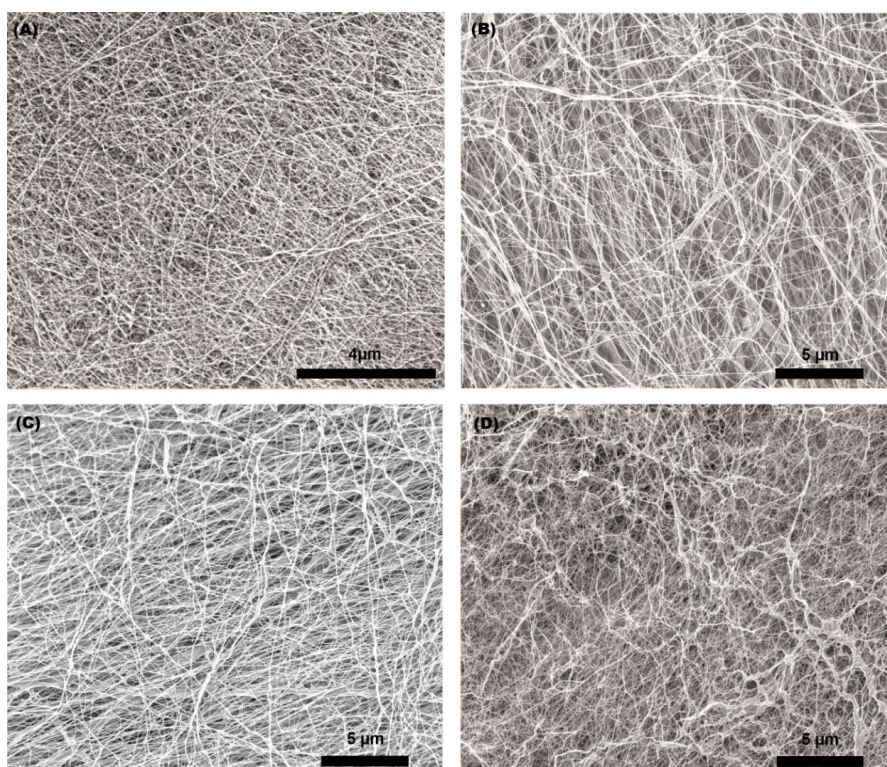


**Figure 3.6** Characterization of the peptide amphiphile nanofiber networks by using scanning electron microscopy. **(A)** Glc-PA/E-PA, **(B)** Glc-PA/SO<sub>3</sub>-PA, **(C)** Glc-PA/SO<sub>3</sub>-PA/E-PA and **(D)** K-PA/E-PA.

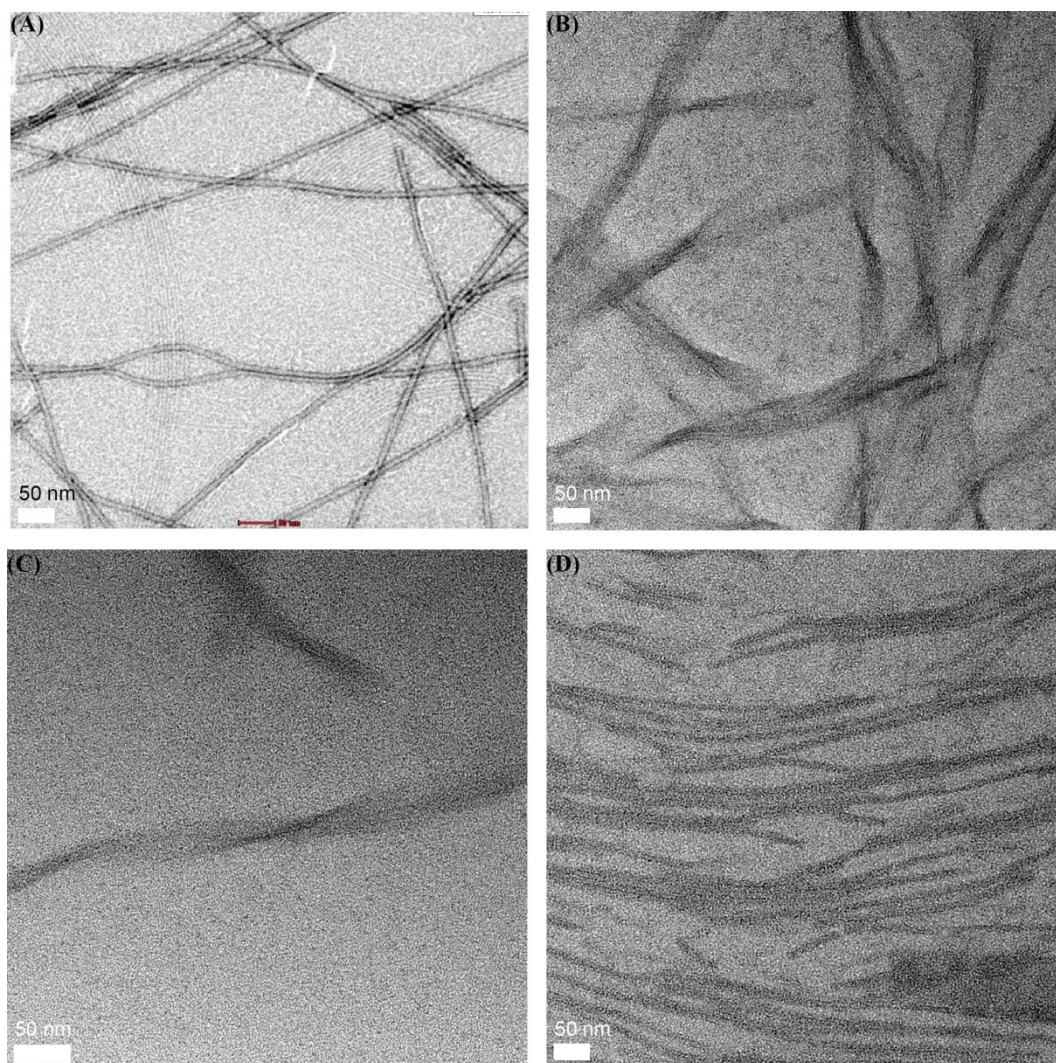


**Figure 3.7** Characterization of the peptide amphiphile nanofiber networks by using transmission electron microscopy. **(A)** Glc-PA/E-PA, **(B)** Glc-PA/SO<sub>3</sub>-PA, **(C)** Glc-PA/SO<sub>3</sub>-PA/E-PA and **(D)** K-PA/E-PA.

## **3.2 EFFECTS OF PEPTIDE NANOFIBER NETWORKS ON RAT MESENCHYMAL STEM CELLS**

Cell culture experiments were performed in two different stages following each other. In the first stage, we examined the effects of peptide nanofiber networks on viability and proliferation of the rat mesenchymal stem cells by using alamar Blue® viability and BrdU (colorimetric) incorporation assays. According to the results of these analyses, we decided whether we can pass to the next stage or not. In the second stage, we examined qualitatively and quantitatively the differentiation of rat mesenchymal stem cells on peptide nanofiber networks by using Alizarin Red-S, Safranin-O and Oil Red-O staining, alkaline phosphatase activity assay and quantitative real-time polymerase chain reaction.

### **3.2.1 THE DESIGN OF 2D CELL CULTURE EXPERIMENTS**

Four different combinations of peptide amphiphile hydrogels were prepared and coated onto tissue culture plates by using Glc-PA, SO<sub>3</sub>-PA, K-PA and E-PA molecules as shown in Figure 3.2. Then, these hydrogels were used to determine the effects of chemical groups represented on peptide nanofibers on the cellular behaviors such as viability, proliferation and differentiation in cell culture. Glc-PA/E-PA nanofiber networks were used to mimic non-sulfated glycosaminoglycan which is hyaluronan. Glc-PA/E-PA/SO<sub>3</sub>-PA nanofiber networks were used to mimic sulfated glycosaminoglycans which are chondroitin sulfate and dermatan sulfate. Glc-PA/SO<sub>3</sub>-PA nanofiber networks were used to mimic over-sulfated

glycosaminoglycans which are heparin and heparan sulfate. K-PA/E-PA nanofiber networks were used as a non-bioactive control group that only contained carboxylic acid residue over nanofiber networks. Uncoated tissue culture plates which lacked peptide coating were used as negative control. Rat mesenchymal stem cells that were at passage # 6 and had multi-lineage differentiation capacities were used in all *in vitro* experiments.

### **3.2.2 BIOCOMPATIBILITY OF PEPTIDE NANOFIBER NETWORKS**

AlamarBlue® (Invitrogen) was used to examine the effects of peptide nanofiber networks on the viability of rat mesenchymal stem cells. AlamarBlue® is an accurate cell viability indicator which uses the natural reducing power of the living cells. Resazurin, a non-toxic, non-fluorescent and cell permeable compound, is the active ingredient of alamarBlue®. Resazurin is continuously reduced to resorufin in viable cells and produces very bright red fluorescence upon this reduction reaction which is used for generating a quantitative measure of viability and cytotoxicity<sup>95-96</sup>.

We checked the toxicological effects of Glc-PA/E-PA, Glc-PA/SO<sub>3</sub>-PA, Glc-PA/SO<sub>3</sub>-PA/E-PA and K-PA/E-PA nanofiber networks on rat mesenchymal stem cells at 24 h. We used 96-well plates and seeded  $5 \times 10^3$  cells/well by using maintenance medium. At the end of 24 h, we incubated the cells for an additional 2 h with 10% (v/v) alamarBlue® and then measured the absorbance by using microplate reader, where the amount of absorbance corresponds to the cells' metabolic activity level. AlamarBlue® results showed that culturing on Glc-PA/E-PA, Glc-PA/SO<sub>3</sub>-PA, Glc-PA/SO<sub>3</sub>-PA/E-PA and K-PA/E-PA nanofiber networks did not alter the viability

of rat mesenchymal stem cells compared to uncoated tissue culture plate (**Figure 3.8**). Cells showed average of 92.42%, 92.58%, 91.74% and 94.19% viability on Glc-PA/E-PA, Glc-PA/SO<sub>3</sub>-PA, Glc-PA/SO<sub>3</sub>-PA/E-PA and K-PA/E-PA nanofiber networks respectively when compared to uncoated tissue culture plate. These results demonstrated that peptide nanofiber systems are biocompatible with rat mesenchymal stem cells and they provide bio-friendly environments where cells can continue their life.

Overall, cellular viability was supported on bioactive peptide nanofiber networks and it was comparable with tissue culture plate. Therefore; we decided to use these nanofiber network systems in further experiments in which we checked the proliferation and differentiation of the cells over these peptide nanofiber networks.

### **3.2.3 PROLIFERATION ANALYSIS OF RAT MESENCHYMAL STEM CELLS ON PEPTIDE NANOFIBER NETWORKS**

Proliferation profiles of rat mesenchymal stem cells on peptide nanofiber networks were analyzed by using BrdU incorporation assay. 5-bromo-2-deoxyuridine (BrdU) is a synthetic uridine derivative and a structural analog of thymidine. It can be incorporated into DNA during the synthesis phase of the cell cycle as a substitute for thymidine, thereby serving as a marker for proliferation<sup>97</sup>. BrdU can also be passed to daughter cells upon replication<sup>98</sup>.

In this experiment, we checked the effects of Glc-PA/E-PA, Glc-PA/SO<sub>3</sub>-PA, Glc-PA/SO<sub>3</sub>-PA/E-PA and K-PA/E-PA nanofiber networks on proliferation of rat mesenchymal stem cells at 72 hours. We used 96-well plates and seeded  $5 \times 10^3$

cells/well by using maintenance medium. At the end of 70 h, we incubated the cells for an additional 2 h with BrdU labeling solution which contained 100  $\mu$ M BrdU. After the incubation period, BrdU assay was applied as described in method part and the results were normalized to uncoated tissue culture plate. In this experiment, we did not observe a significant difference in proliferation of cells seeded on TCP and K-PA/E-PA nanofiber network. This result demonstrated that cells seeded on K-PA/E-PA nanofiber network that contains no bioactive signal acted as cells seeded on tissue culture plate and continued their proliferation. However, we observed significant changes in the proliferation of cells seeded on Glc-PA/E-PA, Glc-PA/SO<sub>3</sub>-PA and Glc-PA/SO<sub>3</sub>-PA/E-PA nanofiber networks when compared to TCP. These results showed that cells seeded on these nanofiber networks that contain biological signals decreased their proliferation and probably started to differentiate into other lineages. We also observed that proliferation of the cells seeded on Glc-PA/SO<sub>3</sub>-PA nanofiber network that was formed by two bioactive signal containing PA macromolecules also decreased significantly compared to Glc-PA/E-PA nanofiber network which was formed by only one bioactive signal containing peptide amphiphile molecules.

Overall, Glc-PA and SO<sub>3</sub>-PA contain bioactive signals and nanofiber networks that were formed by using these peptide amphiphile molecules induced a decreased in the proliferation of rat mesenchymal stem cells perhaps due to differentiation signals according to the degree of sulfonate and carboxylate residues in the nanofibrous networks that the cells encountered. However, K-PA/E-PA nanofiber network which was used as a non-bioactive control did not affect the proliferation of the cells significantly.

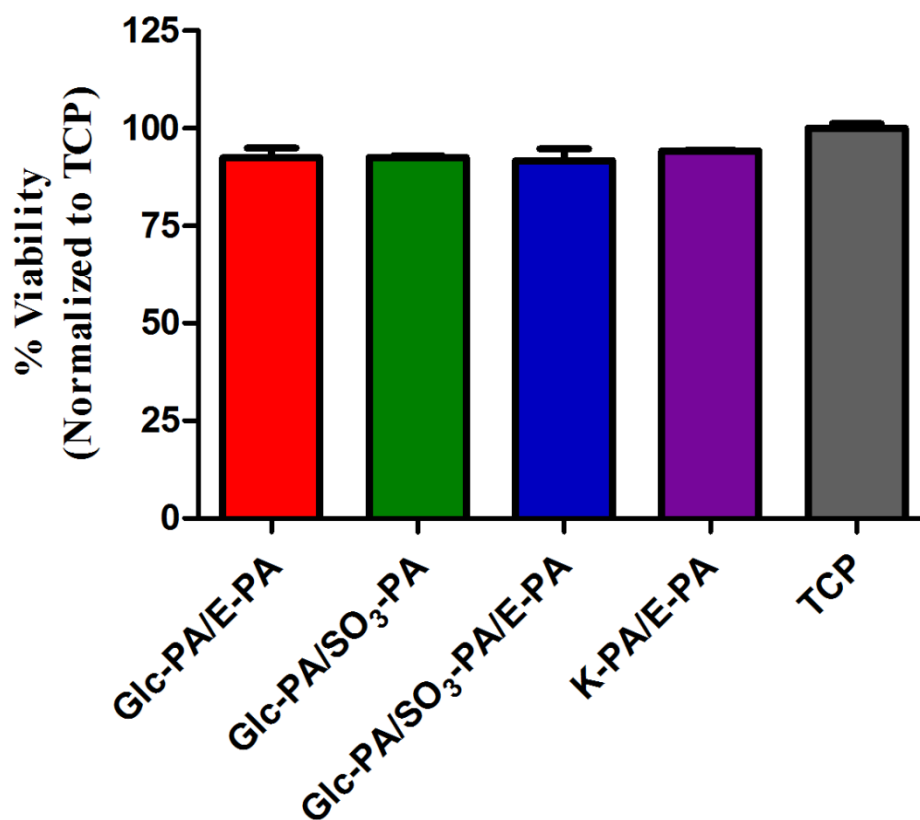


**Figure 3.8** Viability analyses of rat mesenchymal stem cells on different peptide nanofiber networks and uncoated tissue culture plate. AlamarBlue® was used to quantitatively determine the viability of rat mesenchymal stem cells at 24 h. One-way ANOVA with Tukey post test (95% confidence interval) was applied for analyzing the results, and no significant difference was found between each groups.

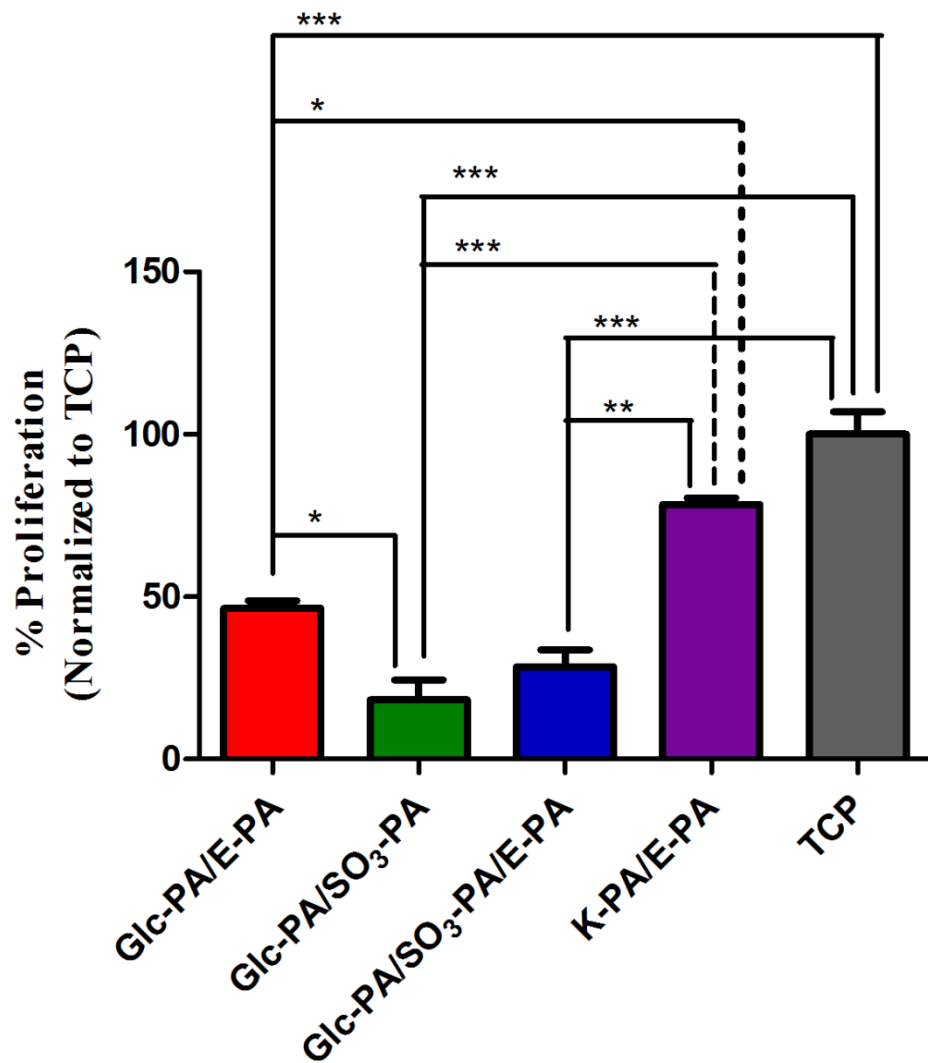


**Figure 3.9** Proliferation analyses of rat mesenchymal stem cells cultured with BrdU on different peptide nanofiber networks and uncoated tissue culture plate at day 3. One-way ANOVA with Tukey post test (95% confidence interval) was applied for analyzing the results and significant differences were expressed as (\*  $p < 0.05$ , \*\*  $p < 0.01$ , \*\*\*  $p < 0.001$ ).

### **3.3 INVESTIGATION OF THE DIFFERENTIATION OF RAT MESENCHYMAL STEM CELLS**

Different experimental methods were used to analyze the differentiation of rat mesenchymal stem cells seeded onto various peptide nanofiber networks and uncoated tissue culture plate towards mesodermal lineages. These methods included histological staining with Safranin-O for analyzing deposition of sulfated glycosaminoglycans, Oil Red-O for investigating deposition of triglycerides and lipids and Alizarin Red-S for examining mineralization, alkaline phosphatase activity measurement, and real-time gene expression analyses of collagen 1 (COL1), collagen 2 (COL2), adiponectin (ADIPOQ), fatty acid binding protein 4 (FABP4), runt-related transcription factor 2 (RUNX2) and transcription factor *SOX-9* (SOX9) as adipogenic, chondrogenic and osteogenic markers.

#### **3.3.1 ANALYSIS OF CALCIUM DEPOSITION AND MINERALIZATION**

First of all, we investigated the osteogenic differentiation of the rat mesenchymal stem cells with Alizarin Red-S staining. Alizarin Red-S, sodium alizarin sulfonate, is the salt of alizarin and it is a specific reagent for calcium when it is used at pH 4.1 to pH 4.3<sup>99</sup>. Alizarin Red-S staining has been used for decades to selectively examine calcium-rich deposits formed by cells in culture<sup>100</sup>. In this study, we used Alizarin Red-S staining to qualitatively and quantitatively analyze the differentiation fate of rat mesenchymal stem cells towards osteogenic lineage. We used different peptide nanofiber networks which were deliberately formed as they

contained glucose residue with sulfonate and/or carboxylate residues in different ratios. The peptide nanofiber networks used in this investigation were Glc-PA/E-PA, Glc-PA/SO<sub>3</sub>-PA, Glc-PA/SO<sub>3</sub>-PA/E-PA and K-PA/E-PA. Tissue culture plate was also used to observe what happened to the cells over non-coated surfaces. Two different media were used in the experiments which were growth medium and osteogenic differentiation medium. Osteogenic differentiation medium was typically composed of growth medium with additional dexamethasone,  $\beta$ -glycerophosphate and ascorbic acid or ascorbic acid analog. It was shown in many studies that mesenchymal stem cells can be induced to differentiate into osteoblasts by using glucocorticoids<sup>101-103</sup>. Dexamethasone is a synthetic corticosteroid and supports osteogenic differentiation<sup>104</sup>. We observed deposition of calcium ions in the mineralized matrix as in red color under light microscopy. We also performed Alizarin Red-S staining over peptide coated wells which did not contain cells to check whether non-specific staining occurred or not. We observed little no staining, which was negligible when compared to cell containing groups. We observed the difference in calcium accumulation when we used osteogenic induction medium at day 7 and day 14. Mineralization was induced in all groups when osteogenic differentiation medium was used. However, mineralization over Glc-PA/E-PA and K-PA/E-PA nanofiber networks increase more than other groups.

Overall, we showed that rMSCs seeded over Glc-PA/E-PA, Glc-PA/SO<sub>3</sub>-PA/E-PA and K-PA/E-PA nanofiber networks started to accumulate calcium deposits which is an indicator for osteogenic differentiation. However, there was no significant calcium deposition over Glc-PA/SO<sub>3</sub>-PA network and TCP. The presence of glucose residue in the nanofiber networks induces the calcium deposition and

therefore osteogenic differentiation of the rMSCs. Carboxylate-to-glucose ratio is also crucial and can be used to direct these cells into osteogenic lineage.

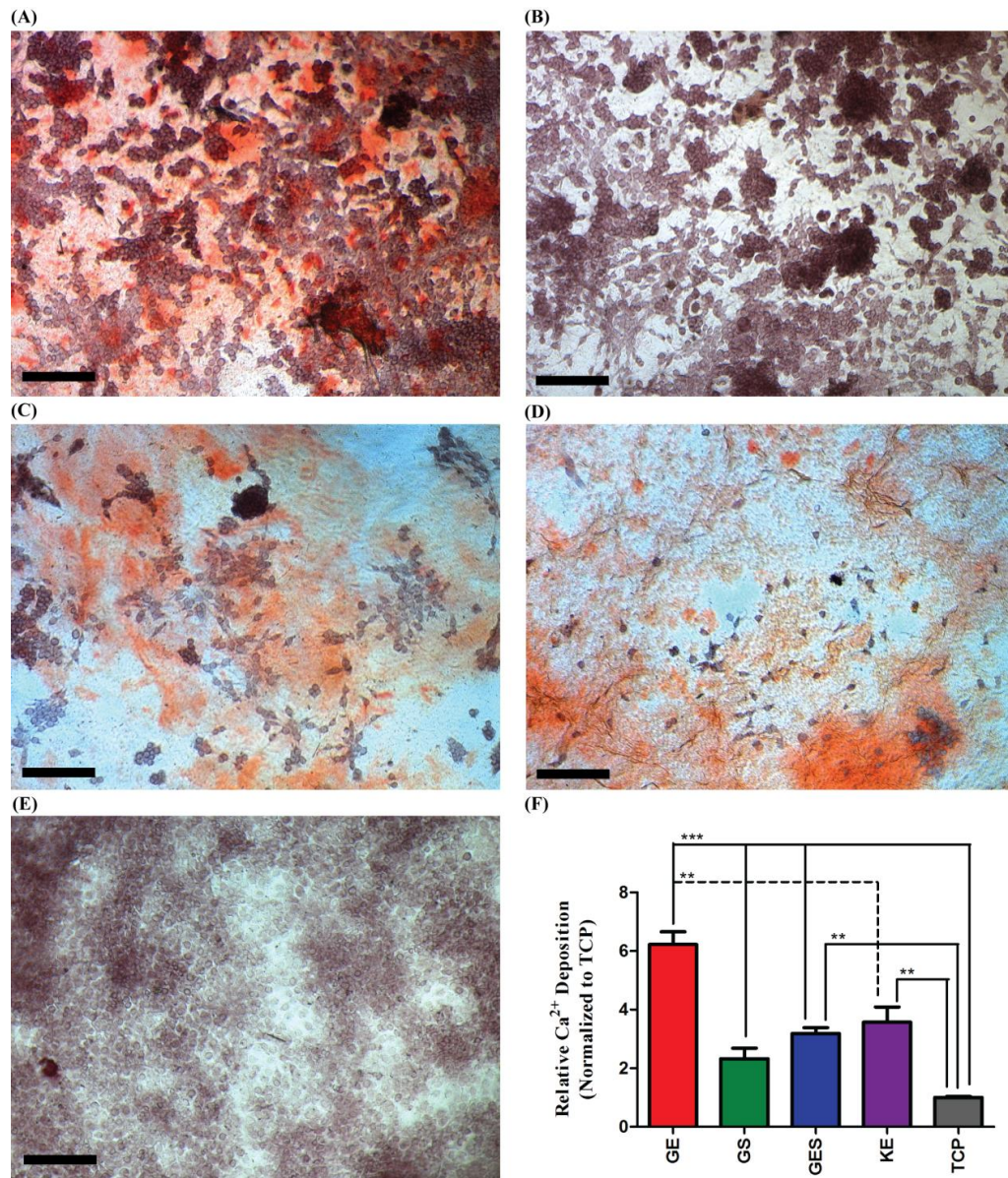


**Figure 3.10** Alizarin Red-S calcium staining of cells cultured with growth medium at day 7. (A) Glc-PA/E-PA, (B) Glc-PA/SO<sub>3</sub>-PA, (C) Glc-PA/SO<sub>3</sub>-PA/E-PA, (D) K-PA/E-PA, (E) TCP and (F) Quantitative analyses of Alizarin Red-S. One-way ANOVA with Tukey post test was applied to analyze the results and significant differences were expressed as (\*\* p<0.01 and \*\*\* p < 0.001). (Scale bars = 200 μm)

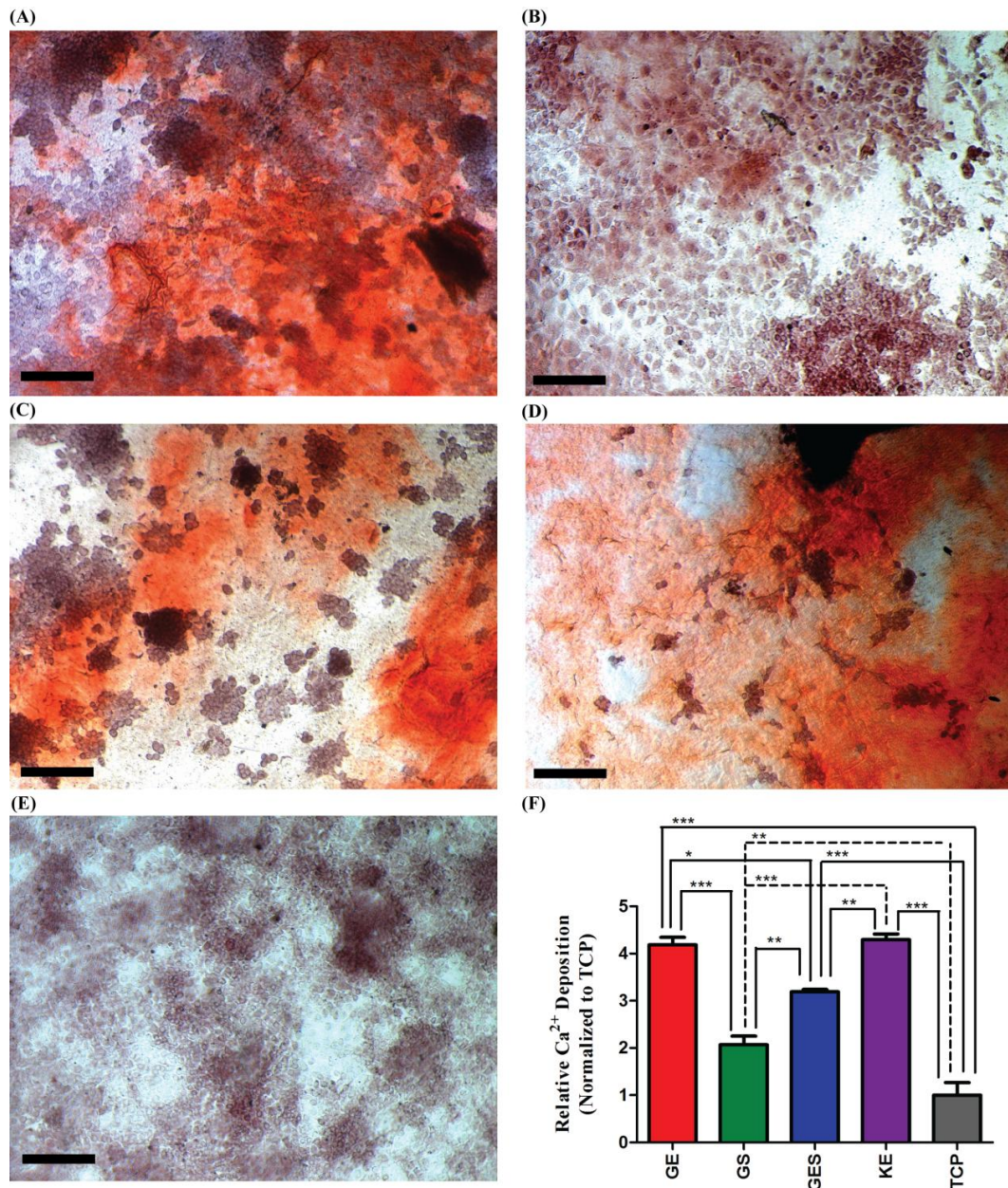


**Figure 3.11** Alizarin Red-S calcium staining of cells cultured with osteogenic medium at day 7. **(A)** Glc-PA/E-PA, **(B)** Glc-PA/SO<sub>3</sub>-PA, **(C)** Glc-PA/SO<sub>3</sub>-PA/E-PA, **(D)** K-PA/E-PA, **(E)** TCP and **(F)** Quantitative analyses of Alizarin Red-S. One-way ANOVA with Tukey post test was applied to analyze the results and significant differences were expressed as (\*  $p < 0.05$ , \*\*  $p < 0.01$  and \*\*\*  $p < 0.001$ ). (Scale bars = 200  $\mu\text{m}$ )

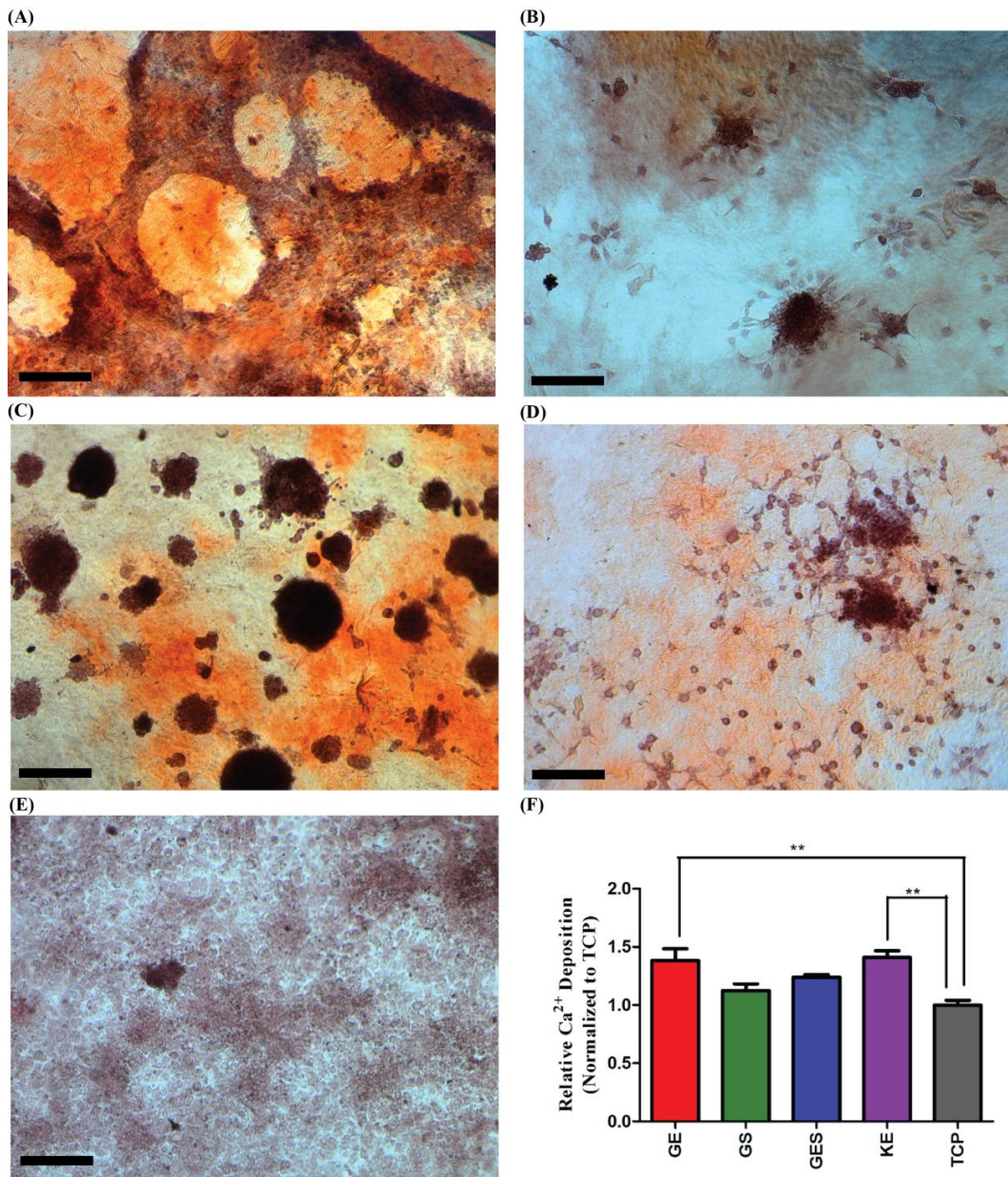


**Figure 3.12** Alizarin Red-S calcium staining of cells cultured with growth medium at day 14. (A) Glc-PA/E-PA, (B) Glc-PA/SO<sub>3</sub>-PA, (C) Glc-PA/SO<sub>3</sub>-PA/E-PA, (D) K-PA/E-PA, (E) TCP and (F) Quantitative analyses of Alizarin Red-S. One-way ANOVA with Tukey post test was applied to analyze the results and significant differences (\*\*) were expressed at  $p < 0.01$ . (Scale bars = 200  $\mu$ m)

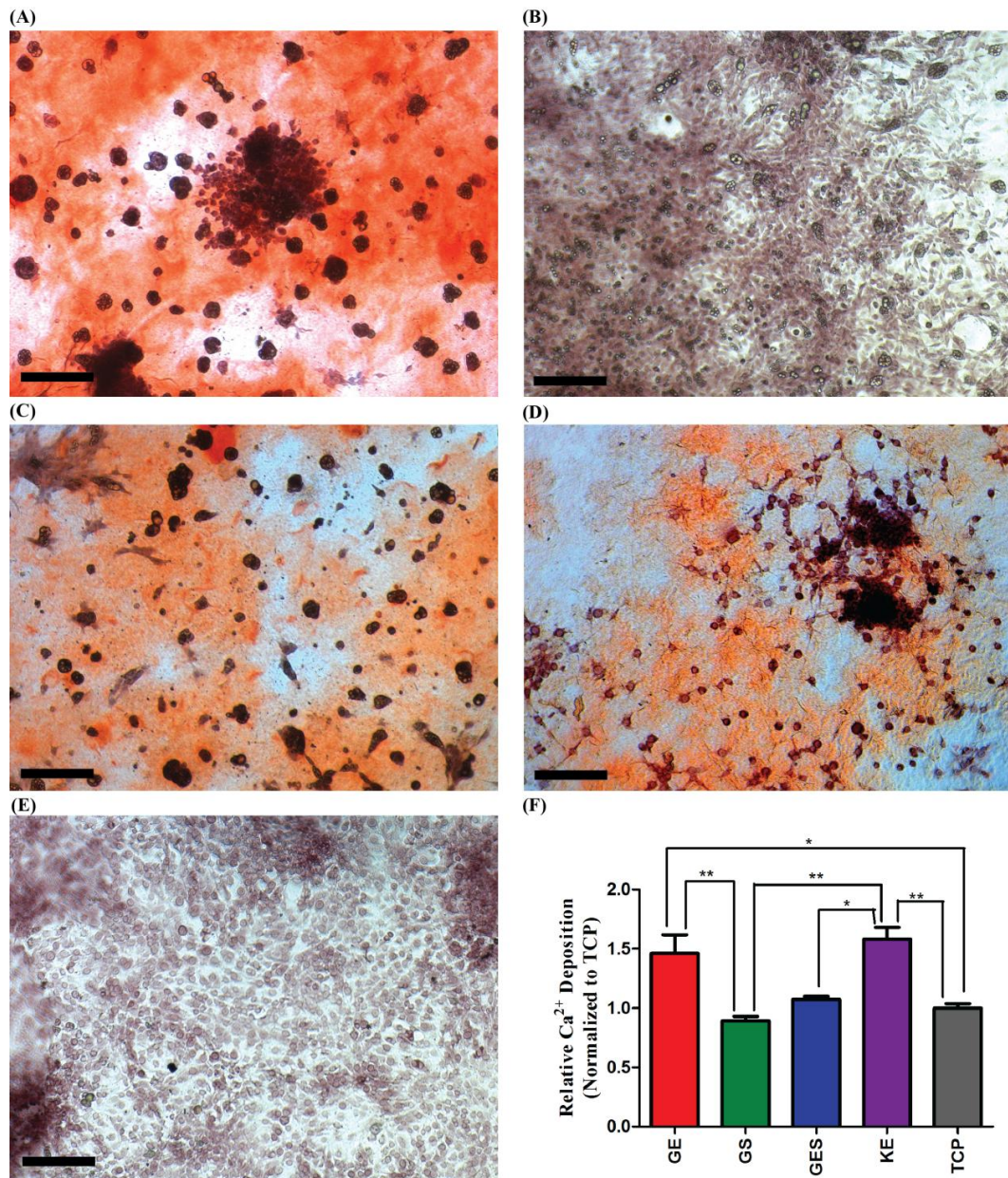


**Figure 3.13** Alizarin Red-S calcium staining of cells cultured with osteogenic medium at day 14. **(A)** Glc-PA/E-PA, **(B)** Glc-PA/SO<sub>3</sub>-PA, **(C)** Glc-PA/SO<sub>3</sub>-PA/E-PA, **(D)** K-PA/E-PA, **(E)** TCP and **(F)** Quantitative analyses of Alizarin Red-S. One-way ANOVA with Tukey post test was applied to analyze the results and significant differences were expressed as (\*  $p < 0.05$  and \*\*  $p < 0.01$ ). (Scale bars = 200  $\mu\text{m}$ )

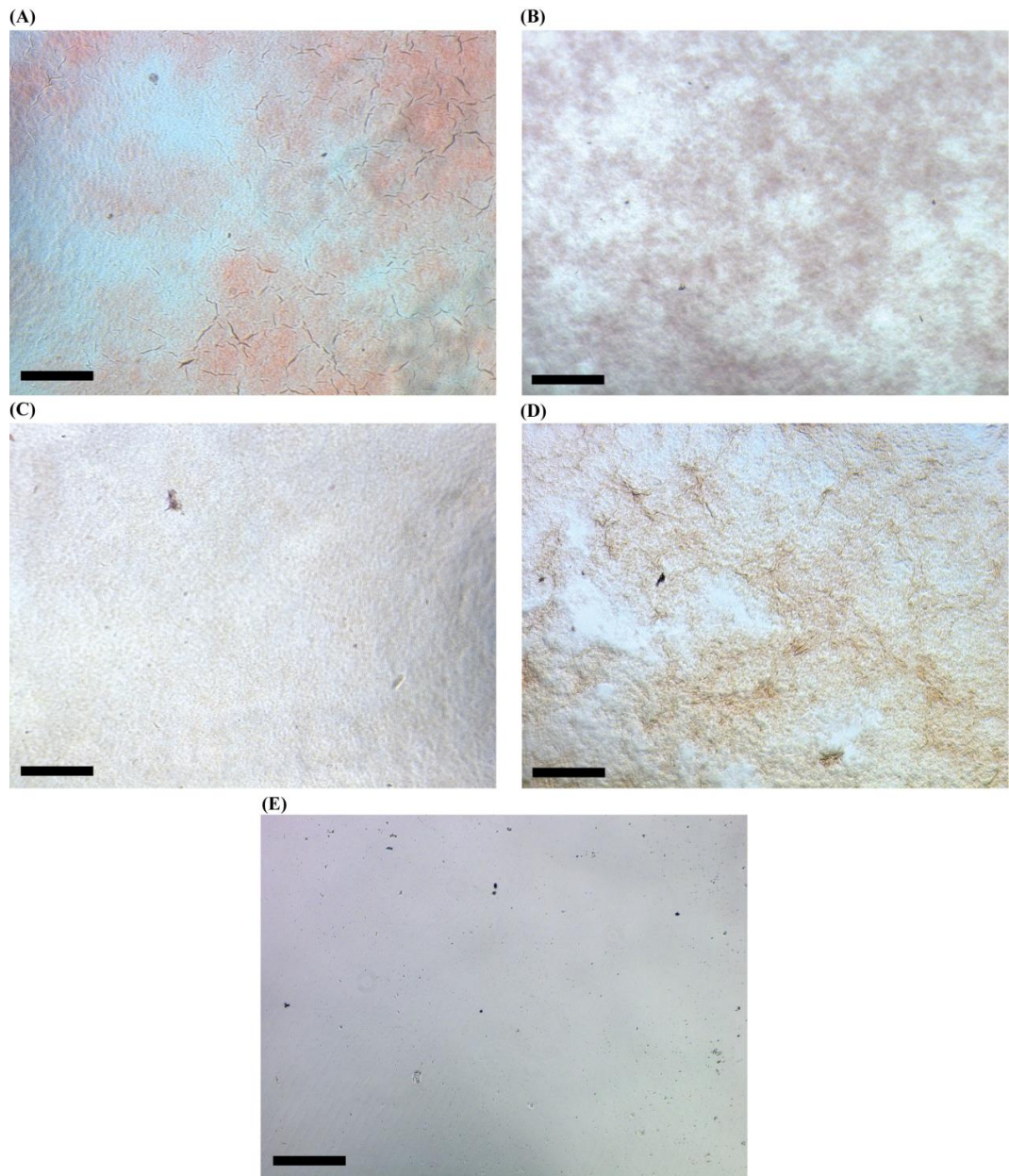


**Figure 3.14** Alizarin Red-S calcium staining of growth medium without cells at day 7, conducted as a control for non-specific calcium deposition. **(A)** Glc-PA/E-PA, **(B)** Glc-PA/SO<sub>3</sub>-PA, **(C)** Glc-PA/SO<sub>3</sub>-PA/E-PA, **(D)** K-PA/E-PA and **(E)** TCP. (Scale bars = 200 μm)

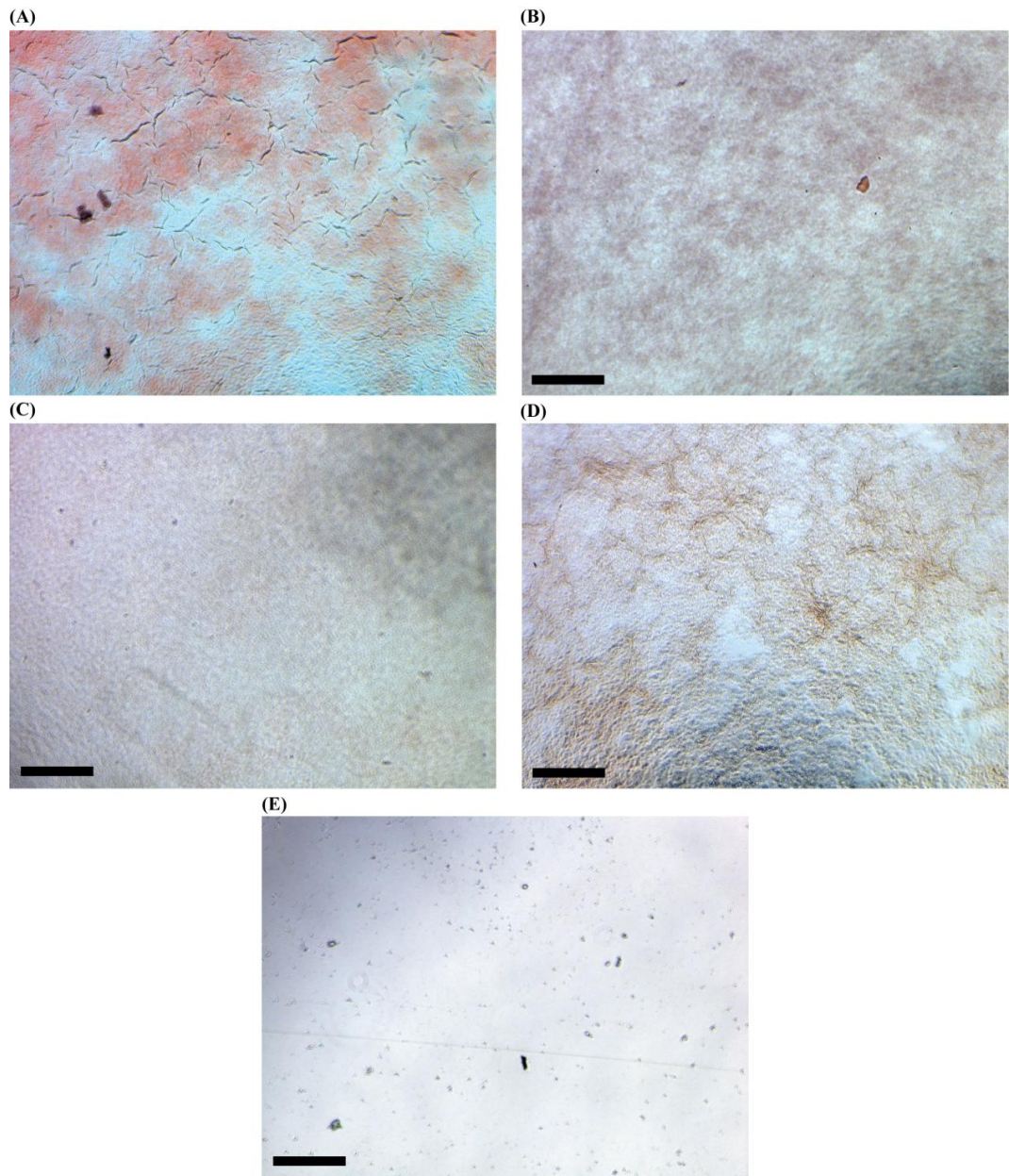


**Figure 3.15** Alizarin Red-S calcium staining of osteogenic differentiation medium without cells at day 7, conducted as a control for non-specific calcium deposition. **(A)** Glc-PA/E-PA, **(B)** Glc-PA/SO<sub>3</sub>-PA, **(C)** Glc-PA/SO<sub>3</sub>-PA/E-PA, **(D)** K-PA/E-PA and **(E)** TCP. (Scale bars = 200  $\mu$ m)

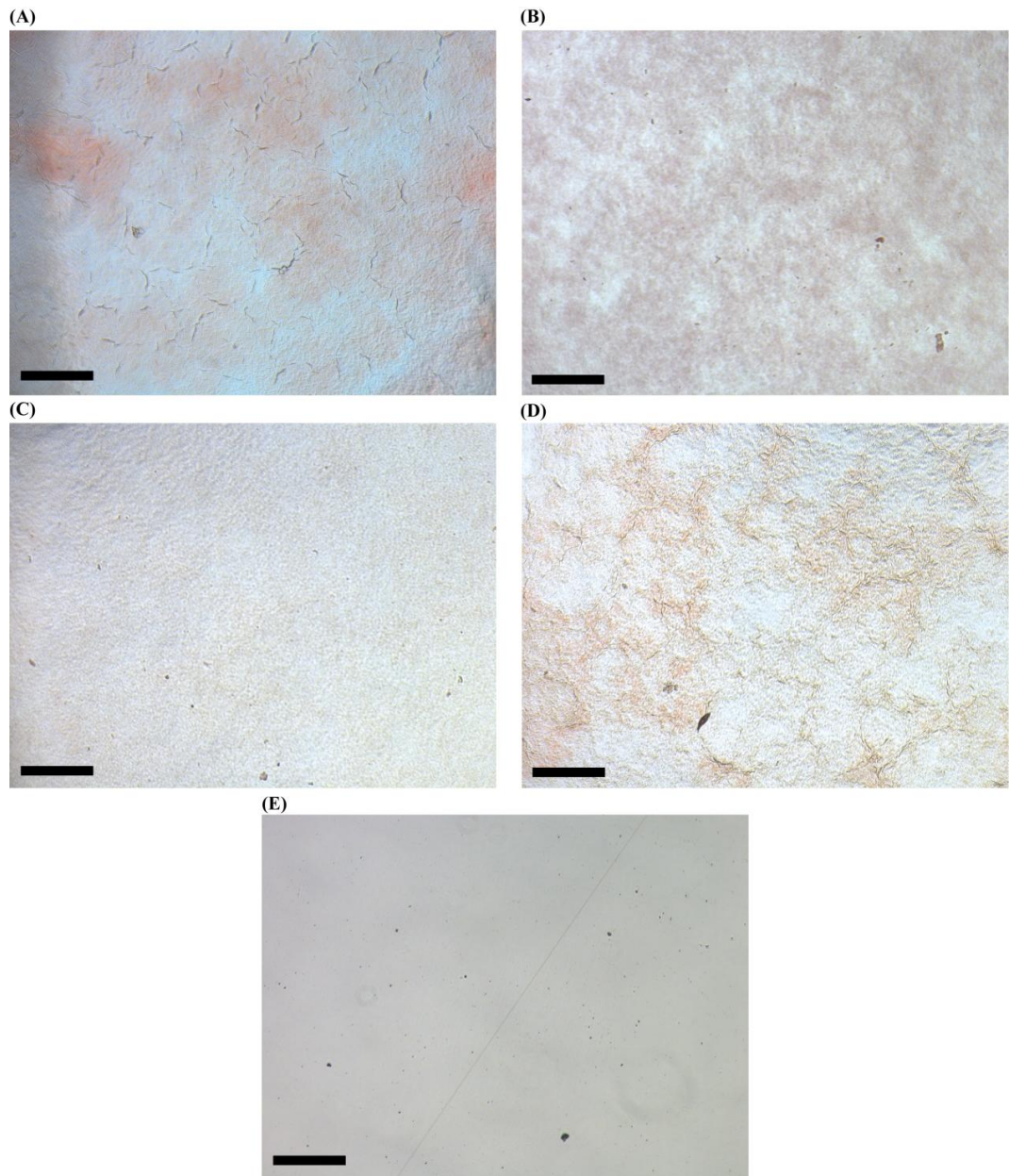


**Figure 3.16** Alizarin Red-S calcium staining of growth medium without cells at day 14, conducted as a control for non-specific calcium deposition. **(A)** Glc-PA/E-PA, **(B)** Glc-PA/SO<sub>3</sub>-PA, **(C)** Glc-PA/SO<sub>3</sub>-PA/E-PA, **(D)** K-PA/E-PA and **(E)** TCP. (Scale bars = 200 μm)

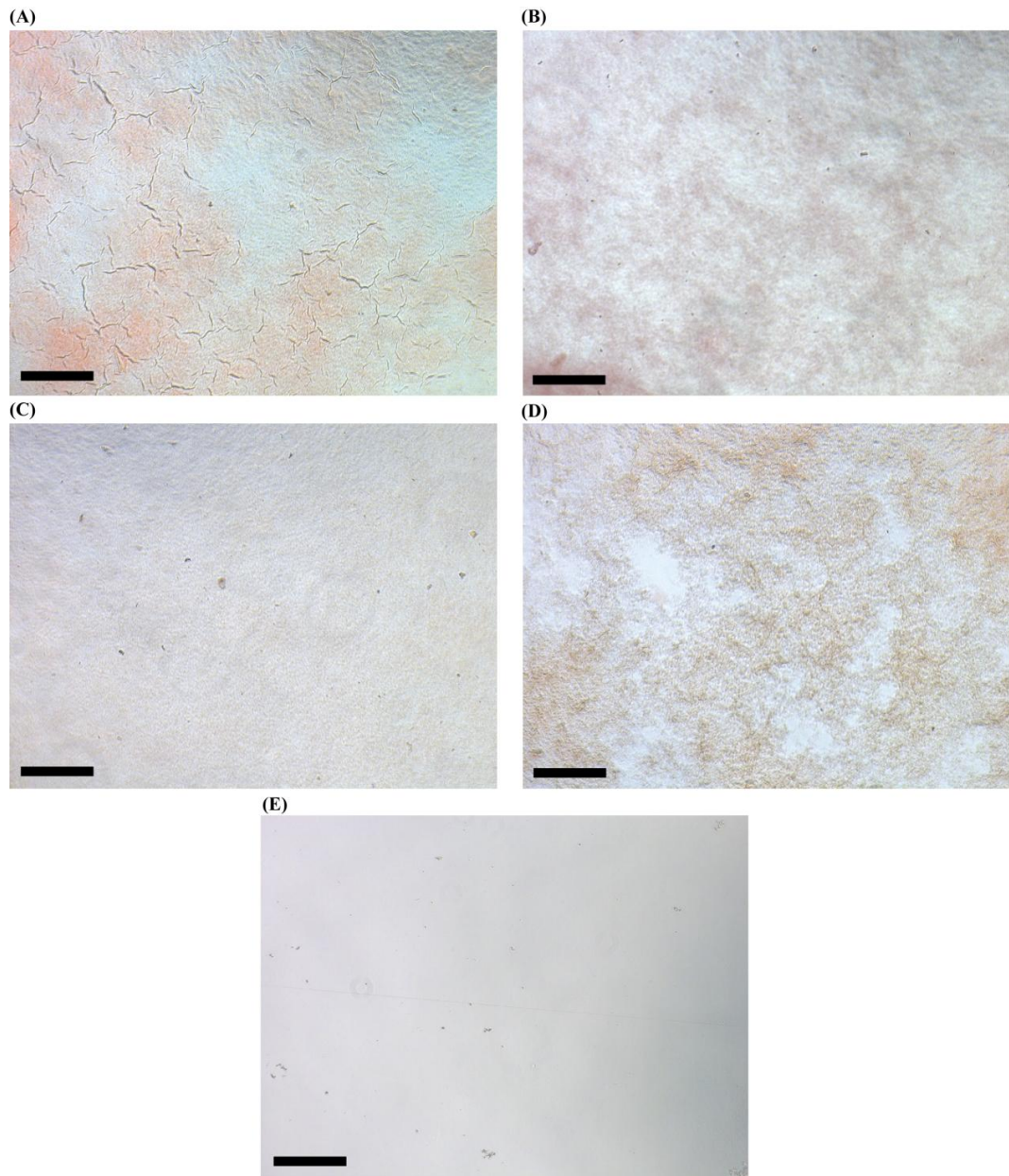


**Figure 3.17** Alizarin Red-S calcium staining of osteogenic differentiation medium without cells at day 14, conducted as a control for non-specific calcium deposition. **(A)** Glc-PA/E-PA, **(B)** Glc-PA/SO<sub>3</sub>-PA, **(C)** Glc-PA/SO<sub>3</sub>-PA/E-PA, **(D)** K-PA/E-PA and **(E)** TCP. (Scale bars = 200  $\mu$ m)

### 3.3.2 ALKALINE PHOSPHATASE ACTIVITY

Alkaline phosphatase activities of the cells seeded over different bio-functionalized nanofibrous networks were investigated for further characterization of the osteogenic differentiation of the rMSCs. Alkaline phosphatase (ALP) is a hydrolase enzyme which is responsible for the removal of phosphate groups from many types of molecules to produce inorganic phosphate<sup>105</sup>. It is demonstrated that it can be used in mineralization process<sup>106</sup>. It was also shown that alkaline phosphatase activity present in 3T3-L1 cells<sup>107</sup>. In another study, the relationship between ALP activity and cellular lipid accumulation in both human preadipocytes and 3T3-L1 cells was investigated by using Pearson correlation. It was demonstrated that there was a very strong positive correlation between ALP activity and intracellular lipid accumulation and therefore it was concluded that ALP activity can also be used as an indicator of intracellular lipid accumulation<sup>108</sup>. In a previous study, ALP activity was also shown in the plasma membrane of multivacuolar preadipocytes. They also demonstrated the correlation between ALP activity and size of preadipocytes and showed strong ALP activity in smaller preadipocytes, moderate ALP activity in intermediate sized preadipocytes and no ALP activity in unicellular mature fat cells and also in preadipocytes exceeding 120  $\mu\text{m}$  in largest diameter<sup>109</sup>. In this study, we tried to analyze the alkaline phosphatase activities of rat mesenchymal stem cells seeded over different peptide nanofiber networks and uncoated tissue culture plate. The peptide nanofiber networks used in this investigation were Glc-PA/E-PA, Glc-PA/SO<sub>3</sub>-PA, Glc-PA/SO<sub>3</sub>-PA/E-PA and K-PA/E-PA. ALP activities of the rMSCs were checked at day 3 and day 7, when the

cells were cultured with growth medium and osteogenic differentiation medium. To investigate ALP activity, protein extraction was performed to obtain whole protein samples from the cells. The protein concentrations of the cells were acquired from coupling of the absorbance values obtained from a microplate reader at 562 nm with the standard curve constituted by using known BSA standard (Figure 3.22). We also formed a standard curve by using *p*-nitrophenol (Figure 3.23) and used this curve to calculate the ALP activities of the rMSCs seeded over different microenvironments. We observed an increase in ALP activities of the cells seeded on Glc-PA/SO<sub>3</sub>-PA and Glc-PA/SO<sub>3</sub>-PA/E-PA nanofiber networks both at day 3 and day 7 compared to other nanofiber networks and uncoated tissue culture plate. We observed enhanced ALP activity from day 3 to day 7, and therefore, we concluded that adipogenic differentiation of the rMSCs proceeded through this time period.

To sum up, it was shown that rMSCs seeded over Glc-PA/SO<sub>3</sub>-PA and Glc-PA/SO<sub>3</sub>-PA/E-PA nanofiber networks exhibited higher ALP activities when compared to other groups. This increase in the ALP activity can be explained with the facts in literature which demonstrated enhancement in the ALP activity in the adipocytes. We did not observe any significant differences between Glc-PA/E-PA and K-PA/E-PA nanofiber networks and this might be explained with the ALP activities due to osteogenic differentiation of the cells over these peptidic scaffolds and Ca<sup>2+</sup> deposition. ALP activity on the Glc-PA/SO<sub>3</sub>-PA/E-PA network also might be caused by the dual effects of adipogenic and osteogenic differentiation of the rMSCs over this nanofiber network.

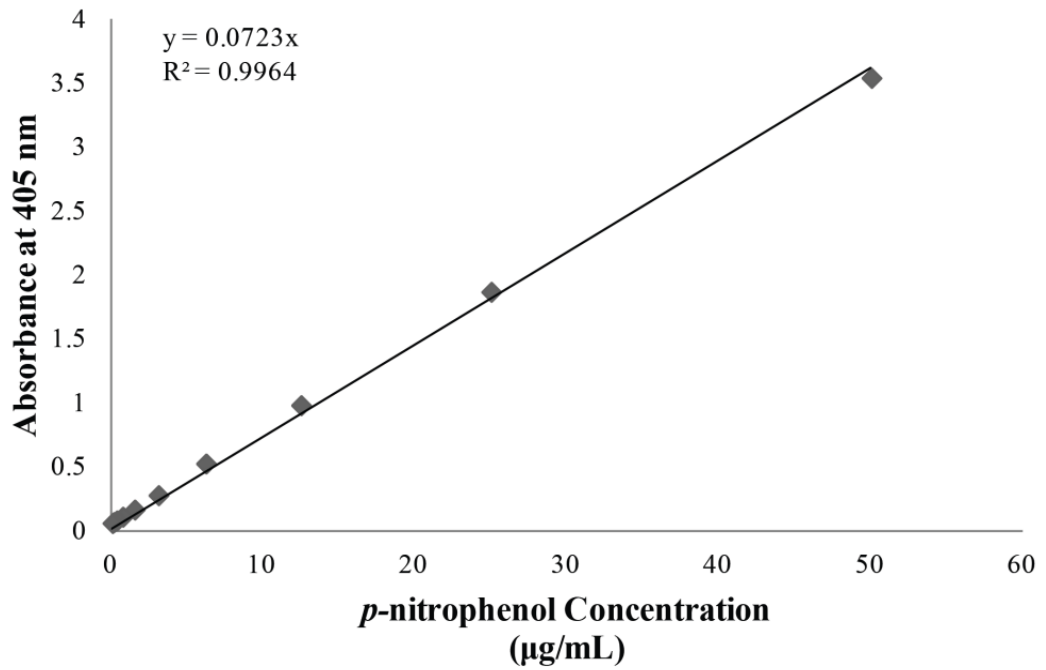


**Figure 3.18** *p*-nitrophenol standard curve obtained by using known *p*-nitrophenol standards. The standard curve was used to analyze the ALP activities of the rMSCs. The slope of the best line was 0.0723.

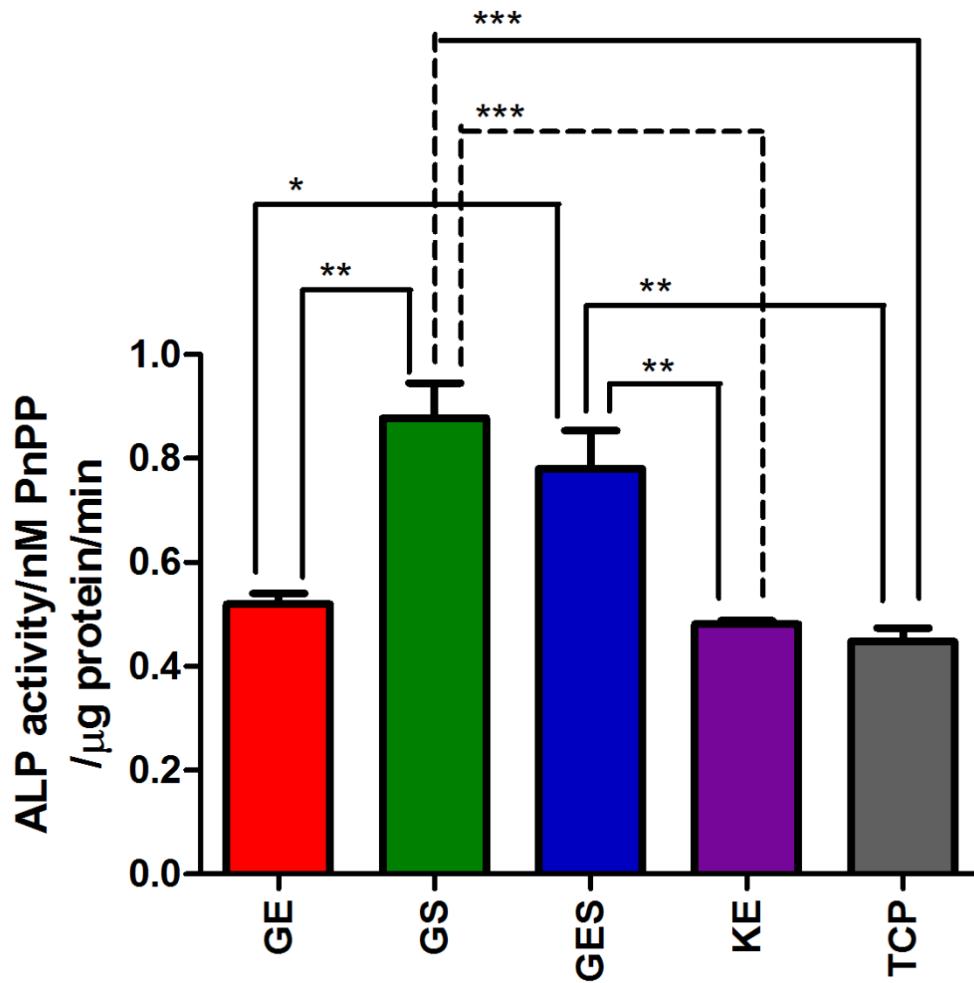


**Figure 3.19** Alkaline phosphatase activity of rat mesenchymal stem cells at day 3. Different nanofiber networks were used to investigate the changes in ALP activity according to the bio-functionality of the microenvironment. ALP activity of the rMSCs roughly correspond to the lipid accumulation characteristics of these cells. One-way ANOVA with Tukey post test was applied to analyze the results and significant differences were expressed as (\*  $p < 0.05$ , \*\*  $p < 0.01$  and \*\*\*  $p < 0.001$ ).

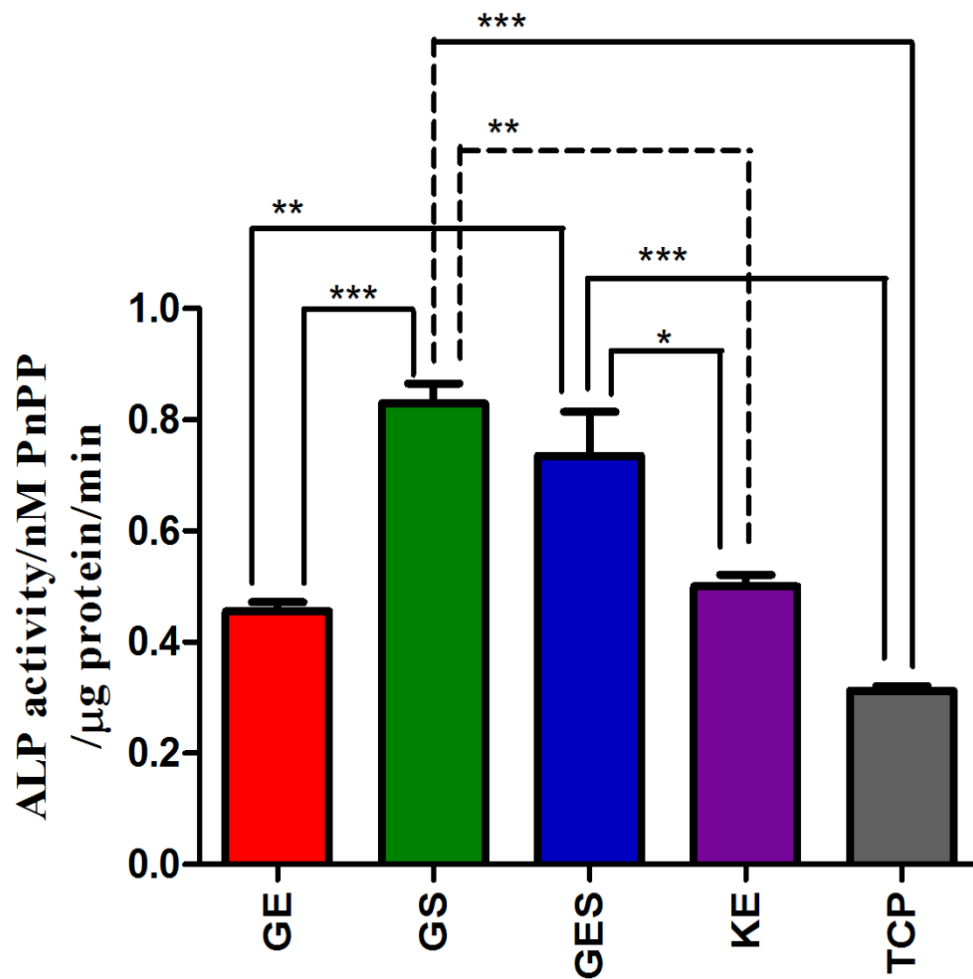


**Figure 3.20** Alkaline phosphatase activity of rat mesenchymal stem cells at day 7. Different nanofiber networks were used to investigate the changes in ALP activity according to the bio-functionality of the microenvironment. ALP activity of the rMSCs roughly correspond to the lipid accumulation characteristics of these cells. One-way ANOVA with Tukey post test was applied to analyze the results and significant differences were expressed as (\*  $p < 0.05$ , \*\*  $p < 0.01$  and \*\*\*  $p < 0.001$ ).

### **3.3.3 EXPRESSION LEVELS OF OSTEOGENIC DIFFERENTIATION MARKERS**

Gene expression profiles of rat mesenchymal stem cells cultured on peptide nanofiber networks coated and uncoated surfaces were analyzed in order to understand differential effects of various peptide nanofiber systems on the differentiation fate of the cells towards osteogenic lineage. Expression levels of two different genes were investigated for understanding differentiation fates of rat mesenchymal stem cells seeded over various peptide nanofiber networks. These genes were collagen 1 (COL1) and runt-related transcription factor 2. COL1 and RUNX2 expression were investigated to understand osteogenic differentiation of rat mesenchymal stem cells. These genes were examined at day 7 and day 14 when rMSCs were cultured with growth medium and osteogenic differentiation medium. COL1 expression level increases during osteogenic differentiation of mesenchymal stem cells <sup>110</sup>. In one study, it was demonstrated that discoidin domain receptor 1, a collagen activated receptor tyrosine kinase, took roles in the stem cell response to and interaction with three dimensional type I collagen, and the inhibition of this receptor caused a decrease in the osteogenic differentiation of the stem cells <sup>111</sup>. RUNX2 plays a crucial role in bone development and early stage of osteogenic differentiation of the pluripotent mesenchymal cells <sup>112</sup>. In this experiment, we observed that the expression levels of RUNX2 gene increased in the cells seeded over Glc-PA/E-PA and K-PA/E-PA networks due to osteochondral differentiation. However, it was still not enough for the cells to differentiate towards osteogenic lineage, and therefore the expression levels of COL1 gene, which directly correlate

with the RUNX2 expression level, did not enhance in all groups. In the experiments in which osteogenic medium was used, it was demonstrated cells responses to the microenvironment also changed according to their culturing conditions.

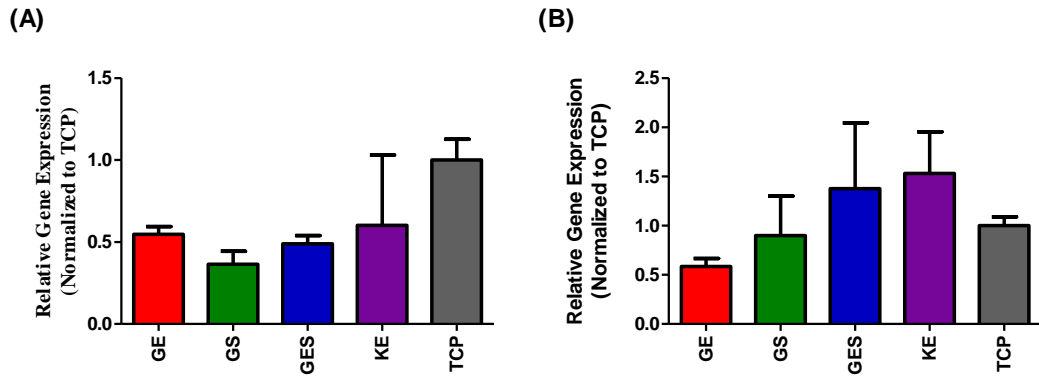


**Figure 3.21** Gene expression analyses of rat mesenchymal stem cells cultured on various nanofiber networks and tissue culture plate with growth medium at day 7. (A) RUNX2 and (B) COL1. The expression level of each gene was normalized against TCP and GAPDH, the latter of which was used as internal control.

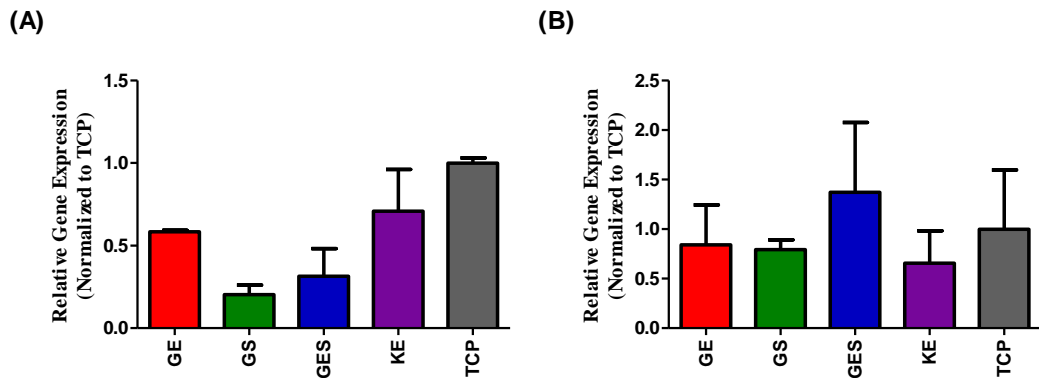


**Figure 3.22** Gene expression analyses of rat mesenchymal stem cells cultured on various nanofiber networks and tissue culture plate with growth medium at day 14. (A) RUNX2 and (B) COL1. The expression level of each gene was normalized against TCP and GAPDH, the latter of which was used as internal control.

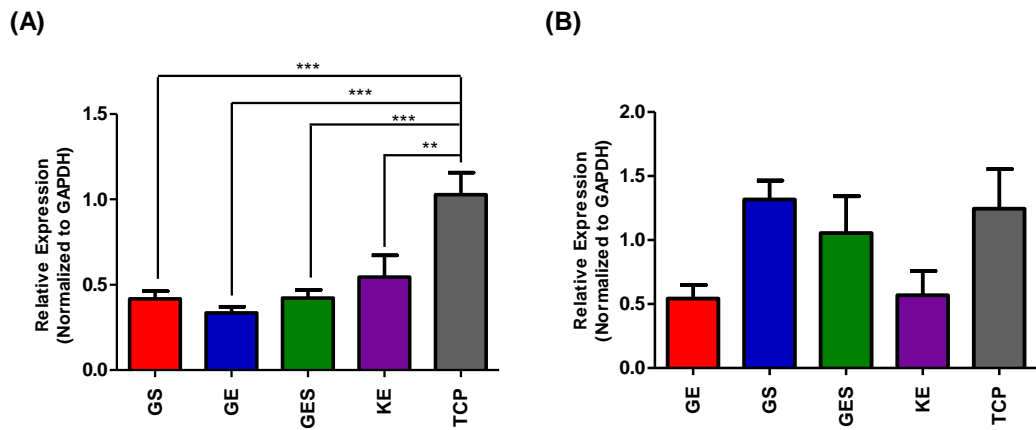


**Figure 3.23** Gene expression analyses of rat mesenchymal stem cells cultured on various nanofiber networks and tissue culture plate with osteogenic differentiation medium at day 7. **(A)** RUNX2 and **(B)** COL1. The expression level of each gene was normalized against TCP and GAPDH, the latter of which was used as internal control. One-way ANOVA with Tukey post test was applied to analyze the results and significant differences were expressed as (\*\*  $p < 0.01$  and \*\*\*  $p < 0.001$ ).

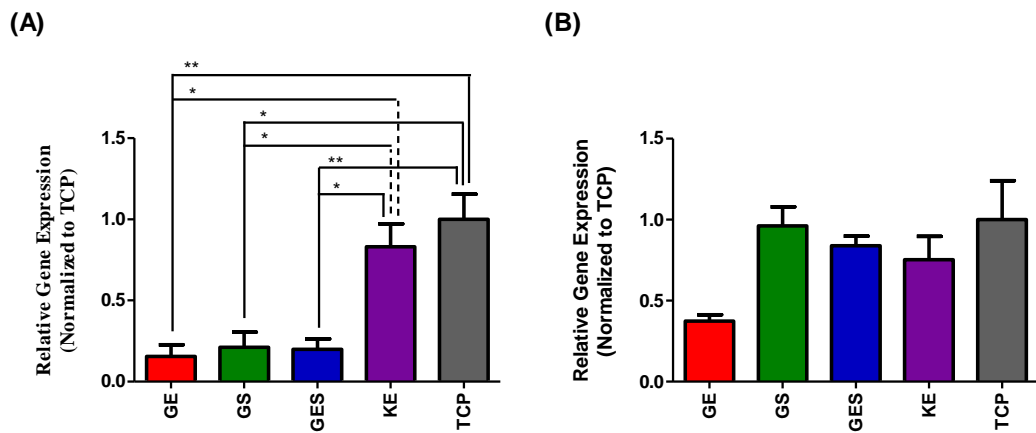


**Figure 3.24** Gene expression analyses of rat mesenchymal stem cells cultured on various nanofiber networks and tissue culture plate with osteogenic differentiation medium at day 14. **(A)** RUNX2 and **(B)** COL1. The expression level of each gene was normalized against TCP and GAPDH, the latter of which was used as internal

control. One-way ANOVA with Tukey post test was applied to analyze the results and significant differences were expressed as (\*  $p < 0.05$  and \*\*  $p < 0.01$ ).

Overall, osteogenic differentiation analyses showed that cells were induced to differentiate into osteogenic lineage more in the absence of sulfonate groups and presence of carboxylate groups, however, the qRT-PCR analyses results were not in correlation with alkaline phosphatase activity assay results. Since ALP activity is also increased during adipogenic differentiation, we further analyzed the cells for adipogenic activity.

### **3.3.4 NEUTRAL TRIGLYCERIDE AND LIPID PRODUCTION ANALYSES**

Oil Red-O staining was performed in order to visualize neutral triglycerides and lipids accumulations by rMSCs on different peptide nanofiber networks and uncoated tissue culture plate. We analyzed the neutral triglyceride and lipid depositions in cells cultured by using growth medium over functionalized nanofiber networks. Oil Red-O, which is a fat soluble diazole dye, stains neutral lipids and cholesteryl esters. It gives a maximum absorption at 518 nm and does not stain biological membranes<sup>113</sup>. The positive effect of glucose residues was observed on the accumulation of neutral lipid vacuoles, which is a sign of adipogenic differentiation. Furthermore, it was quantitatively demonstrated that the incorporation of sulfonate residues and carboxylate residues into the these functionalized platforms also contributed to adipogenic differentiation. We did not observed any significant difference in adipogenic differentiation between K-PA/E-PA nanofiber network and un-coated tissue culture plate which also supported this

conclusion. In one study, it was demonstrated that heparin can be used to promote adipocyte differentiation due to its dose dependent inhibitory effects on differentiation of osteoblast *in vitro* and inhibitory effects on the formation of bone *in vivo*<sup>114-115</sup>. In accordance with these reports, lipid accumulation started from day 7 over Glc-PA/SO<sub>3</sub>-PA and Glc-PA/SO<sub>3</sub>-PA/E-PA nanofiber networks in which osteogenic differentiation of the rat mesenchymal stem cells were diminished. We did not observe any lipid accumulation over K-PA/E-PA nanofiber network and uncoated tissue culture plates perhaps because these experimental groups did not contain enough functionalization which support adipogenic differentiation. We also observed that the significant difference between Glc-PA/SO<sub>3</sub>-PA nanofiber network and TCP and Glc-PA/SO<sub>3</sub>-PA/E-PA nanofiber network and TCP increased from day 7 to day 14, which was an indicator for the continuum of adipogenic differentiation.

To conclude, we found out that the nanofiber networks that formed from sulfonate residue containing peptide amphiphile molecules supported adipogenic differentiation of rMSCs cultured with growth medium. Furthermore, we also demonstrated that presence of glucose group in the microenvironment also supported the adipogenic differentiation of rMSCs however presence of sulfate group in the microenvironment started this differentiation earlier. We did not observe any lipid accumulation over K-PA/E-PA nanofiber network and uncoated tissue culture plate and therefore concluded that presence of glucose residue is the primary requirement for the adipogenic differentiation over our bio-functionalized nanofiber platforms.

### **3.3.5 EXPRESSION LEVELS OF ADIPOGENIC DIFFERENTIATION MARKERS**

Subsequent to lipid accumulation analyses with Oil Red-O staining, gene expression profiles of rat mesenchymal stem cells cultured on peptide nanofiber network coated and uncoated surfaces were further analyzed in order to understand differential effects of various peptide nanofiber systems on the differentiation fate of the cells towards adipogenic lineage. Expression levels of two different genes were investigated for understanding differentiation fates of rMSCs seeded over various peptide nanofiber networks. These genes were adiponectin (ADIPOQ) and fatty acid binding protein 4 (FABP4). These gene were examined at day 7 and day 14 when rMSCs were cultured with growth medium. Fatty acid binding proteins are a family of lipid binding transport proteins and they take roles in the regulation of fatty acid uptake and intracellular transport <sup>124</sup>. FABP4 which is also known as adipocyte protein 2 is the member of this family that is primarily expressed in adipocytes and macrophages <sup>125</sup>. Expression levels of FABP4 and ADIPOQ increase during the late stage of adipogenic differentiation <sup>126</sup>. In these experiments, the effects of glucose and sulfonate residues on the adipogenic differentiation of rMSCs were also illustrated at gene level by analyzing the expression levels of adiponectin and fatty acid binding protein 4 genes. The expression levels of both ADIPOQ and FABP4 were enhanced at day 7 and day 14 by the cells seeded over Glc-PA/E-PA, Glc-PA/SO<sub>3</sub>-PA and Glc-PA/SO<sub>3</sub>-PA/E-PA nanofiber networks and these increases in the gene expressions were related with the adipogenic differentiation of the rMSCs. The presence of glucose residue in the microenvironment had positive effect on the differentiation of rat mesenchymal stem cells. However, the presence of sulfonate

residue in the nanofibrous networks is also important and has positive effect on the lipid accumulation and adipogenic differentiation of the rat mesenchymal stem cells.

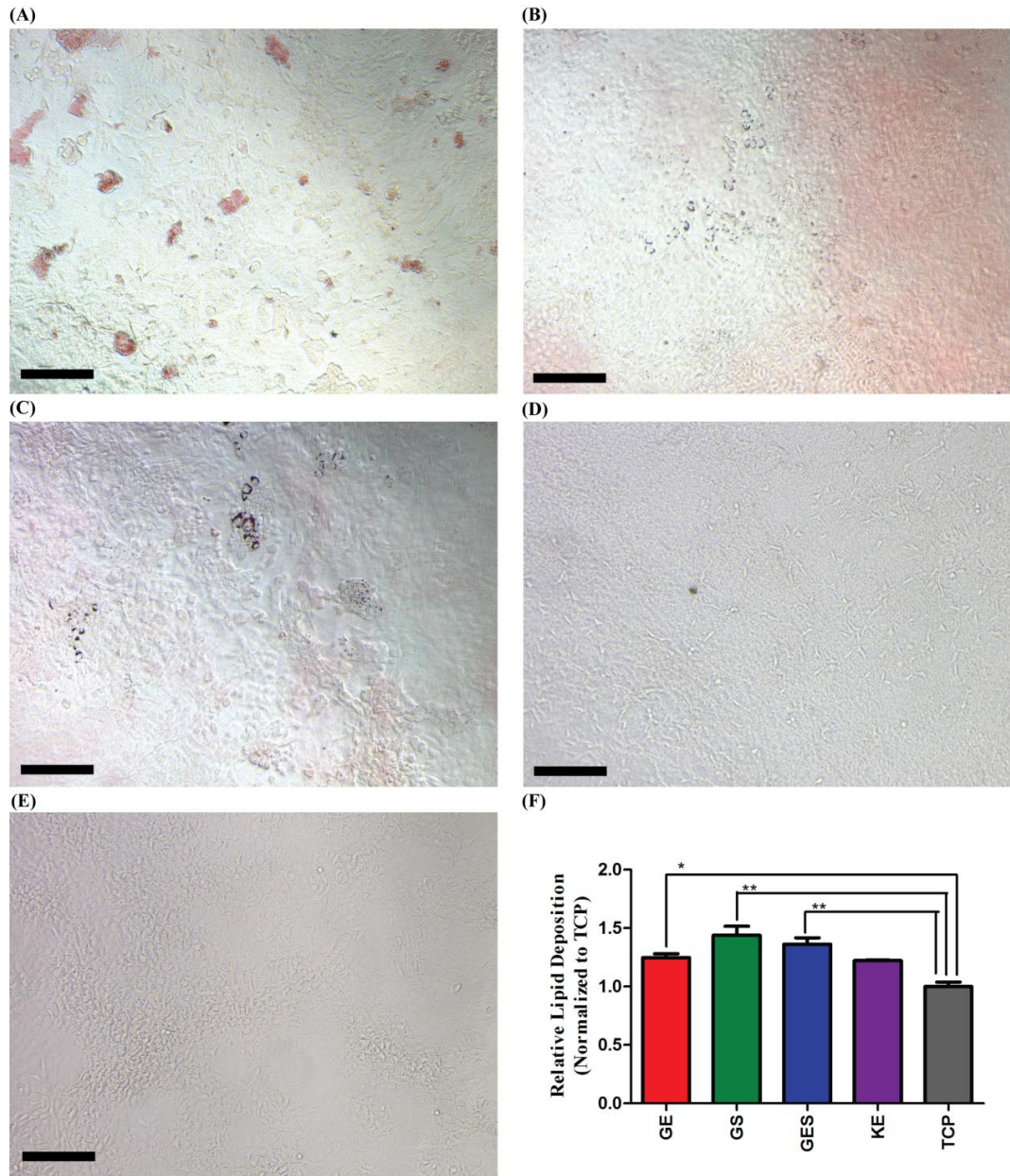


**Figure 3.25** Oil Red-O staining of cells in growth medium at day 7, showing the extent of lipid deposition. (A) Glc-PA/E-PA, (B) Glc-PA/SO<sub>3</sub>-PA, (C) Glc-PA/SO<sub>3</sub>-PA/E-PA, (D) K-PA/E-PA, (E) TCP and (F) Quantification of Oil Red O. One-way ANOVA with Tukey post test was applied to analyze the results and significant differences were expressed as (\* p<0.05 and \*\* p<0.01). (Scale bars = 200 μm)

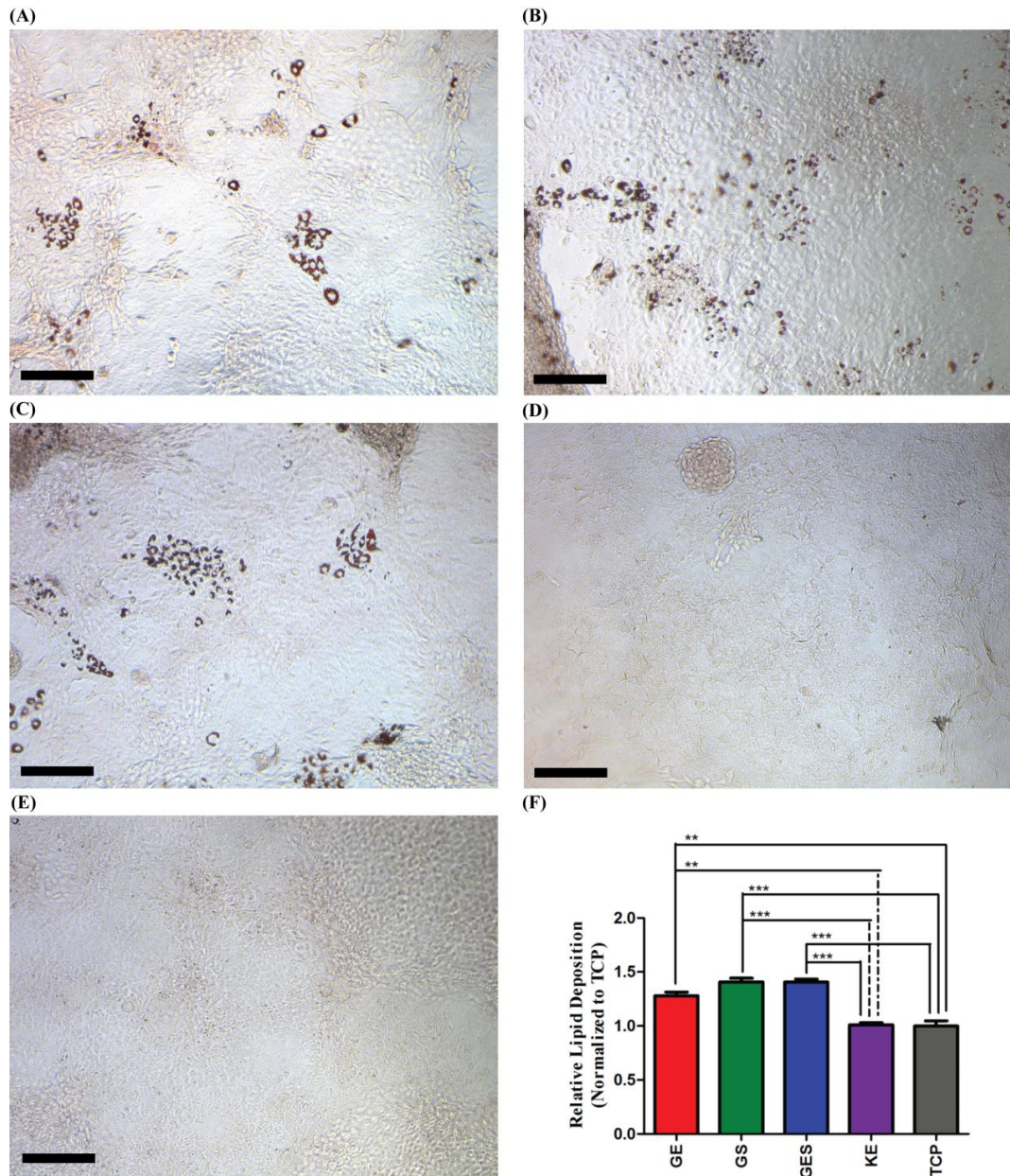


**Figure 3.26** Oil Red-O staining of cells in growth medium at day 14, showing the extent of lipid deposition. **(A)** Glc-PA/E-PA, **(B)** Glc-PA/SO<sub>3</sub>-PA, **(C)** Glc-PA/SO<sub>3</sub>-PA/E-PA, **(D)** K-PA/E-PA, **(E)** TCP and **(F)** Quantification of Oil Red O. One-way ANOVA with Tukey post test was applied to analyze the results and significant differences were expressed as (\*\* p<0.01 and \*\*\* p<0.001). (Scale bars = 200 μm)

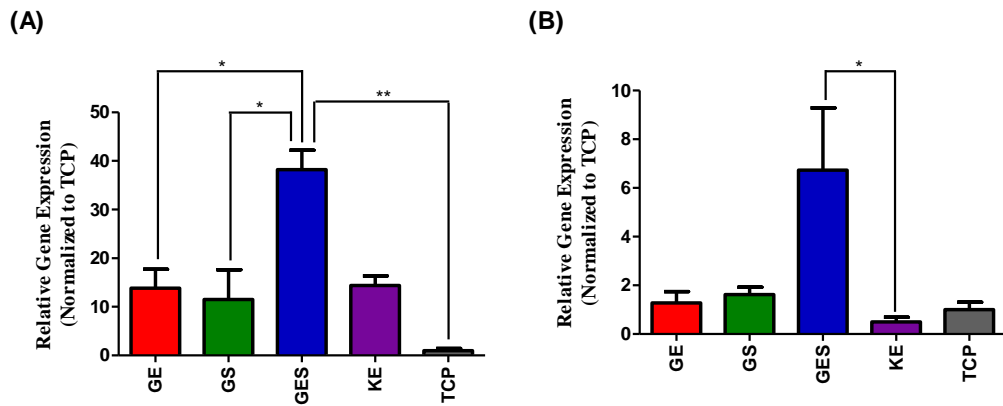


**Figure 3.27** Gene expression analyses of rat mesenchymal stem cells cultured on various nanofiber networks and tissue culture plate with growth medium at day 7. (A) FABP4 and (B) ADIPOQ. The expression level of each gene was normalized against TCP and GAPDH, the latter of which was used as internal control. One-way ANOVA with Tukey post test was applied to analyze the results and significant differences were expressed as (\*  $p < 0.05$  and \*\*  $p < 0.01$ ).

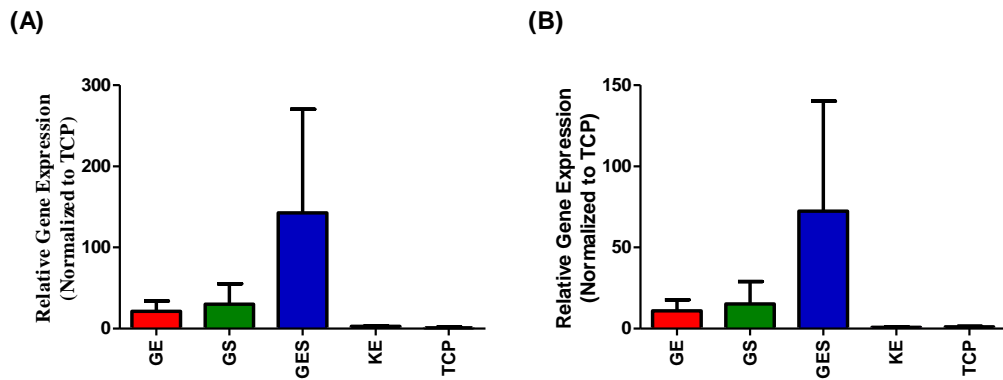


**Figure 3.28** Gene expression analyses of rat mesenchymal stem cells cultured on various nanofiber networks and tissue culture plate with growth medium at day 14. (A) FABP4 and (B) ADIPOQ. The expression level of each gene was normalized against TCP and GAPDH, the latter of which was used as internal control.

Overall, the adipogenic and osteogenic differentiation analyses showed that cells were induced to differentiate into adipogenic lineage in the presence of sulfonate groups and more to the osteogenic lineage in the absence of sulfonate groups in growth medium. Osteogenic differentiation of mesenchymal stem cells is strongly correlated with chondrogenic differentiation and these two pathways are altogether known as osteochondrogenic differentiation. Thus, we further analyzed the cells for the presence or absence of chondrogenic markers.

### **3.3.6 SULFATED GLYCOSAMINOGLYCAN PRODUCTION ANALYSES**

Finally, safranin-O staining was performed to investigate the chondrogenic differentiation of the cells, the last remaining mesodermal lineage that mesenchymal stem cells can also differentiate. It was used in order to visualize sulfated glycosaminoglycan accumulation by rMSCs that were seeded over different peptide nanofiber networks and uncoated tissue culture plate. Safranin-O staining has been used for many decades for the detection of articular cartilage formation<sup>116</sup>. Safranin-O is a cationic dye that binds to sulfated glycosaminoglycans specifically and stoichiometrically<sup>117</sup>. Therefore, secreted cartilaginous extracellular matrix can be indexed by Safranin-O staining and the intensity of staining is directly proportional to the glycosaminoglycan content. In this study, we analyzed the sulfated glycosaminoglycan depositions on peptide nanofiber networks at day 7 and day 14 when the cells cultured by using growth medium.

Nodule like structures were observed over Glc-PA/E-PA and K-PA/E-PA nanofiber networks at day 7 which were indicators of chondrogenic differentiation of

the mesenchymal stem cells (Figure 3.18). We also observed formation of small nodule like structures over Glc-PA/SO<sub>3</sub>-PA/E-PA nanofiber network at day 14 in addition to Glc-PA/E-PA and K-PA/E-PA nanofiber networks. For each experimental day (Day 7 and Day 14), we did not observe any cell aggregation which showed resemblance to cartilage formation and positive Safranin-O staining over Glc-PA/SO<sub>3</sub>-PA nanofiber network. Glc-PA/E-PA network system mimic hyaluronan. During embryonic cartilage development, hyaluronan can be found in high amounts in the ECM of the cells and it also takes roles in and assist the integration of engineered cartilage tissues <sup>118</sup>. Therefore cells seeded over this scaffold had a tendency towards chondrogenic lineage. We also observed nodule-like structures over K-PA/E-PA nanofiber network and this could be explained due to structural similarity between this network and Glc-PA/E-PA network. We analyzed small nodule-like structures over Glc-PA/SO<sub>3</sub>-PA/E-PA nanofiber network in Safranin-O staining at day 14. We thought this functionalized network system resembled chondroitin sulfate glycosaminoglycan. In a study, it was shown that integration of chondroitin sulfate into scaffold may promote secretion of collagen 2 and proteoglycans <sup>119</sup>. In another research, it was also demonstrated that bone marrow derived mesenchymal stem cells in chondroitin sulfate based bioactive hydrogels aggregated in such a way that produced cartilaginous tissues <sup>120</sup>. On Glc-PA/SO<sub>3</sub>-PA nanofiber network and uncoated tissue culture plate, we did not observe any Safranin-O staining and concluded that there was no chondrogenesis over these groups. Thus, elevated sulfonate residues per glucose levels in the nanofiber network platform might cause a decrease in the differentiation of rMSCs towards chondrogenic lineage.

To sum up, Glc-PA/E-PA and K-PA/E-PA nanofiber networks supported chondrogenic differentiation starting from day 7 and continued this support still at the end of day 14. While over Glc-PA/SO<sub>3</sub>-PA/E-PA nanofiber network, differentiation of rMSCs toward chondrogenic lineage was only observed at the end of day 14, in which we concluded that over Glc-PA/E-PA and K-PA/E-PA nanofiber networks chondrogenic differentiation was enhanced compared to Glc-PA/SO<sub>3</sub>-PA/E-PA bioactive scaffold. Finally, we did not observe any differentiation towards chondrogenic lineage on Glc-PA/SO<sub>3</sub>-PA and uncoated tissue culture plate.

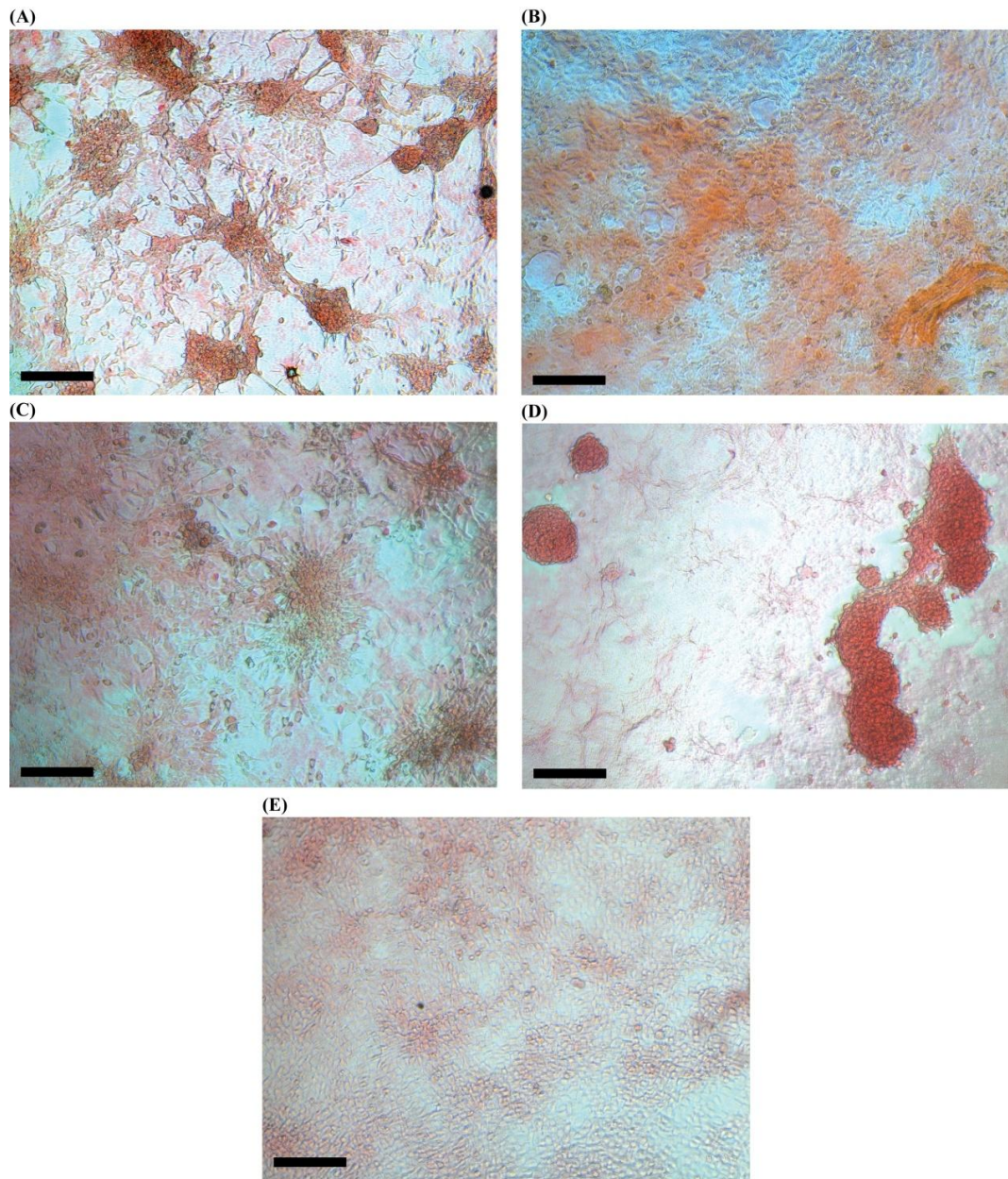


**Figure 3.29** Safranin-O staining at day 7 for the analysis of sulfated glycosaminoglycan incorporation. Cells were cultured with growth medium. (A) Glc-PA/E-PA, (B) Glc-PA/SO<sub>3</sub>-PA, (C) Glc-PA/SO<sub>3</sub>-PA/E-PA, (D) K-PA/E-PA and (E) TCP. (Scale bars = 200  $\mu$ m)

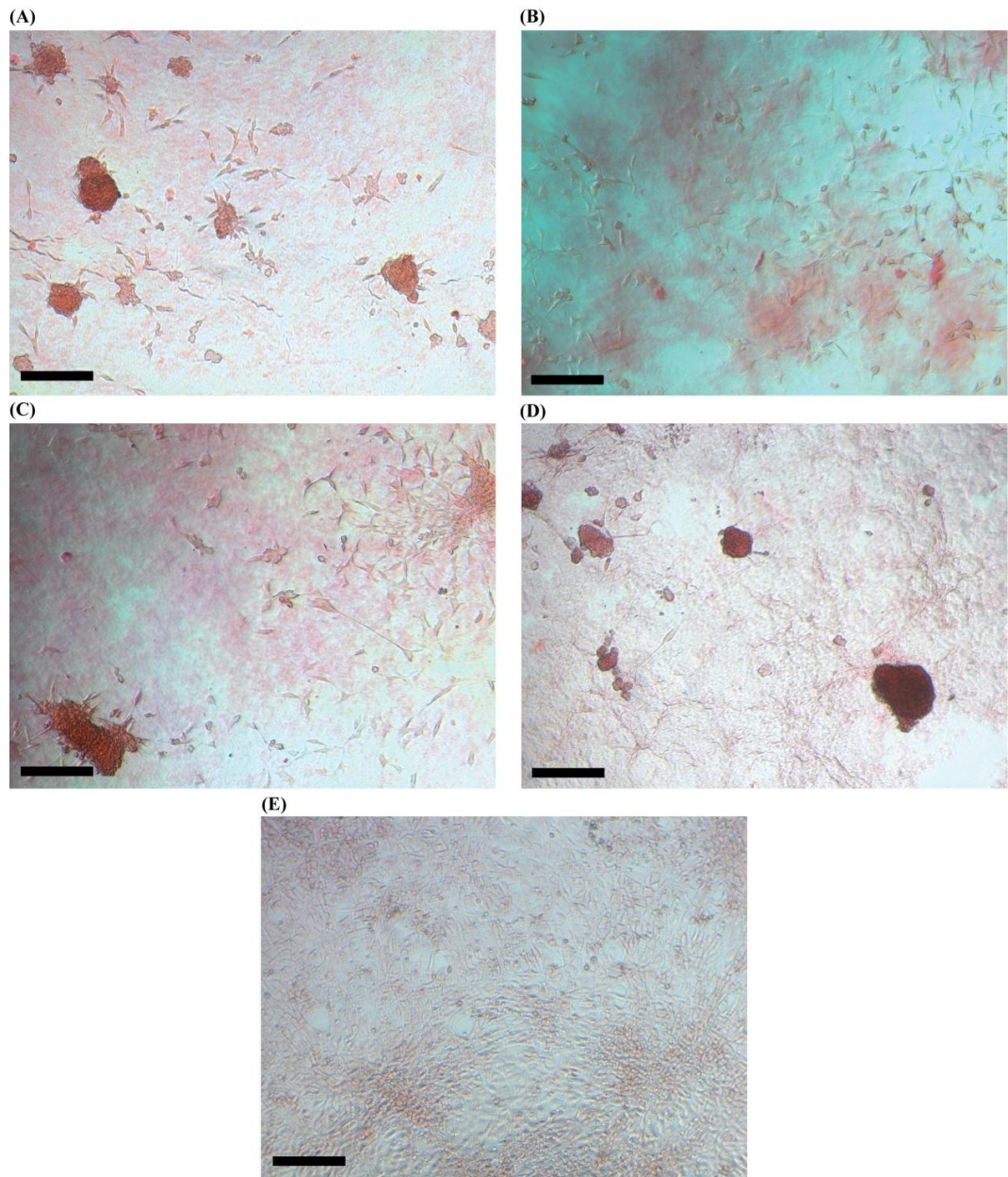


**Figure 3.30** Safranin-O staining at of cells in growth medium at day 7, showing the extent of sulfated glycosaminoglycan incorporation. (A) Glc-PA/E-PA, (B) Glc-PA/SO<sub>3</sub>-PA, (C) Glc-PA/SO<sub>3</sub>-PA/E-PA, (D) K-PA/E-PA and (E) TCP. (Scale bars = 200  $\mu$ m)

### **3.3.7 EXPRESSION LEVELS OF CHONDROGENIC DIFFERENTIATION MARKERS**

Following to sulfated glycosaminoglycan deposition analyses with safranin-O staining, gene expression profiles of rMCSs cultured on peptide nanofiber network coated and uncoated surfaces were analyzed in order to further investigate the differentiation potential of the cells towards chondrogenic lineage. Expression levels of two different genes were investigated for understanding differentiation fates of rMSCs seeded over various peptide nanofiber networks towards chondrogenic lineage. These genes were collagen 2 (COL2) and transcription factor *SOX-9* (SOX9). COL2 and SOX9 expression were analyzed to understand chondrogenic differentiation of rMSCs. Collagens, a multigene family, are structural proteins found in the extracellular matrix <sup>121</sup>. COL2/COL1 ratio decreases during the late phase of chondrogenic differentiation which means expression level of collagen 1 starts to increase compared to collagen 2 expression level <sup>122</sup>. Increase in the expression level of SOX9 is correlated to a high expression of collagen 2 in mesenchymal stem cells <sup>123</sup>. It was shown that the expression level of SOX9 gene increased at day 7 in the cells seeded over Glc-PA/E-PA and K-PA/E-PA nanofiber networks and the expression level of COL1 gene increased at day 14 in the cells seeded over Glc-PA/E-PA nanofiber network. These results were related with the early stage of chondrogenic differentiation in which SOX9 expression starts to increase and induces COL2 expression for fully differentiation. qRT-PCR analyses of these markers and osteogenic markers demonstrated that rMSCs seeded on Glc-PA/E-PA

and K-PA/E-PA networks started to differentiate by using osteochondral differentiation pathway.

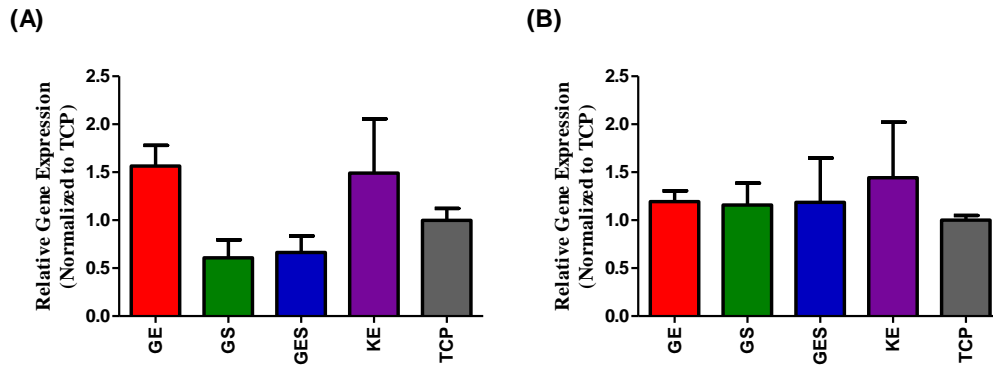


**Figure 3.31** Gene expression analyses of rat mesenchymal stem cells cultured on various nanofiber networks and tissue culture plate with growth medium at day 7. **(A)** SOX9 and **(B)** COL2. The expression level of each gene was normalized against TCP and GAPDH, the latter of which was used as internal control.

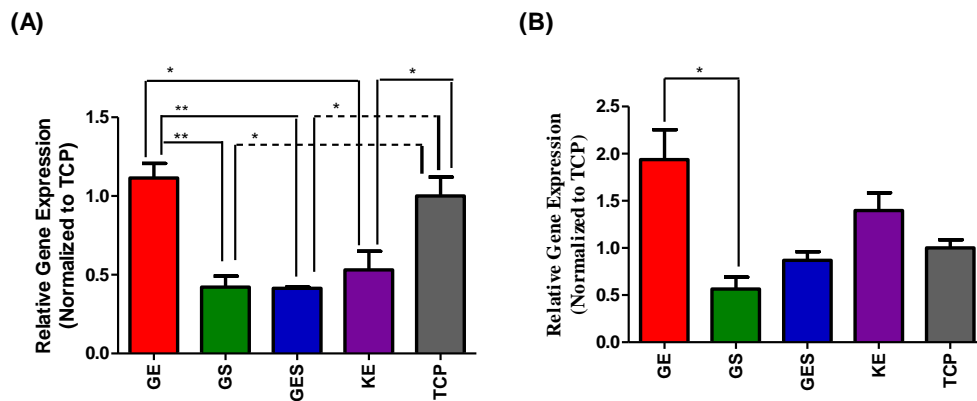


**Figure 3.32** Gene expression analyses of rat mesenchymal stem cells cultured on various nanofiber networks and tissue culture plate with growth medium at day 14. **(A)** SOX9 and **(B)** COL2. The expression level of each gene was normalized against TCP and GAPDH, the latter of which was used as internal control. One-way ANOVA with Tukey post test was applied to analyze the results and significant differences were expressed as (\*  $p < 0.05$  and \*\*  $p < 0.01$ ).

## **CHAPTER 4**

### **CONCLUSION AND FUTURE PERSPECTIVES**

The microenvironment of the cells is composed of various fibrous proteins and glycosaminoglycans in the form of proteoglycans. It is crucial to mimic the glycosaminoglycan content of the extracellular matrix to control the differentiation fate of the mesenchymal stem cells. Peptide amphiphile molecules provide good opportunities to mimic the native ECM microenvironments of the cells. They can form long nanofibrous networks due to their self-assembly properties and can be modified with various biological signals to mimic ECM of different tissue types.

In this study, we tried to form glycosaminoglycan mimetic nanofibrous networks by using four different peptide amphiphile molecules. These peptide amphiphile molecules contained different chemical groups including glucose, sulfonate and carboxylate on their peptide backbone. We controlled the amount of chemical groups in the microenvironment by changing the concentration of the molecules. By this way, we constituted different ECM mimetic systems where we tested the changes in the differentiation potentials of the rat mesenchymal stem cells. We demonstrated that when the degree of sulfonation increased in the nanofibrous networks, the rat mesenchymal stem cells started to differentiate towards adipogenic lineage and when the degree of carboxylation increased in the nanofibrous networks, the cells started to differentiate towards osteochondrogenic lineages. We also demonstrated that the presence of glucose residues in the microenvironment as attached to the peptide nanofibers drastically decreases the proliferation of rat mesenchymal stem cells and perhaps contributes to the specialization and differentiation of these cells.

Overall, this study offers a general strategy for the development of functional peptide nanofiber platforms for mimicking sulfated and non-sulfated natural

glycosaminoglycans. It was demonstrated that well ordered peptidic nanostructures can be formed by using various self-assembled nanofibers which were formed by using bottom-up design strategy. It was also shown that the content of the nanofiber networks can be controlled according to the demand and application of interests. As a future perspective, differentiation of the rat mesenchymal stem cells can be further characterized by using flow cytometry. With this technique, we can quantify the percentage of differentiated cells in the nanofibrous microenvironments by labeling specific surface markers of the cells according to their differentiation states. The effects of glucose, sulfonate or carboxylate residue containing peptide amphiphile molecules on the differentiation fates of rat mesenchymal stem cells can be also examined by supplying these molecules as a soluble factor when the cells are seeded over non-bioactive scaffolds. With this experiment, we can test the response of the cells when their surroundings are saturated with a specific differentiation signal. We can further analyze the differentiation pathways activated in mesenchymal stem cells by these peptide nanofiber networks with surface receptor blocking experiments. The amounts of calcium, lipid and/or sulfated glycosaminoglycan depositions can also be adjusted to the DNA concentration in the microenvironments for obtaining more accurate and specific differentiation results. The differentiation diversities of the rat mesenchymal stem cells even in the same microenvironment can be demonstrated with immunocytochemistry. Finally, the efficiency of cell differentiation and future success of these functionalized platforms can be tested and evaluated with an *in vivo* study and further translated into clinical studies.

## BIBLIOGRAPHY

- 1 Daar, A. S. & Greenwood, H. L. A proposed definition of regenerative medicine. *Journal of tissue engineering and regenerative medicine* **1**, 179-184, doi:10.1002/term.20 (2007).
- 2 Lennard, A. L. & Jackson, G. H. Stem cell transplantation. *Bmj* **321**, 433-437 (2000).
- 3 Cima, L. G., Vacanti, J. P. & Vacanti, C. Tissue engineering by cell transplantation using degradable polymer substrates. *Journal of ...* (1991).
- 4 Mertsching, H., Walles, T., Hofmann, M. & Schanz, J. Engineering of a vascularized scaffold for artificial tissue and organ generation. *Biomaterials* (2005).
- 5 Zhou, Q. & Melton, D. A. Extreme makeover: converting one cell into another. *Cell Stem Cell* (2008).
- 6 Stocum, D. L. *Regenerative Biology and Medicine*. (Academic Press, 2012).
- 7 Berthiaume, F., Maguire, T. J. & Yarmush, M. L. Tissue engineering and regenerative medicine: history, progress, and challenges. *Annual review of chemical and biomolecular engineering* **2**, 403-430, doi:10.1146/annurev-chembioeng-061010-114257 (2011).
- 8 Lee, E. H. & Hui, J. H. P. The potential of stem cells in orthopaedic surgery. *Journal of Bone & Joint Surgery*, doi:10.1302/0301-620x.88b7.17305 (2006).
- 9 Takebe, T., Sekine, K., Enomura, M., Koike, H. & Kimura, M. Vascularized and functional human liver from an iPSC-derived organ bud transplant. *Nature*, doi:10.1038/nature12271 (2013).
- 10 Yan, Y. *et al.* Fabrication of viable tissue-engineered constructs with 3D cell-assembly technique. *Biomaterials* **26**, 5864-5871 (2005).
- 11 Längle, D., Halver, J., Rathmer, B. & Willems, E. Small molecules targeting in vivo tissue regeneration. *ACS chemical ...*, doi:10.1021/cb4008277 (2014).
- 12 Zhu, S., Wei, W. & Ding, S. Chemical strategies for stem cell biology and regenerative medicine. *Annual review of biomedical engineering*, doi:10.1146/annurev-bioeng-071910-124715 (2011).
- 13 Chambers, S. M., Fasano, C. A. & Papapetrou, E. P. Highly efficient neural conversion of human ES and iPS cells by dual inhibition of SMAD signaling. *Nature ...*, doi:10.1038/nbt.1529 (2009).
- 14 Wu, X., Ding, S., Ding, Q. & Gray, N. S. A small molecule with osteogenesis-inducing activity in multipotent mesenchymal progenitor cells. *Journal of the American ...*, doi:10.1021/ja0283908 (2002).
- 15 Russell, J. L., Goetsch, S. C. & Aguilar, H. R. Targeting native adult heart progenitors with cardiogenic small molecules. *ACS chemical ...*, doi:10.1021/cb200525q (2012).
- 16 MacMillan, K. S., Naidoo, J., Liang, J. & Melito, L. Development of proneurogenic, neuroprotective small molecules. *Journal of the ...*, doi:10.1021/ja108211m (2011).
- 17 Caplan, A. I. & Bruder, S. P. Mesenchymal stem cells: building blocks for molecular medicine in the 21st century. *Trends in molecular medicine* (2001).

- 18 Pittenger, M. F., Mackay, A. M., Beck, S. C. & Jaiswal, R. K. Multilineage potential of adult human mesenchymal stem cells. *science*, doi:10.1126/science.284.5411.143 (1999).
- 19 Mackay, A. M., Beck, S. C., Murphy, J. M. & Barry, F. P. Chondrogenic differentiation of cultured human mesenchymal stem cells from marrow. *Tissue ...*, doi:10.1089/ten.1998.4.415 (1998).
- 20 Bruder, S. P., Jaiswal, N. & Ricalton, N. S. Mesenchymal stem cells in osteobiology and applied bone regeneration. ... *and related research*, doi:10.1097/00003086-199810001-00025 (1998).
- 21 Dominici, M., Blanc, L. K., Mueller, I. & Slaper-Cortenbach, I. Minimal criteria for defining multipotent mesenchymal stromal cells. The International Society for Cellular Therapy position statement. *Cytotherapy* (2006).
- 22 Cohnheim, J. Ueber entzündung und eiterung. *Virchows Archiv* (1867).
- 23 Friedenstein, A. J. & Gorskaja, J. F. Fibroblast precursors in normal and irradiated mouse hematopoietic organs. *Experimental ...* (1976).
- 24 Mafi, R., Hindocha, S., Mafi, P. & Griffin, M. Suppl 2: Sources of Adult Mesenchymal Stem Cells Applicable for Musculoskeletal Applications-A Systematic Review of the Literature. *The open orthopaedics ...* (2011).
- 25 Paul, S. F., Sandra, P., Daniel, L. & Christoph, S. Mesenchymal stem cell: keystone of the hematopoietic stem cell niche and a stepping-stone for regenerative medicine. *Annual review of immunology* **31**, 285-316 (2013).
- 26 Digirolamo, C. M. *et al.* Propagation and senescence of human marrow stromal cells in culture: a simple colony-forming assay identifies samples with the greatest potential to propagate and differentiate. *British journal of haematology* **107**, 275-281 (1999).
- 27 D'Ippolito, G., Schiller, P. C., Ricordi, C., Roos, B. A. & Howard, G. A. Age-related osteogenic potential of mesenchymal stromal stem cells from human vertebral bone marrow. *Journal of bone and mineral research : the official journal of the American Society for Bone and Mineral Research* **14**, 1115-1122, doi:10.1359/jbmr.1999.14.7.1115 (1999).
- 28 Oreffo, R. O. C., Bord, S. & Triffitt, J. T. Skeletal progenitor cells and ageing human populations. *Clinical Science* (1998).
- 29 Murphy, J. M., Dixon, K., Beck, S. & Fabian, D. Reduced chondrogenic and adipogenic activity of mesenchymal stem cells from patients with advanced osteoarthritis. *Arthritis & ...*, doi:10.1002/art.10118 (2002).
- 30 Lodie, T. A., Blickarz, C. E. & Devarakonda, T. J. Systematic analysis of reportedly distinct populations of multipotent bone marrow-derived stem cells reveals a lack of distinction. *Tissue ...*, doi:10.1089/10763270260424105 (2002).
- 31 Barry, F., Boynton, R. E., Liu, B. & Murphy, J. M. Chondrogenic differentiation of mesenchymal stem cells from bone marrow: differentiation-dependent gene expression of matrix components. *Experimental cell research* (2001).
- 32 Bruder, S. P. *et al.* Bone regeneration by implantation of purified, culture-expanded human mesenchymal stem cells. *Journal of orthopaedic research : official publication of the Orthopaedic Research Society* **16**, 155-162, doi:10.1002/jor.1100160202 (1998).

- 33 Jaiswal, R. K., Jaiswal, N., Bruder, S. P. & Mbalaviele, G. Adult human mesenchymal stem cell differentiation to the osteogenic or adipogenic lineage is regulated by mitogen-activated protein kinase. *Journal of Biological ...*, doi:10.1074/jbc.275.13.9645 (2000).
- 34 Mesenchymal stem cells: clinical applications and biological characterization. *The International Journal of Biochemistry & Cell Biology* **36**, doi:10.1016/j.biocel.2003.11.001 (2004).
- 35 Frantz, C., Stewart, K. M. & Weaver, V. M. The extracellular matrix at a glance. *Journal of cell science*, doi:10.1242/jcs.023820 (2010).
- 36 Xian, X., Gopal, S. & Couchman, J. R. Syndecans as receptors and organizers of the extracellular matrix. *Cell and tissue research*, doi:10.1007/s00441-009-0829-3 (2010).
- 37 Harburger, D. S. & Calderwood, D. A. Integrin signalling at a glance. *Journal of cell science*, doi:10.1242/jcs.018093 (2009).
- 38 Schmidt, S. & Friedl, P. Interstitial cell migration: integrin-dependent and alternative adhesion mechanisms. *Cell and tissue research*, doi:10.1007/s00441-009-0892-9 (2010).
- 39 Alberts, B. *et al. Essential Cell Biology, Fourth Edition.* (Taylor & Francis Group, 2013).
- 40 Rozario, T. & DeSimone, D. W. The extracellular matrix in development and morphogenesis: a dynamic view. *Developmental biology* (2010).
- 41 Gordon, M. K. & Hahn, R. A. Collagens. *Cell and tissue research*, doi:10.1007/s00441-009-0844-4 (2010).
- 42 Smith, M. L., Gourdon, D., Little, W. C. & Kubow, K. E. Force-induced unfolding of fibronectin in the extracellular matrix of living cells. *PLoS biology*, doi:10.1371/journal.pbio.0050268 (2007).
- 43 Tsang, K. Y., Cheung, M. C. H., Chan, D. & Cheah, K. S. E. The developmental roles of the extracellular matrix: beyond structure to regulation. *Cell and tissue research*, doi:10.1007/s00441-009-0893-8 (2010).
- 44 Kim, S. H., Turnbull, J. & Guimond, S. Extracellular matrix and cell signalling: the dynamic cooperation of integrin, proteoglycan and growth factor receptor. *Journal of Endocrinology* (2011).
- 45 Murray, R. K., Granner, D. K., Mayes, P. A. & Rodwell, V. W. *Harper's Illustrated Biochemistry.* (McGraw-Hill, 2003).
- 46 Nelson, D. L. & Cox, M. M. *Lehninger Principles of Biochemistry.* (W.H. Freeman, 2013).
- 47 Sasisekharan, R. & Raman, R. Glycomics approach to structure-function relationships of glycosaminoglycans. *Annu. Rev. Biomed. ...*, doi:10.1146/annurev.bioeng.8.061505.095745 (2006).
- 48 Fraser, J. R. E. & Laurent, T. C. Hyaluronan: its nature, distribution, functions and turnover. *Journal of internal ...*, doi:10.1046/j.1365-2796.1997.00170.x (1997).
- 49 Nikitovic, D., Zafiroopoulos, A. & Tzanakakis, G. N. Effects of glycosaminoglycans on cell proliferation of normal osteoblasts and human osteosarcoma cells depend on their type and fine chemical compositions. *Anticancer ...* (2005).

- 50 Gorio, A., Lesma, E. & Vergani, L. Glycosaminoglycan supplementation promotes nerve regeneration and muscle reinnervation. *European journal of ...*, doi:10.1111/j.1460-9568.1997.tb01532.x (1997).
- 51 Antonio, J. D. S., Winston, B. M. & Tuan, R. S. Regulation of chondrogenesis by heparan sulfate and structurally related glycosaminoglycans. *Developmental biology* (1987).
- 52 Salbach, J., Rachner, T. D., Rauner, M. & Hempel, U. Regenerative potential of glycosaminoglycans for skin and bone. *Journal of molecular ...*, doi:10.1007/s00109-011-0843-2 (2012).
- 53 Norrby, K. & Sörbo, J. Heparin enhances angiogenesis by a systemic mode of action. *International journal of experimental pathology* (1992).
- 54 Sasisekharan, R., Shriver, Z. & Venkataraman, G. Roles of heparan-sulphate glycosaminoglycans in cancer. *Nature Reviews ...*, doi:10.1038/nrc842 (2002).
- 55 Roden, L. Structure and metabolism of connective tissue proteoglycans. *The biochemistry of glycoproteins and proteoglycans*, doi:10.1007/978-1-4684-1006-8\_7 (1980).
- 56 Laurent, T. C. & Fraser, J. R. Hyaluronan. *The FASEB Journal* (1992).
- 57 Jiang, D., Liang, J. & Noble, P. W. Hyaluronan in tissue injury and repair. *Annu. Rev. Cell Dev. Biol.*, doi:10.1146/annurev.cellbio.23.090506.123337 (2007).
- 58 Gilbert, M. E., Kirker, K. R., Gray, S. D. & Ward, P. D. Chondroitin sulfate hydrogel and wound healing in rabbit maxillary sinus mucosa. *The ...*, doi:10.1097/00005537-200408000-00017 (2004).
- 59 Iozzo, R. V. & Murdoch, A. D. Proteoglycans of the extracellular environment: clues from the gene and protein side offer novel perspectives in molecular diversity and function. *The FASEB Journal* (1996).
- 60 Baeurle, S. A., Kiselev, M. G., Makarova, E. S. & Nogovitsin, E. A. Effect of the counterion behavior on the frictional–compressive properties of chondroitin sulfate solutions. *Polymer* (2009).
- 61 Kwok, J. C. F., Warren, P. & Fawcett, J. W. Chondroitin sulfate: a key molecule in the brain matrix. *... journal of biochemistry & cell biology* (2012).
- 62 Galtrey, C. M. & Fawcett, J. W. The role of chondroitin sulfate proteoglycans in regeneration and plasticity in the central nervous system. *Brain research reviews* (2007).
- 63 Trowbridge, J. M. & Gallo, R. L. Dermatan sulfate: new functions from an old glycosaminoglycan. *Glycobiology*, doi:10.1093/glycob/cwf066 (2002).
- 64 Singla, S. K. Dermatan sulphate: Structure, biosynthesis and functions. *Biochemical Education*, doi:10.1016/0307-4412(88)90192-6 (1988).
- 65 Shinmyozu, K., Takahashi, T. & Ariyoshi, W. Dermatan sulfate inhibits osteoclast formation by binding to receptor activator of NF-κB ligand. *Biochemical and ...* (2007).
- 66 Vitale, C., Verdecchia, C., Bagnis, C. & Ganzaroli, M. Effects of dermatan sulfate for anticoagulation in continuous renal replacement therapy. *Journal of ...* (2008).

- 67 Dreyfuss, J. L., Regatieri, C. V. & Jarrouge, T. R. Heparan sulfate proteoglycans: structure, protein interactions and cell signaling. *Anais da Academia ...*, doi:10.1590/s0001-37652009000300007 (2009).
- 68 Rabenstein, D. L. Heparin and heparan sulfate: structure and function. *Natural product reports*, doi:10.1039/b100916h (2002).
- 69 Jiao, X., Billings, P. C., O'Connell, M. P. & Kaplan, F. S. Heparan sulfate proteoglycans (HSPGs) modulate BMP2 osteogenic bioactivity in C2C12 cells. *Journal of Biological ...*, doi:10.1074/jbc.M513414200 (2007).
- 70 Funderburgh, J. L. MINI REVIEW Keratan sulfate: structure, biosynthesis, and function. *Glycobiology*, doi:10.1093/glycob/10.10.951 (2000).
- 71 Kitayama, K., Hayashida, Y. & Nishida, K. Enzymes responsible for synthesis of corneal keratan sulfate glycosaminoglycans. *Journal of Biological ...*, doi:10.1074/jbc.M703695200 (2007).
- 72 Hayashi, M., Kadomatsu, K. & Ishiguro, N. Keratan sulfate suppresses cartilage damage and ameliorates inflammation in an experimental mice arthritis model. *Biochemical and biophysical ...* (2010).
- 73 Jones, L. L. & Tuszynski, M. H. Spinal cord injury elicits expression of keratan sulfate proteoglycans by macrophages, reactive microglia, and oligodendrocyte progenitors. *The Journal of neuroscience*, doi:20026464 (2002).
- 74 Alberts, B. *et al. Molecular Biology of the Cell 4th Edition: International Student Edition.* (Routledge, 2002).
- 75 Schaefer, L. & Schaefer, R. M. Proteoglycans: from structural compounds to signaling molecules. *Cell and tissue research* **339**, 237-246, doi:10.1007/s00441-009-0821-y (2010).
- 76 Schaefer, L. & Iozzo, R. V. Biological functions of the small leucine-rich proteoglycans: from genetics to signal transduction. *Journal of Biological Chemistry*, doi:10.1074/jbc.R800020200 (2008).
- 77 Goldoni, S. & Iozzo, R. V. Tumor microenvironment: Modulation by decorin and related molecules harboring leucine-rich tandem motifs. *International journal of cancer*, doi:10.1002/ijc.23930 (2008).
- 78 Oschatz, C., Maas, C., Lecher, B., Jansen, T. & Björkqvist, J. Mast cells increase vascular permeability by heparin-initiated bradykinin formation in vivo. *Immunity* (2011).
- 79 Munoz, E. M. & Linhardt, R. J. Heparin-binding domains in vascular biology. ..., doi:10.1161/01.ATV.0000137189.22999.3f (2004).
- 80 Laurent, T. C., Laurent, U. B. G. & Fraser, J. R. E. The structure and function of hyaluronan: An overview. *Immunology and cell biology*, doi:10.1038/icb.1996.32 (1996).
- 81 Cui, H., Webber, M. J. & Stupp, S. I. Self-assembly of peptide amphiphiles: From molecules to nanostructures to biomaterials. *Peptide Science*, doi:10.1002/bip.21328 (2010).
- 82 Hartgerink, J. D., Beniash, E. & Stupp, S. I. Peptide-amphiphile nanofibers: a versatile scaffold for the preparation of self-assembling materials. *Proceedings of the National Academy of Sciences* **99**, 5133-5138, doi:10.1073/pnas.072699999 (2002).

- 83 Guler, M. O., Hsu, L., Soukasene, S. & Harrington, D. A. Presentation of RGDS epitopes on self-assembled nanofibers of branched peptide amphiphiles. ..., doi:10.1021/bm060161g (2006).
- 84 Storrie, H., Guler, M. O., Abu-Amara, S. N., Volberg, T. & Rao, M. Supramolecular crafting of cell adhesion. *Biomaterials* (2007).
- 85 D'Andrea, L. D. & Iaccarino, G. Targeting angiogenesis: structural characterization and biological properties of a de novo engineered VEGF mimicking peptide. *Proceedings of the ...* (2005).
- 86 Spoerke, E. D., Anthony, S. G. & Stupp, S. I. Enzyme directed templating of artificial bone mineral. *Advanced Materials*, doi:10.1002/adma.200802242 (2009).
- 87 Hartgerink, J. D., Beniash, E. & Stupp, S. I. Self-assembly and mineralization of peptide-amphiphile nanofibers. *Science (New York, N.Y.)* **294**, 1684-1688, doi:10.1126/science.1063187 (2001).
- 88 Mata, A., Geng, Y., Henrikson, K. J., Aparicio, C. & Stock, S. R. Bone regeneration mediated by biomimetic mineralization of a nanofiber matrix. *Biomaterials* (2010).
- 89 Kocabey, S., Ceylan, H., Tekinay, A. B. & Guler, M. O. Glycosaminoglycan mimetic peptide nanofibers promote mineralization by osteogenic cells. *Acta biomaterialia* (2013).
- 90 Ustun, S., Tombuloglu, A., Kilinc, M. & Guler, M. O. Growth and differentiation of prechondrogenic cells on bioactive self-assembled peptide nanofibers. ..., doi:10.1021/bm301538k (2012).
- 91 Mammadov, B., Mammadov, R., Guler, M. O. & Tekinay, A. B. Cooperative effect of heparan sulfate and laminin mimetic peptide nanofibers on the promotion of neurite outgrowth. *Acta biomaterialia* (2012).
- 92 Benoit, D. S. W., Schwartz, M. P., Durney, A. R. & Anseth, K. S. Small functional groups for controlled differentiation of hydrogel-encapsulated human mesenchymal stem cells. *Nature materials*, doi:10.1038/nmat2269 (2008).
- 93 Stanford, C. M., Jacobson, P. A., Eanes, D. E., Lembke, L. A. & Midura, R. J. Rapidly forming apatitic mineral in an osteoblastic cell line (UMR 10601 BSP). *Journal of Biological Chemistry* **270**, 9420-9428, doi:10.1074/jbc.270.16.9420 (1995).
- 94 Niece, K. L., Hartgerink, J. D., Donners, J. & Stupp, S. I. Self-assembly combining two bioactive peptide-amphiphile molecules into nanofibers by electrostatic attraction. *Journal of the American Chemical Society* **125**, 7146-7147, doi:10.1021/ja028215r (2003).
- 95 Nakayama, G. R., Caton, M. C., Nova, M. P. & Parandoosh, Z. Assessment of the Alamar Blue assay for cellular growth and viability in vitro. *Journal of immunological methods* **204**, 205-208 (1997).
- 96 Nociari, M. M., Shalev, A., Benias, P. & Russo, C. A novel one-step, highly sensitive fluorometric assay to evaluate cell-mediated cytotoxicity. *Journal of immunological ...* (1998).
- 97 Dolbeare, F. & Gratzner, H. Flow cytometric measurement of total DNA content and incorporated bromodeoxyuridine. *Proceedings of the ...*, doi:10.1073/pnas.80.18.5573 (1983).

- 98 Kee, N., Sivalingam, S., Boonstra, R. & Wojtowicz, J. M. The utility of Ki-67 and BrdU as proliferative markers of adult neurogenesis. *Journal of neuroscience methods* **115**, 97-105 (2002).
- 99 McGee-Russell, S. M. Histochemical methods for calcium. *Journal of Histochemistry & Cytochemistry*, doi:10.1177/6.1.22 (1958).
- 100 Puchtler, H., Meloan, S. N. & Terry, M. S. On the history and mechanism of alizarin and alizarin red S stains for calcium. *Journal of Histochemistry & Cytochemistry* **17**, 110-124, doi:10.1177/17.2.110 (1969).
- 101 Barling, P. M., Bennett, J. H., Triffitt, J. T. & Owen, M. E. The adenylate cyclase response to parathyroid hormone in cultured rabbit marrow fibroblastic cells. *Bone and mineral* **7**, 23-30 (1989).
- 102 Kamalia, N., McCulloch, C. A. & Tenebaum, H. C. Dexamethasone recruitment of self-renewing osteoprogenitor cells in chick bone marrow stromal cell cultures. ... (1992).
- 103 Leboy, P. S., Beresford, J. N. & Devlin, C. Dexamethasone induction of osteoblast mRNAs in rat marrow stromal cell cultures. *Journal of cellular ...*, doi:10.1002/jcp.1041460306 (1991).
- 104 Atmani, H., Audrain, C., Mercier, L., Chappard, D. & Basle, M. F. Phenotypic effects of continuous or discontinuous treatment with dexamethasone and/or calcitriol on osteoblasts differentiated from rat bone marrow stromal cells. *Journal of cellular biochemistry* **85**, 640-650, doi:10.1002/jcb.10165 (2002).
- 105 Millan, J. L. *Mammalian Alkaline Phosphatases: From Biology to Applications in Medicine and Biotechnology*. (Wiley, 2006).
- 106 Addison, W. N., Azari, F. & Sørensen, E. S. Pyrophosphate inhibits mineralization of osteoblast cultures by binding to mineral, up-regulating osteopontin, and inhibiting alkaline phosphatase activity. *Journal of Biological ...*, doi:10.1074/jbc.M701116200 (2007).
- 107 Ali, A. *et al.* Alkaline phosphatase is involved in the control of adipogenesis in the murine preadipocyte cell line, 3T3-L1. *Clinica chimica acta* **354**, 101-109 (2005).
- 108 Ali, A. T., Penny, C. B., Paiker, J. E., Psaras, G. & Ikram, F. The relationship between alkaline phosphatase activity and intracellular lipid accumulation in murine 3T3-L1 cells and human preadipocytes. *Analytical ...* (2006).
- 109 Bianco, P., Costantini, M. & Dearden, L. C. Alkaline phosphatase positive precursors of adipocytes in the human bone marrow. *British journal of ...*, doi:10.1111/j.1365-2141.1988.tb04225.x (1988).
- 110 Lanza, R. P. *Handbook of Stem Cells*. (Elsevier Academic, 2004).
- 111 Lund, A. W., Stegemann, J. P. & Plopper, G. E. Mesenchymal stem cells sense three dimensional type I collagen through discoidin domain receptor 1. *The open stem cell journal* **1**, 40 (2009).
- 112 Komori, T. Regulation of skeletal development by the Runx family of transcription factors. *Journal of cellular biochemistry*, doi:10.1002/jcb.20420 (2005).
- 113 Ramirez-Zacarias, J. L., Castro-Munozledo, F. & Kuri-Harcuch, W. Quantitation of adipose conversion and triglycerides by staining intracytoplasmic lipids with Oil red O. *Histochemistry* **97**, 493-497, doi:10.1007/bf00316069 (1992).

- 114 Luo, W., Shitaye, H., Friedman, M. & Bennett, C. N. Disruption of cell–matrix interactions by heparin enhances mesenchymal progenitor adipocyte differentiation. *Experimental cell ...* (2008).
- 115 Hausser, H. J. & Brenner, R. E. Low doses and high doses of heparin have different effects on osteoblast-like Saos-2 cells in vitro. *Journal of cellular biochemistry*, doi:10.1002/jcb.20007 (2004).
- 116 Rosenberg, L. Chemical basis for the histological use of safranin O in the study of articular cartilage. *The Journal of Bone & Joint Surgery* (1971).
- 117 Banaszkiwicz, P. A. & Kader, D. F. *Classic Papers in Orthopaedics*. (Springer London, Limited, 2014).
- 118 Solchaga, L. A. & Goldberg, V. M. Cartilage regeneration using principles of tissue engineering. *Clinical orthopaedics and ...*, doi:10.1097/00003086-200110001-00016 (2001).
- 119 Sechriest, V. F., Miao, Y. J. & Niyibizi, C. GAG-augmented polysaccharide hydrogel: A novel biocompatible and biodegradable material to support chondrogenesis. *Journal of ...*, doi:10.1002/(sici)1097-4636(20000315)49:4<534::aid-jbm12>3.0.co;2-# (2000).
- 120 Varghese, S., Hwang, N. S., Canver, A. C. & Theprungsirikul, P. Chondroitin sulfate based niches for chondrogenic differentiation of mesenchymal stem cells. *Matrix Biology* (2008).
- 121 Ottani, V., Martini, D., Franchi, M., Ruggeri, A. & Raspanti, M. Hierarchical structures in fibrillar collagens. *Micron* (2002).
- 122 Marlovits, S., Hombauer, M. & Truppe, M. Changes in the ratio of type-I and type-II collagen expression during monolayer culture of human chondrocytes. *Journal of Bone & ...*, doi:10.1302/0301-620x.86b2.14918 (2004).
- 123 Karlsson, C., Brantsing, C. & Svensson, T. Differentiation of human mesenchymal stem cells and articular chondrocytes: Analysis of chondrogenic potential and expression pattern of differentiation-related .... *Journal of ...*, doi:10.1002/jor.20287 (2007).
- 124 Chmurzyńska, A. The multigene family of fatty acid-binding proteins (FABPs): function, structure and polymorphism. *Journal of applied genetics*, doi:10.1007/bf03194597 (2006).
- 125 Baxa, C. A., Sha, R. S., Buelt, M. K., Smith, A. J. & Matarese, V. Human adipocyte lipid-binding protein: purification of the protein and cloning of its complementary DNA. *Biochemistry*, doi:10.1021/bi00448a003 (1989).
- 126 Vater, C., Kasten, P. & Stiehler, M. Culture media for the differentiation of mesenchymal stromal cells. *Acta biomaterialia* (2011).